

NON-DARCIAN FLOW IN A FRACTURED AQUIFER

A THESIS SUBMITTED TO
THE GRADUATE SCHOOL OF NATURAL AND APPLIED SCIENCE
OF
MIDDLE EAST TECHNICAL UNIVERSITY

BY

ADNAN ALTAY ALTINÖRS

IN PARTIAL FULFILLMENT OF THE REQUIREMENTS
FOR
THE DEGREE OF DOCTOR OF PHILOSOPHY
IN
CIVIL ENGINEERING

AUGUST 2005

Approval of the Graduate School of Natural and Applied Sciences

Prof. Dr. Canan Özgen
Director

I certify that this thesis satisfies all the requirements as a thesis for the degree of Doctor of Philosophy

Prof. Dr. Erdal Çokça
Head of Department

This is to certify that we have read this thesis and that in our opinion it is fully adequate, in scope and quantity, as a thesis for the degree of Doctor of Philosophy.

Prof. Dr. Halil Önder
Supervisor

Examining Committee Members

Prof. Dr. Uygur Şendil	(METU, CE)	_____
Prof. Dr. Halil Önder	(METU, CE)	_____
Prof. Dr. Nurkan Karahanoğlu	(METU, GEOE)	_____
Assoc. Prof. Dr. İsmail Aydın	(METU, CE)	_____
Assoc. Prof. Dr. Lale Balas	(Gazi University, CE)	_____

I hereby declare that all information in this document has been obtained and presented in accordance with academic rules and ethical conduct. I also declare that, as required by these rules and conduct, I have fully cited and referenced all material and results that are not original to this work.

Adnan Altay Altınörs

ABSTRACT

NON-DARCIAN FLOW IN A FRACTURED AQUIFER

Altınörs, Adnan Altay

Ph. D., Department of Civil Engineering

Supervisor: Prof. Dr. Halil Önder

August 2005, 147 pages

Non-Darcian flow in a finite fractured aquifer is studied in this thesis. A stream bounds the aquifer at one side and an impervious stratum at the other. The aquifer consists of fractures capable of transmitting water rapidly and porous blocks which mainly store water. Unsteady flow in the aquifer due to a sudden or a gradual rise in the stream level is analysed by the double-porosity conceptual model. Governing equations for the flow in fractures and blocks are developed using the continuity equation. The fluid velocity in fractures is often too high for the linear Darcian flow so that the governing equation for fracture flow is modified by Forcheimer's equation which incorporates a nonlinear term. Governing equations are coupled by an interaction term that controls the quasi-steady state fracture-block interflow. Governing equations are solved numerically by the Crank-Nicolson implicit scheme. The numerical results are compared to the analytical results for the same problem which assumes Darcian flow both in fractures and blocks. Numerical and analytical solutions give same results when Reynold's number is less than 0.1. The effect of non-linearity on the flow appears when Reynold's number is greater than 0.1. The larger the piezometric head gradient, the higher the flow rate and, thus, higher the non-linearity is. The effect of aquifer parameters on the flow is also investigated. The proposed model and its numerical solution is a unique application of non-linear flow models to the fractured aquifers. It can be used in predicting water levels in fractured aquifers and evaluating time dependent flow rates in the analysis of recession hydrographs.

Keywords: Fractured aquifer, Non-Darcian flow, Forcheimer's equation

ÖZ

ÇATLAKLI AKÜFERDE DARCY KANUNUNA UYMAYAN AKIM

Altınörs, Adnan Altay

Doktora, İnşaat Mühendisliği Bölümü

Tez Yöneticisi: Prof. Dr. Halil Önder

Ağustos 2005, 147 sayfa

Bu tezde sınırlı çatlaklı aküferde Darcy Kanunu'na uymayan akım çalışılmıştır. Aküferi bir yanda nehir, diğer yanda ise geçirgen olmayan bir tabaka sınırlamaktadır. Nehirdeki su seviyesinin aniden yükselmesi sonucunda aküferde oluşan zamana bağlı akım ikili gözenek kavramsal modeliyle incelenmiştir. Çatlaklardaki ve bloklardaki akımları tasvir eden denklemler süreklilik denklemi kullanılarak elde edilmiştir. Çatlaklardaki akım hızı genelde doğrusal Darcy Kanunu için yüksek olduğundan çatlaklardaki akım denklemi, doğrusal olmayan akımı modelleyen bir ifadeyi içeren Forcheimer Denklemi'yle geliştirilmiştir. Akım denklemleri çatlaklar ve bloklar arasındaki su geçişini belirleyen bir etkileşim ifadesi ile eşleştirilmiş ve Crank-Nicolson yöntemiyle sayısal olarak çözülmüştür. Sayısal çözümler aynı problem için mevcut olan, ancak çatlaklardaki akımın da doğrusal Darcy Kanunu'na uyduğunu kabul eden analitik çözümlerle karşılaştırılmıştır. Sayısal ve analitik çözümler Reynold sayısı 0.1'den küçükken aynı sonuçları vermiştir. Doğrusal olmayan akımın etkisi Reynold sayısı 0.1'den büyükken ortaya çıkmaktadır. Piezometrik basınç farkı yükseldikçe aküferdeki akım da artmakta, dolayısıyla doğrusal olmayan akımın etkisi büyümektedir. Aküferin özelliklerinin akım üzerindeki etkisi de araştırılmıştır. Önerilen model ve sayısal çözümü doğrusal olmayan akım modellerinin çatlaklı aküferlere özgün bir uygulanmasıdır. Bu model çatlaklı aküferlerde su seviyesinin tespiti ile taşkın ve çekilme hidrograflarının analizinde zamana bağlı akımın tespitinde kullanılabilir.

Anahtar kelimeler: Çatlaklı aküfer, Darcy Kanunu'na uymayan akım,
Forcheimer Denklemi

ACKNOWLEDGMENTS

I wish to express my deepest gratitude to my supervisor Prof. Dr. Halil Önder for his guidance, advice, support and criticism throughout this research. I would also like to mention my sincere appreciation for the excellent communication between us.

I am grateful to Prof. Dr. Uygur Şendil and Prof. Dr. Nurkan Karahanoğlu, the members of the thesis supervising committee, for their valuable comments and constructive suggestions.

I would also like to thank to my superiors in the Ministry of Foreign Affairs for their support and tolerance throughout my Ph. D. study.

My personal thanks go to Assoc. Prof. Dr. Serkan Özgen, Mr. Uğraş Başaran and Mr. Tolga Yaşa for their kind assistance and encouragement.

TABLE OF CONTENTS

PLAGIARISM	iii
ABSTRACT	iv
ÖZ	v
ACKNOWLEDGEMENTS	vi
TABLE OF CONTENTS	vii
LIST OF SYMBOLS.....	x
CHAPTER	
1. INTRODUCTION	1
2. THEORETICAL BACKGROUND	4
2.1 Literature Survey	4
2.2 Darcy's Law	14
2.3 Hydraulic Conductivity	18
2.4 Non-Darcian Flow	18
2.5 Forcheimer's Equation	21
2.6 Reynold's Number.....	24
2.7 Continuity Equation	24
2.8 Governing Equations	26
2.9 Fluid Transfer Rate	30
2.10 Initial and Boundary Conditions	32
2.11 Governing Equations Presented by Önder (1998) for the Same Problem.....	34
3. NUMERICAL SOLUTION OF THE PROBLEM	37
3.1 Non-Dimensionalization of the Governing Equations and Boundary Conditions	37
3.2 Introductory Remarks for Numerical Solution	43
3.3 Discretization of the Governing Equations	46
3.4 Calculation of the Scalar Function F(q).....	49
3.5 Discretization of the Boundary Conditions	52

3.6 Calculation of the Flow Rate from the Stream to the Aquifer.....	53
3.7 Stability, Consistency and Convergence	54
3.8 Accuracy	57
3.9 Discrete Perturbation Stability Analysis.....	58
4. SOLUTION AND RESULTS.....	61
4.1 Basic Data and Solution Procedure	61
4.2 Stability of the Finite Difference Equations of the Fractures and the Blocks.....	67
4.3 Comparison of the Numerical Solution with the Analytical Solution - Determination of Appropriate Step Size and Mesh Size	69
4.4 Drawdown in the Aquifer	79
4.5 Effect of the Non-Linear Forcheimer Parameter, b , on the Drawdown in the Fractures	83
4.6 Effect of the Storativity Contrast, η , on the Drawdown in the Fractures	89
4.7 Effect of the Conductivity Contrast, κ , on the Drawdown in the Fractures	92
4.8 Effect of the Fluid Transfer Parameter, ε , on the Drawdown in the Fractures	94
4.9 Effect of the Non-Linear Forcheimer's Parameter, b , on the Flow Rate	94
4.10 Effect of the Storativity Contrast, η , on the Flow Rate	99
4.11 Effect of the Conductivity Contrast, κ , on the Flow Rate....	101
4.12 Linear Rise in the Stream Level.....	104
4.13 Response of the Aquifer to an Arbitrary Stage Hydrograph.....	107
5. CONCLUSIONS	110
REFERENCES	114

APPENDICES

A. COMPUTER PROGRAM	119
B. APPLICATION OF THE DISCRETE PERTURBATION ANALYSIS.....	123
C. COMPARISON OF NUMERICAL AND ANALYTICAL SOLUTIONS	130
D. PUBLISHED DATA ON POROUS MEDIA.....	135
E. RAW DATA	137
F. SOME EXAMPLES TO THE RESULTS OF DISCRETE PERTURBATION STABILITY ANALYSIS.....	143
CURRICULUM VITAE.....	147

LIST OF SYMBOLS

a	: Forcheimer's linear term, reciprocal of hydraulic conductivity
A	: Area
b	: Forcheimer's non-linear term
B	: Thickness of aquifer
c	: Half length of fracture width
e	: Error or perturbation
F(q)	: Scalar function of the magnitude of specific discharge vector
g	: Gravitational acceleration
h	: Piezometric head
J	: Hydraulic gradient
k	: Intrinsic permeability
K	: Hydraulic conductivity
l	: Half length of fractures and blocks in contact
L	: Length of aquifer
M	: Izbash's non-Darcian flow coefficient
N	: Number of points, unknowns or equations
n	: Porosity
m	: Izbash's constant
p	: Pressure
q	: Specific discharge
Q	: Flow rate
Q _d	: Dimensionless flow rate
R _e	: Reynold's number
RMS	: Root mean square
s	: Drawdown in stream level
s _d	: Dimensionless drawdown in stream level
S	: Storativity
t	: Time

T	: Transmissivity
u	: Dependent variable
V	: Velocity
x	: Horizontal coordinate
y	: Vertical coordinate
z	: The third coordinate
z	: Dimensionless drawdown
α	: Ratio between time step and square of grid size
α_T	: Shape factor
β	: Dimensionless Forcheimer's non-linear parameter
Γ	: Parameter used in the application of Discrete Perturbation Analysis
γ	: Coefficient of the combined method
γ_s	: Specific weight of fluid
δ	: Diffusivity contrast
κ	: Conductivity contrast
Λ	: Parameter used in the application of Discrete Perturbation Analysis
η	: Storativity contrast
ξ	: Shape factor
ε	: Fluid transfer parameter
θ	: Dimensionless time variable
λ	: Dimensionless space variable in horizontal coordinate axis
ψ	: Constant coefficient
μ	: Dynamic viscosity
ν	: Kinematic viscosity
ν_d	: Interaction term, volume of water transfer between blocks and fractures per unit area per unit time
ρ	: Density
b	: Subscript for blocks
f	: Subscript for fractures
0	: Subscript for initial conditions

CHAPTER I

INTRODUCTION

Groundwater has an important role in the development and management of water resources. There exists an increasing demand for information on groundwater hydrology and hydraulics. Aquifers, which are the main resources of groundwater, need special attention in this regard.

Aquifers are geological porous formations, or group of geological formations, that contain water as well as permit water to flow through. The pressure distribution in an aquifer, the discharge to or from an aquifer and river-aquifer or well-aquifer interactions have significant importance in solving various engineering problems.

Aquifers often exhibit a variety of heterogeneities, such as fractures, fissures, cracks and macro-pores (Gerke and Genuchten, 1993). These structures affect water movement at macroscopic level by creating non-uniform flow fields with widely different velocities.

Fractured aquifers, which consist of fractures and matrix blocks, are one of the most common types of aquifers. The flow behaviour in fractured aquifers is significantly different from the flow behaviour in conventional aquifers (Bai *et al.*, 1993). Flow of water in a fractured aquifer is primarily through high-permeability fractures surrounding individual porous blocks.

Darcy's law of flow describing a linear relationship between volumetric flow rate and pressure gradient in porous media has been the fundamental principle in analyzing flow in porous media. Any deviation from this linear relation may be defined as non-Darcian flow (Wu, 2002), in other words non-linear flow. The fluid velocity in fractures is often too high for the linear Darcian flow so that the flow in

fractures should be modeled by different relationships which incorporate non-linear term.

The objective of this study is to investigate the behavior of non-Darcian groundwater flow in a finite fractured confined aquifer system using a numerical solution method. The proposed model is a unique application of non-linear flow models to the fractured aquifers. It can be used in predicting water levels in fractured aquifers and evaluating time dependent flow rates in the analysis of recession hydrographs.

The general description of the stream-aquifer system is shown in *Figure 1.1*. The aquifer is bounded by a stream at one side and an impervious layer at the other. The response of the aquifer to three different conditions in the stream level, i.e. sudden rise, linear (gradual) rise and arbitrary stage hydrograph, has been investigated. However, the effect of a sudden rise in the stream level on piezometric head distribution in the aquifer and in flow of water from the stream to the aquifer is the primary concern.

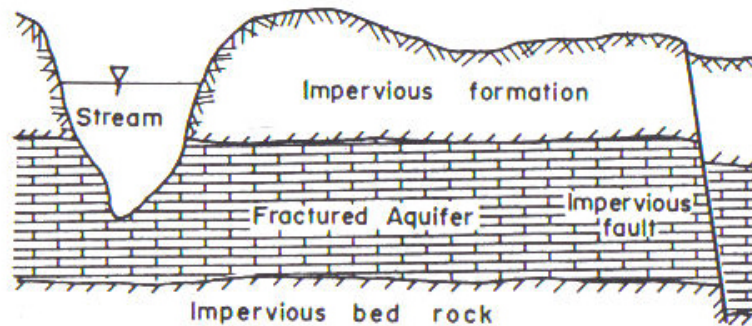


Figure 1.1: Stream and finite fractured confined aquifer system (Önder, 1998)

Following the introduction, the theoretical background of the problem is given in *Chapter 2*. First of all, physical and mathematical concepts as well as the

previous studies related to the problem explored in the literature are presented. Secondly, Darcian and non-Darcian types of flow are described. Then, the procedure for derivation of the governing equations, which are based on the continuity equation and the double porosity conceptual model is explained. The flow in fractures is modeled by Forcheimer's equation and the flow in blocks is described by Darcy's law. Quasi-steady transfer of water between fractures and blocks is assumed.

Chapter 3 covers the numerical solution of the problem. Firstly, non-dimensionalization procedures for the governing equations and related initial and boundary conditions are presented. Then, the numerical method, i.e. the Crank-Nicolson implicit scheme, used to solve the governing equations is explained. Concepts of stability, consistency, convergence and accuracy are summarized and the discrete perturbation stability analysis is described.

Chapter 4 is devoted to the solution procedure, results and discussions. Numerical solution gives piezometric head variation along the aquifer with time and rate of water flow from the stream to the aquifer. Primarily the non-Darcian effect on the piezometric head distribution and the flow rate has been investigated. Comparison of the results of the numerical solution with the results of the available analytical solution, which is presented by Önder (1998) for the same problem but for the special case of Darcian flow in fractures, has helped to determine the accuracy of the numerical solution and to show the non-Darcian effect on the flow in the aquifer more precisely. Furthermore, effects of the various aquifer parameters on the piezometric head distribution and the flow rate are elaborated. Finally, conclusions are presented in *Chapter 5*.

CHAPTER 2

THEORETICAL BACKGROUND

2.1 Literature Survey

There exists interaction between surface water and ground water in various means including natural or artificial recharge or drainage, seepage from irrigation or river waters, precipitation, evaporation and evapotranspiration. Numerous studies examining these problems are available in the literature.

The behaviour of groundwater flow in a finite aquifer between a stream and an impervious boundary under natural or artificial conditions has to be known in various engineering applications such as prediction of time dependent flow in the analysis of storm and recession hydrographs, evaluation of the base flow during dry seasons, predicting water levels and determination of the hydraulic properties of aquifers,.

Figure 2.1 shows diagrammatic cross-sections through idealised finite confined aquifers. These aquifers are bounded at one side by a stream boundary and by an impermeable formation or barrier at the other. *Case (a)* represents a homogenous and uniform (single porosity) aquifer. *Case (b)* represents a non-uniform aquifer which consists of two distinct homogeneous regions. *Case (c)* represents a double (dual) porosity fractured aquifer comprising a homogeneous fracture system within a homogeneous porous block system (Önder, 2002).

A common feature in these situations is that the head varies because of a change in stream stage, which means the head at the stream boundary is imposed as an excitation (input).

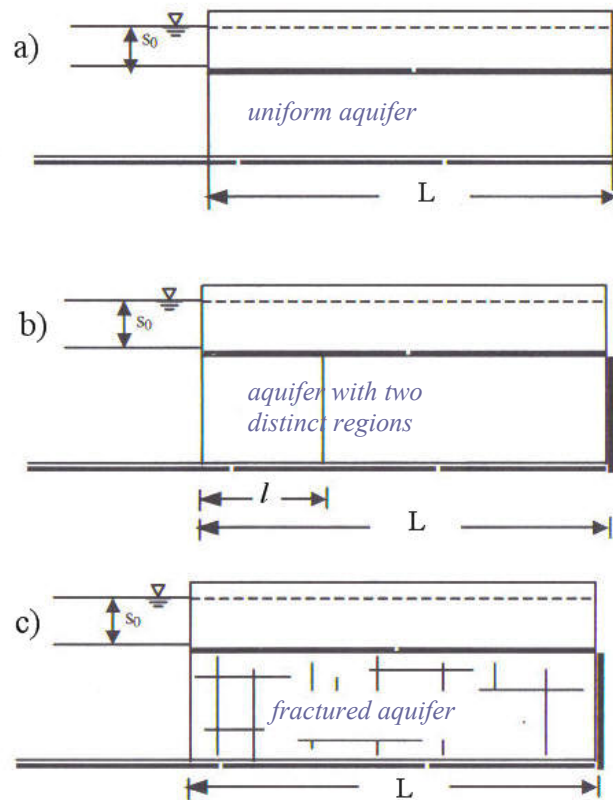


Figure 2.1: Finite confined aquifers (Önder, 2002).

The link between the excitation and the groundwater system should be established in order to evaluate the responses (outputs). In prediction of the response of groundwater systems to diverse inputs, modelling is used as a tool to obtain answers to questions posed by water resource managers. Various mathematical and physical models have been developed.

Analytical solutions for stream-aquifer interaction problems are available in the literature for the cases depicted in *Figure 2.1*. However, when the boundary conditions or the aquifer characteristics are variable, the response of a groundwater flow system to such excitations is complex and often simulated by numerical models.

The constant rise or drawdown condition in the stream stage is encountered not as frequently as the constant discharge condition from the aquifer. However, in the channels of flood plains, when appropriate control structures are present, the changes in water level may reasonably be approximated by a step rise or drawdown. Several researchers (Lane and Zinn, 1981, Henry and Palmer, 1981) have observed such field conditions created by recharge weirs which are constructed to enhance the rate of groundwater inflow from the streams. These observations may be considered as adequate evidence that a step change may occur in streams adjacent to aquifers.

Rorabaugh (1960), Rorabaugh (1964), Pinder *et al.* (1970) and Önder (1994) are some examples of the researchers who have studied the flow behaviour in a finite aquifer system due to a sudden rise or decline of the water level in the adjacent stream. In these studies, aquifers composed of granular media (single porosity aquifers) were considered. However, a widely encountered type of aquifer is the fractured rock aquifer (Önder, 1998).

The behaviour of naturally fractured aquifers is radically different from that of the conventional aquifers composed solely of inter-granular porosity (Bai *et al.* 1993). The reason for this is that fractures affect water movement at the macroscopic level by creating non-uniform flow fields with widely different velocities. Therefore, in fractured media, the application of conventional single-porosity flow models has proven inadequate.

Fractured porous media may be represented by two completely overlapping continua, one representing the porous matrix and the other representing the fractures. This type of formation, which is shown in *Figure 2.2*, is commonly qualified as a heterogeneous medium in which low permeability blocks of primary porosity are separated by highly permeable fractures of low volume. In a typical fractured medium, the fractures provide high conductivity conduits amenable to rapid hydraulic flows, whereas the high porosity matrix blocks contain the majority of the storage (Bai *et al.*, 1993).

When dealing with flow in a fractured porous medium, the microscopic flow patterns inside the individual pores or fractures are overlooked and it is considered that some fictitious average flow is taking place. Therefore, the concept of continuum is employed. The obvious reason for employing the continuum approach in flow through porous medium is that it is practically impossible to describe in any exact mathematical manner the complicated geometry of the solid surfaces that bound the flowing fluid (Bear, 1979).

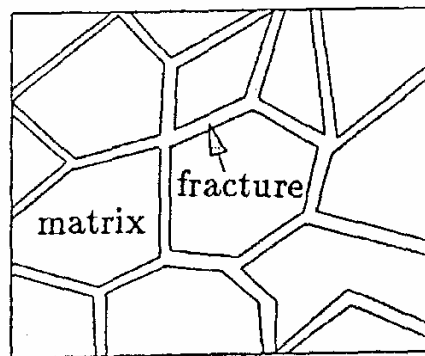


Figure 2.2: Fractured porous medium.

It was only in the early 1950's that a qualitative evaluation of fluid flow and rock properties was undertaken, and attempts were made to interpret fissure flow properties. The study was carried out mainly by petroleum geologists, as the world's largest and important oil production fields are associated with fractured rocks. From the very beginning of these investigations, it was recognized that fluid flow behaviour and basic reservoir parameters, namely permeability and storage capacity, of the fissured formation differ from the behaviour and parameters of a porous medium (Streltsova, 1976).

The hydrodynamic aspects of flow in fissured rocks were first considered by Barenblatt *et al.* (1960). Two overlapping continuum media, porous and fissured, each filling the entire domain flow domain, were assumed to represent a fractured

formation, consisting of an extreme system of randomly distributed and arbitrarily oriented fissures in a rock of primary porosity.

Barenblatt *et al.* (1960) recognized that one can assume the permeability of the porous blocks in a fractured reservoir to be very low relative to the permeability of the fractures. This assumption was credited later by Warren and Root (1963) by putting this concept into a mathematical-physical statement that assumes that the matrix blocks are arranged in a systematic array of identical, rectangular parallelepipeds that provide flow to the fractures which, in turn, transport the fluid. Odeh (1965) attempted to generalize the concept of Warren and Root (1963) to accommodate a fractured reservoir in which the pattern of fractures is not known. This conceptual jump was consistent with the fundamental postulates of modern continuum theory, but it was ignored by many later researchers. Warren and Root (1963) and Odeh (1965) developed analytical solutions using their models.

These analytical solutions subsequently were extended by Kazemi *et al.* (1969). They presented the assumptions for which their conceptual models hold as:

- The matrix porosity has a high storage capacity but low flow capacity. The converse is true of the fracture porosity.
- Flow occurs only through the fracture network. Matrix flow occurs into the fractures.
- Matrix flow to the fractures is quasi-steady and fracture flow is unsteady.
- The reservoir is horizontal and infinitely large.
- Vertical pressure gradients are negligible.

Much later than these studies, Bai *et al.* (1993) proposed several conceptual flow models in order to provide more flexible tools to match geological variations in the fractured media and to avoid an unrealistic prediction of reservoir storage and flow characteristics. They are single-porosity/single-permeability, double-porosity/single-permeability, double-porosity/double-permeability, triple-

porosity/double-permeability and triple-porosity/triple-permeability conceptual models based on deformation dependent flow.

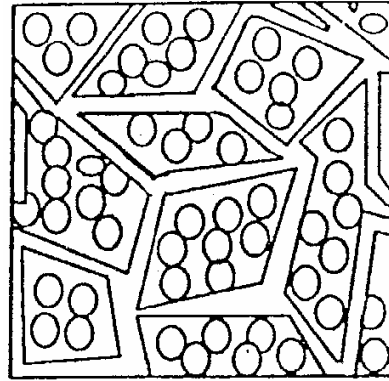


Figure 2.3: Double-porosity/double-permeability fractured medium
(Bai *et al.*, 1993).

The double-porosity/double-permeability conceptual model of Bai *et al.* (1993), which is schematically shown in *Figure 2.3*, is actually the same model introduced by Barenblatt *et al.* (1960). In this model, an exchange of water between fractures and blocks is taken into account; however, there is no flow between any two blocks. Hence, the fractures provide the main path for fluid flow, whereas the blocks act as a source or sink to the fractures.

Double porosity models assume that water flow in a fractured medium can be described by two equations that are coupled using a term characterizing the exchange of fluid between two pore regions. Central to the double porosity approach is the assumption that the medium can be separated into two distinct pore systems, both of which are treated as homogenous media with separate hydraulic properties. The double-porosity medium is considered to be a superposition of these two systems over the same volume (Dykhuizen, 1987, and Gerke and van Genuchten, 1993). The two pore systems interact by exchanging water in response to the pressure head

gradient. Hence, macroscopically, the porous medium at any point in time and space is characterized by two flow velocities and two pressure heads (Gerke and van Genuchten, 1993).

Streltsova (1975) presented drawdown equations for the flow in fractures and porous matrix to a well discharging at a constant rate in a fractured confined aquifer of finite thickness, based on Darcy's law and the equation of continuity. She assumed that the aquifer and the water contained in it are compressible. Initially, before pumping, fissures of all orientation and porous blocks are compressed equally by hydrostatic pressure. A reduction in the fluid pressure, as soon as pumping commences, causes the elastic response of the aquifer. The volume of water released causes horizontal flow.

Streltsova (1975) also studied unsteady two-dimensional flow in a semi-infinite unconfined aquifer adjacent to a surface reservoir, canal or river. The initial state of the aquifer is of uniform head distribution. A sudden rise or fall of the water boundary level causes a discontinuity of the heads at the boundary, creating a non-uniform distribution of heads along the vertical, which results in the downward or upward variable movement of the water in the aquifer.

Studies on the fractured media are often based on the assumption that the flow of water through fractures and porous matrix blocks complies with Darcy's law which postulates a linear relation between the specific discharge (macroscopic velocity) and the hydraulic gradient. However, while using Darcy's linearity for various problems, it is always necessary to be cautious about the applicability in the high velocity zone. Widely available experimental data to justify the validity and applicability of Darcy's law have helped to evolve a general consensus that there is an upper as well as a lower limit beyond which Darcy's linear law does not hold (Basak, 1977).

Many researchers have proposed various forms of velocity-gradient relationship that are mainly based on extensive experimental results. A summary of available relations is given by Basak (1977).

The most widely used flow relations for non-Darcian flow are that of Izbash and Forcheimer (Basak, 1977). While Izbash's equation is purely empirical, Forcheimer's equation, though initially based on the experimental results alone, is found to have theoretical justification. It can be characterized as the empirical modification of the Darcy's model.

Basak (1976) presented an analytical solution for the case of steady-state unconfined flow through embankments using Forcheimer's equation. In this study, the effect of non-linearity in the flow response of discharge characteristics and piezometric pressure distribution corresponding to the Darcian case are brought out.

Basak (1977) also obtained analytical solutions using Izbash's equation for two seepage problems, which are the drainage spacing in ditch drainage system and the steady-state seepage through a confined aquifer of variable thickness. The primary objective of this study was to bring out the necessity of consideration of non-Darcian flow at low and high velocities.

Bordier and Zimmer (1999), who studied drainage systems made up of coarse materials, have shown experimentally that Izbash's and Forcheimer's equations are suitable to describe the flow equation in different coarse materials.

Choi *et al.* (1996) investigated single phase fluid flow in fractured formations using the double-porosity conceptual flow model. They solved the governing equations for the flow in fractures and blocks provided by Bai *et al.* (1993) numerically using the successive over-relaxation scheme. Forcheimer's equation was used to describe fluid flow through fractures while maintaining Darcian flow through blocks. Basic data supplied from field data were used in calculations. Numerical

solutions results indicate that the non-linear model predicts a higher flow rate compared to the Darcian model.

Kohl *et al.* (1997) carried out field tests in order to investigate non-Darcian flow transients in fractured rock and concluded that a transition from Darcian flow to a turbulent flow regime occurs in fractures.

Venkataraman *et al.* (1998) identified the ranges of the Reynold's number where the flow through porous media is Darcian, transitional and turbulent, and derived a formulation for the friction factor.

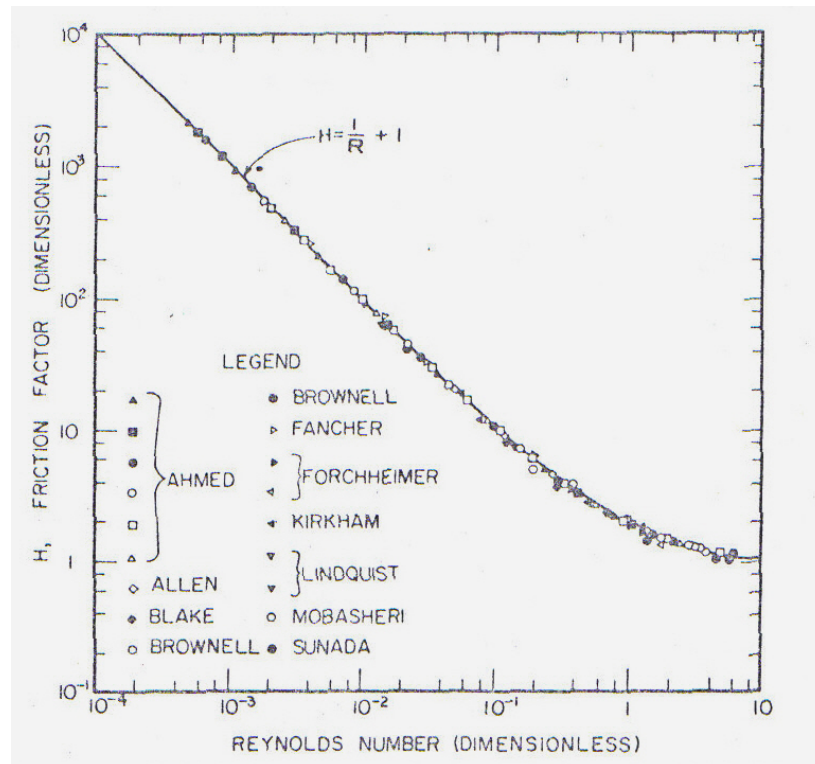


Figure 2.4: Graphical correlation of friction factor and Reynold's number, Ahmed and Sunada (1969).

Ahmed and Sunada (1969) pointed out that turbulence in porous media is small compared to the convective acceleration resulting from the curved path that the fluid must follow in pores. They presented the experimental data, which are shown in *Figure 2.4*, for various porous media in terms of friction factor and Reynold's number, and concluded that non-Darcian flow starts to take place when Reynold's number is around 0.1 .

Based on the previous experimental studies, Cornell and Katz (1953) also demonstrated that the non-linear flow of natural gas or air occurs in consolidated porous media (sandstones, canyon reef limestones, dolamites and porous metals) when Reynold's number is slightly greater than 0.1 .

On the other hand, Beawers and Sparrow (1969) showed that significant departures of the experimental results from Darcy's law first occur at Reynold's numbers in the order of 1 .

Depending on the characteristic length used in the definition of Reynold's number and the type of the porous material, the start of non-Darcian flow occurs when Reynold's number is between 0.1 and 1 .

Wu (2002a) studied non-Darcian flow toward a well in fractured media modifying Warren and Root's (1963) analytical solution using Forcheimer's equation.

Wu (2002b) also described a numerical method incorporating the Forcheimer equation to investigate single-phased and multi-phased non-Darcian flow in porous and fractured reservoirs. He verified his numerical method by comparing its results against those of analytical methods. Wu also found out that the quasi-steady flow assumption in Warren and Root's model provides a good approximation to non-Darcian flow cases as long as the double porosity concept applies.

Rafiqul *et al.* (1998) studied the mixed convection heat transfer in an infinitely long horizontal porous duct applying Darcy's and Forcheimer's equations. They stated that the scale of the axial velocity as well as the inertial parameter in the Forcheimer's equation determine the flow characteristics in the duct.

Şen (1986) provided an approximate analytical solution incorporating the Forcheimer's equation to be used to analyse time-drawdown data observed in wells in coarse grained or fractured medium producing radial non-Darcian flow effects.

It appears that there is a need for a further study on the non-Darcian flow in a fractured aquifer in general and on the one-dimensional flow in particular as it has not been considered in the literature.

2.2 Darcy's Law

The theory of flow through porous media originated almost 150 years ago when Henry Darcy published an empirical relationship as a result of his experimental studies, which has since been called Darcy's law. Darcy concluded that the rate of flow, Q , is proportional to the cross-sectional area, A , and the piezometric head difference, Δh , and inversely proportional to the length, L , of the porous medium. These conclusions gave the famous Darcy's formula:

$$Q = \frac{KA(h_1 - h_2)}{L} = \frac{KA\Delta h}{L} \quad 2.1$$

where K is the coefficient of proportionality and h_1 and h_2 are piezometric heads measured with respect to some arbitrary horizontal datum.

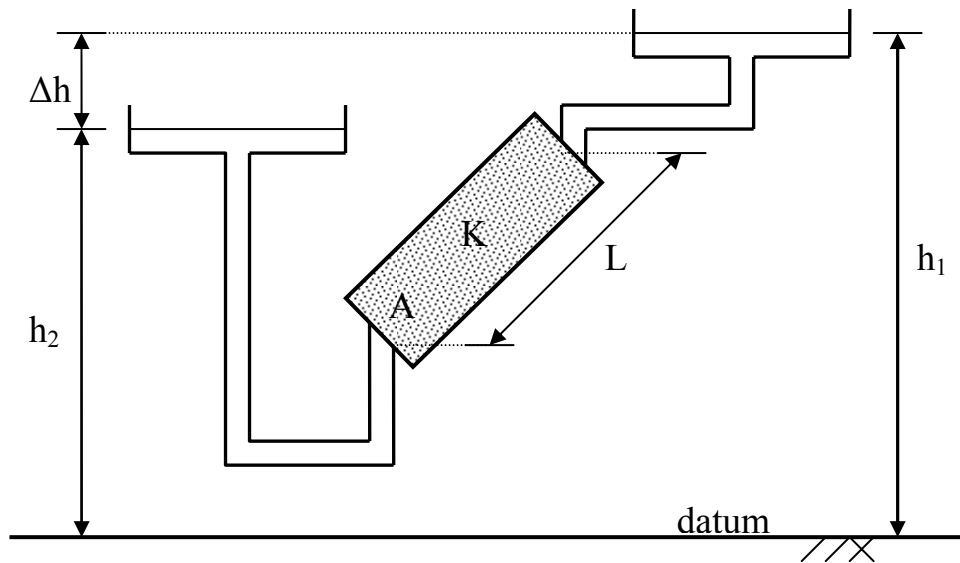


Figure 2.5: General layout of the Darcy's experimental set up.

Given that the piezometric head describes (in terms of head of water) the sum of pressure and potential energies of the fluid per unit weight, $\frac{(h_1 - h_2)}{L}$ is to be interpreted as hydraulic gradient. Denoting this gradient by J and defining the specific discharge, q , as the volume of water flowing per unit time through a unit cross-sectional area normal to the direction of flow, then:

$$q = KJ \tag{2.2}$$

where

$$q = \frac{Q}{A} \tag{2.3}$$

Thus:

$$q = \frac{K(h_1 - h_2)}{L} = KJ \quad 2.4$$

is another form of the Darcy's formula. Darcy's linear law may also be extended to flow through an inclined homogenous column of porous medium (Bear, 1979).

The piezometric head, h , is expressed as

$$h = z + \frac{p}{\gamma_s} \quad 2.5$$

where z is an arbitrarily specified reference level, p is the pressure, γ_s is the specific weight, ν is the kinematic viscosity, g is the gravitational acceleration and $\frac{p}{\gamma_s}$ is the pressure head.

There exists an energy loss due to friction in the flow through the narrow tortuous parts of the porous medium. Actually, in Darcy's law, the kinetic energy of water has been neglected as, in general, changes in the piezometric head along the flow path are much larger than the changes in kinetic energy. It is important to note that the flow takes place from a higher piezometric head to a lower head and not from a higher to lower pressure.

The flow takes place only through the void space of the cross-sectional area of the column of porous medium, the remaining part being occupied by the solid matrix of the porous medium. Since it can be shown that the average areal porosity is equal to the volumetric porosity, n , the portion of the area, A , available for flow is nA . Accordingly, the average velocity, V , of the flow through the column is

$$V = \frac{Q}{nA} = \frac{q}{n} \quad 2.6$$

The coefficient of proportionality, K , appearing in Darcy's law is called the hydraulic conductivity of the porous medium. It depends on properties of both the porous matrix and the fluid.

The experimentally derived equation of motion in the form of Darcy's law is limited to one-dimensional flow of a homogenous incompressible fluid. When the flow is three dimensional, the generalization of Darcy's law is

$$\vec{q} = K\vec{J} \quad 2.7$$

$$\vec{V} = \vec{q}/n \quad 2.8$$

where \vec{V} is the velocity vector with components V_x , V_y and V_z , and \vec{q} is the specific discharge vector with components q_x , q_y and q_z in the directions of the Cartesian coordinates x , y and z respectively. Then the hydraulic gradient components are:

$$J_x = -\frac{\partial h}{\partial x}, \quad J_y = -\frac{\partial h}{\partial y}, \quad J_z = -\frac{\partial h}{\partial z} \quad 2.9$$

in the x , y and z -directions.

When the flow takes place through a homogenous and isotropic medium, the coefficient K is a constant scalar, and the specific discharge in x , y and z -directions can be written as

$$q_x = KJ_x = -K \frac{\partial h}{\partial x} = nV_x \quad 2.10$$

$$q_y = KJ_y = -K \frac{\partial h}{\partial y} = nV_y \quad 2.11$$

$$q_z = KJ_z = -K \frac{\partial h}{\partial z} = nV_z \quad 2.12$$

Equations 2.10, 2.11 and 2.12 apply to non-homogenous (heterogeneous) medium where $K = K(x,y,z)$, as long as the medium is isotropic.

2.3 Hydraulic Conductivity

In an isotropic medium the hydraulic conductivity, K , may be defined as the specific discharge per unit hydraulic gradient. It is a scalar that expresses the ease with which a fluid is transported through porous matrix. It is, therefore, a coefficient which depends on both matrix and fluid properties. The relevant fluid properties are density, ρ , and dynamic viscosity, μ , (or in the combined form of kinematic viscosity, ν). The relevant solid matrix properties are mainly grain (or pore) size distribution, shape of grains (or pores), tortuosity, specific surface and porosity. The hydraulic conductivity may be expressed as

$$K = \frac{k\rho g}{\mu} = \frac{kg}{\nu} \quad 2.13$$

where k is permeability or intrinsic permeability of the porous matrix, which depends solely on properties of the solid matrix. Various formulas relating k to the various properties of the solid matrix are presented in the literature. Some of these formulas are purely empirical (Bear, 1979).

2.4 Non-Darcian Flow

Darcy's law postulates a linear relation between the macroscopic velocity and the hydraulic gradient. However, widely available experimental data, which have accumulated for many years, to justify the validity and applicability of Darcy's law

have helped to evolve a general consensus that there is an upper as well as a lower limit beyond which Darcy's linear law does not hold. Combining the works of various investigators over different velocities or Reynold's numbers, Re , (based on macroscopic velocity) zones, the shape of velocity gradient response for any type of soil over a wide range of velocities can be represented by *Figure 2.6*. Different zones of flow that are expected are demarcated in the same figure. The total flow regimes are divided into five zones and they are:

1. *No flow zone*: This zone is likely to exist only in case of dense porous media of high colloid content. In this zone, surface forces are strong enough to counteract a certain portion applied gradient called initial, limiting or threshold gradient and is denoted by J_0 .
2. *Non-Darcy prelinear laminar zone*: Any surface active porous media is likely to show this zone. The surface forces arising out of the solid-fluid interaction due to strong negative charges on the clay particle surfaces and dipolar nature of water molecules causes the velocity-gradient response to be nonlinear and thus non-Darcian. Various authors have suggested various forms of equations to describe the flow process in this zone.
3. *Darcian linear regime*: Almost all the natural soils exhibit this zone to a certain extent though the width of this zone may vary widely depending on the type of soil. In this zone the effect of surface forces is not felt, and the influence of inertial forces are negligibly small compared to viscous forces.
4. *Non-Darcy post-linear laminar zone*: This is the zone where flow is still laminar but a gradual increase in inertial force makes the flow deviate from Darcian linearity. Various available equations for this high velocity zone proposed by various authors.
5. *Non-Darcy post-linear turbulent zone*: Here, the onset of turbulence is first noted and the substantial part applied gradient becomes dissipated in overcoming the

inertial forces and consequently the rate of velocity gain is very much less compared to earlier regimes.

Recall that for all soils, all the flow zones previously mentioned may not exist. For clays, the existence of the last two zones is highly improbable whereas for sands and other coarse inert materials, the first two zones may not exist or may not be noticeable within the ordinary experimental accuracy. Moreover, neither any unified theory nor any consistent experimental data available for critical gradients or velocities demarcating different zones of flow mentioned.

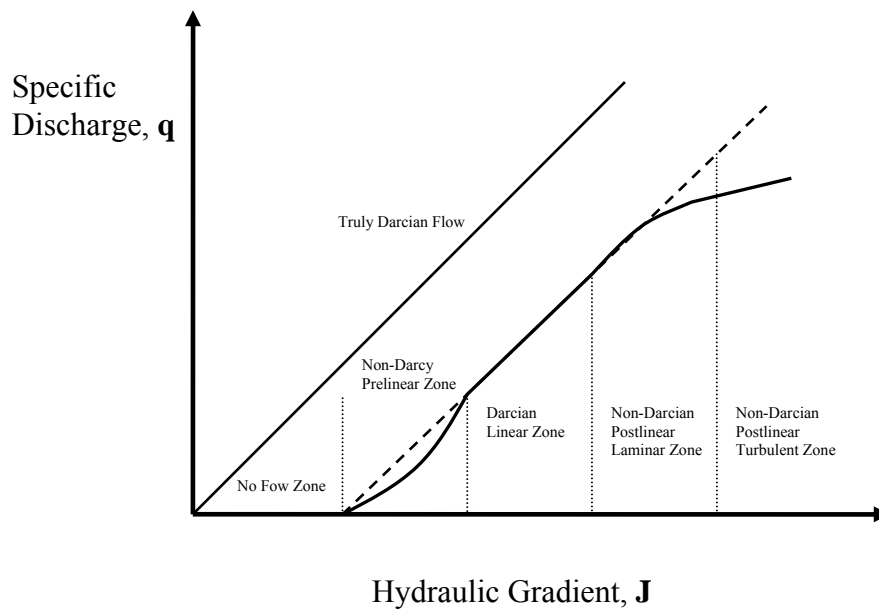


Figure 2.6: Probable velocity-gradient relationship over large range of velocity (Basak, 1975).

The preceding analysis points to the fact that while using Darcy's linearity for various field problems, one should be careful in interpreting and using the results in pre-linear and post-linear regime. If the published experimental velocity-gradient

response for the last few decades for clays and under low gradients is any indication of the actual state of affair, then the majority of flow problems in clayey, loamy and organic soils, as well as fine grained sandy deposits under low gradients, would be largely met by the preliminary regime.

So far as flow through coarse sand under medium to high gradient goes, it is more or less accepted that the flow is initially linear and, then, it enters into the post-linear regime. Thus, it seems to be necessity to have solutions of various seepage problems incorporating a velocity-gradient response representing all the flow zones mentioned. But, unfortunately, no general equation is available which gives the actual shape over the entire gradient range. A single equation covering the prelinear, linear and post-linear regimes is very much lacking. In this mitigating circumstance, one of the alternatives is to use Izbash's flow equation of the type:

$$q = MJ^m \tag{2.14}$$

which is one of the most widely used non-Darcy flow equations, the other being Forcheimer's equation (Basak, 1977) which reads:

$$J = aq + bq^2 \tag{2.15}$$

where M , m , a and b are constants and J is the hydraulic gradient (Basak, 1977).

Forcheimer's equation can be characterized as the empirical modification of Darcy's equation (Choi *et al.*, 1996).

2.5 Forcheimer's Equation

Forcheimer's equation is the equation most widely used to describe the non-Darcian flow. It can be presented in the vectorial form of *equation 2.15* as:

$$\vec{\nabla}h = -F(q)\vec{q} \quad 2.16$$

where $\vec{\nabla}$ is gradient operator and \vec{q} is the specific discharge vector. Furthermore:

$$F(q) = a + bq \quad 2.17$$

where $F(q)$ is a scalar function of the magnitude of the specific discharge vector at any point, a and b are the Forcheimer parameters and q is the magnitude of the specific discharge vector:

$$q = \sqrt{q_x^2 + q_y^2 + q_z^2} \quad 2.18$$

where q_x , q_y and q_z are the components of the specific discharge vector in the x , y and z -directions respectively.

For one-dimensional flow in the x -direction, using q for q_x , the Forcheimer's equation takes the form:

$$-\frac{dh}{dx} = aq + bq^2 \quad 2.19$$

or

$$-\frac{dh}{dx} = F(q)q \quad 2.20$$

Note that *equations 2.19* and *2.20* are same as *equation 2.15* with $J = -\frac{dh}{dx}$.

Obviously, when $b=0$, both *equation 2.19* and *equation 2.20* become identical with Darcy's law:

$$q = -\frac{1}{a} \frac{dh}{dx} \tag{2.21}$$

Basak (1976) has presented the reported values for Forcheimer parameters a and b for sand and gravel. Bordier and Zimmer (2000) also tabulated Forcheimer parameters for gravel, geonet and geo-composite materials. Venkataraman *et al.* (1998) summarized the published data on the properties of porous media, i.e. particle size, porosity, intrinsic permeability and the nonlinear parameter, b .

Venkataraman *et al.* (1998) assumed that the linear parameter, a , depends upon the fluid properties and intrinsic permeability, k , on the other hand, the non-linear parameter b is dependent upon the media properties such as size and shape of the media and porosity. They summarized the published data on properties of porous media. The list of parameters is presented in *Appendix D* in *Table D.1*.

Given that the non-linear parameter b of a fractured medium should be much greater than that of the large sized porous media, it should be greater than the maximum value of in the Venkataraman's list which is almost $1 \cdot 10^{-3} \text{ m}^2/\text{day}^2$. Then, it would be appropriate to assume that b is $O(10^{-2})$ for fractured aquifers.

When the quadratic part is discarded, Forcheimer's equation turns into Darcy's linear model. Therefore, a is the reciprocal of the hydraulic conductivity, K .

$$a = \frac{1}{K} \quad \text{or} \quad K = \frac{1}{a} \tag{2.22}$$

Ward (1964) also obtained the same expression for a as a function of intrinsic permeability, dynamic viscosity and specific gravity.

2.6 Reynold's Number

Based on the previous studies, Venkatamaran *et. al.* (1998) defined the Reynold's number in porous media as:

$$R_e = \frac{q\sqrt{k}}{\nu} \quad 2.23$$

where R_e is the Reynold's number, q is the specific discharge, k is the intrinsic permeability and ν is the kinematic viscosity. This equation can be applied to fractured porous media as well.

Recalling that:

$$K = \frac{kg}{\nu} \quad \text{or} \quad k = \frac{K\nu}{g} \quad 2.13$$

Then,

$$R_e = q\sqrt{\frac{K}{g\nu}} \quad 2.24$$

2.7 Continuity Equation

In order to derive the continuity equation for flow the in a fractured porous medium, an elementary representative volume shown in *Figure 2.7* is considered. The representative elementary volume is large enough compared to the dimensions of the individual blocks and fractures to allow meaningful spatial averaging and yet small enough to characterize variations in reservoir properties at scales of interest (Huyakorn and Pinder, 1983). Furthermore, it consists of a sufficient number of blocks and fractures having random distribution, orientation and size.

In a pheratic aquifer, water is stored in the void spaces and an increase in storage is followed by a rise in the pheratic surface. On the other hand, in a confined aquifer, water is stored on account of water and solid matrix compressibility and, an increase in storage is followed by a rise in the piezometric head. The aquifer storativity could be introduced as the volume of water added to a unit horizontal area of an aquifer per unit rise in the piezometric head (Bear, 1979). Storativity is a property of a confined aquifer.

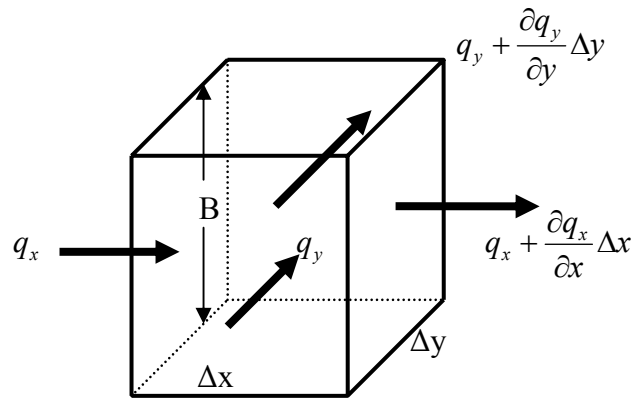


Figure 2.7: A representative elementary volume and flow components.

The continuity condition requires that the difference between all inflows and outflows should be equal to the water stored in or released from the representative elementary volume. Therefore, the continuity equation of the flow in the elementary volume can be written as:

$$-\left(\frac{\partial q_x}{\partial x} \Delta x \Delta y + \frac{\partial q_y}{\partial y} \Delta y \Delta x\right) B \Delta t = S \Delta x \Delta y \Delta h \quad 2.25$$

where q is the specific discharge, S is the storage coefficient, B is the depth of the elementary representative volume and h is the piezometric head.

Dividing both sides of *equation 2.25* by Δx , Δy , and Δt yields:

$$-B \left(\frac{\partial q_x}{\partial x} + \frac{\partial q_y}{\partial y} \right) = S \frac{\Delta h}{\Delta t} \quad 2.26$$

As Δt approaches to zero:

$$-B \left(\frac{\partial q_x}{\partial x} + \frac{\partial q_y}{\partial y} \right) = S \frac{\partial h}{\partial t} \quad 2.27$$

2.8 Governing Equations

For fractured porous media, the continuity of fluid flow both in the porous blocks and the fractures needs to be taken into consideration. Therefore, the continuity equation of the flow in the blocks can be written as:

$$-B \left(\frac{\partial q_{bx}}{\partial x} + \frac{\partial q_{by}}{\partial y} \right) = S_b \frac{\partial h_b}{\partial t} \quad 2.28$$

where the subscript, b , represents the blocks.

Assuming that Darcy's law is valid for the flow through the porous blocks and that the fractured medium is homogenous and isotropic, i.e., K is constant, then the specific discharge equations for the blocks in the x and y -directions can be written as $q_{bx} = -K_b \frac{\partial h_b}{\partial x}$ and $q_{by} = -K_b \frac{\partial h_b}{\partial y}$ respectively. When these equations are introduced into *equation 2.28*, the mass balance equation for the blocks is obtained:

$$BK_b \left(\frac{\partial^2 h_b}{\partial x^2} + \frac{\partial^2 h_b}{\partial y^2} \right) = S_b \frac{\partial h_b}{\partial t} \quad 2.29$$

For one-dimensional flow through the blocks:

$$BK_b \frac{\partial^2 h_b}{\partial x^2} = S_b \frac{\partial h_b}{\partial t} \quad 2.30$$

On the other hand, the continuity equation to the flow through the fractures can be written as:

$$-B \left(\frac{\partial q_{fx}}{\partial x} + \frac{\partial q_{fy}}{\partial y} \right) = S_f \frac{\partial h_f}{\partial t} \quad 2.31$$

where the subscript, f , represents the fractures.

For the non-Darcian fracture flow, *equation 2.27* should be modified by replacing Darcy's law with Forcheimer's equation .

Recall that Forcheimer's equation in vectorial form is *equation 2.16*:

$$\vec{\nabla} h = -F(q)\vec{q} \quad 2.16$$

or

$$\vec{q} = -\frac{1}{F(q)} \vec{\nabla} h \quad 2.16$$

If the derivative of *equation 2.16* is taken with respect to x and y , then *equations 2.31* and *2.32* are obtained:

$$\frac{\partial q_{fx}}{\partial x} = -\frac{\partial}{\partial x} \left[\frac{1}{F(q)} \left(\frac{\partial h_f}{\partial x} \right) \right] \quad 2.31$$

$$\frac{\partial q_{fy}}{\partial y} = -\frac{\partial}{\partial y} \left[\frac{1}{F(q)} \left(\frac{\partial h_f}{\partial y} \right) \right] \quad 2.32$$

Recalling that $F(q)$ is a function of space variables, the fractured medium is assumed to be homogenous and isotropic in order to eliminate the non-linearity in equations 2.31 and 2.32. Therefore:

$$F(q) = f(x, y) \quad 2.33$$

Note that Choi *et al.* (1996) also made same assumption.

Then, equations 2.31 and 2.32 take the form:

$$\frac{\partial q_{fx}}{\partial x} = -\frac{1}{F(q)} \left(\frac{\partial^2 h_f}{\partial x^2} \right) \quad 2.34$$

$$\frac{\partial q_{fy}}{\partial y} = -\frac{1}{F(q)} \left(\frac{\partial^2 h_f}{\partial y^2} \right) \quad 2.35$$

When equations 2.34 and 2.35 are introduced into the equation 2.29, the non-Darcian continuity equation for the fractures is obtained.

$$\frac{B}{F(q)} \left(\frac{\partial^2 h_f}{\partial x^2} + \frac{\partial^2 h_f}{\partial y^2} \right) = S_f \frac{\partial h_f}{\partial t} \quad 2.36$$

For one-dimensional fracture flow:

$$\frac{B}{F(q)} \frac{\partial^2 h_f}{\partial x^2} = S_f \frac{\partial h_f}{\partial t} \quad 2.37$$

According to the double-porosity conceptual model, fluid transfer between the porous blocks and the fractures should be taken into consideration. In this regard, the fluid transfer rate between the blocks and fractures v_d should be added to *equations 2.30 and 2.37*:

$$BK_b \frac{\partial^2 h_b}{\partial x^2} = S_b \frac{\partial h_b}{\partial t} - v_d \quad 2.38$$

$$\frac{B}{F(q)} \frac{\partial^2 h_f}{\partial x^2} = S_f \frac{\partial h_f}{\partial t} + v_d \quad 2.39$$

Notice that the signs of the fluid transfer rate term in *equations 2.38 and 2.39* are different, which means that flow occurs between fractures and blocks according to the pressure difference between these two media.

Equations 2.38 and 2.39 are valid under the assumptions that:

- Darcy's law is valid for the flow in the blocks.
- The flow in the fractures is non-Darcian and governed by Forcheimer's equation.
- Fractures and blocks are homogenous and isotropic.
- The aquifer is confined and non-leaky.
- Depth of the aquifer is constant.
- Flow occurs only in x -direction.
- The geometry of fractures is unaffected by chemical dissolution or deposition.
- The flow is fully saturated.

2.9 Fluid Transfer Rate

For the flow in a fractured medium, fracture-matrix interactions, in other words the exchange of water between fractures and blocks, can be handled with the double-porosity model which is presented in the existing literature (Barenblatt *et al.*, 1960, Warren and Root, 1963, Önder, 1998 and Wu, 2002b). The double-porosity model relies on quasi-steady-state flow assumption to account for fracture-matrix interflow (Wu, 2002b). The transfer of water between the blocks and the fractures occurs in quasi-steady state while the flow takes place through matrix blocks and the fractures. The rate of transfer depends on the pressure difference between blocks and fractures as well as the geometry and other properties of the fractured medium. The fluid transfer rate v_d can be expressed as:

$$v_d = \xi \Delta p \tag{2.40}$$

where ξ is the interaction term which incorporates the geometry as well as other properties of the aquifer and Δp is the pressure difference. If the interaction term is written in terms of piezometric head difference:

$$v_d = \xi \gamma_s \Delta h \tag{2.41}$$

where γ_s is the specific weight of the fluid.

It could be interpreted that v_d is the volume of water transfer per unit horizontal area per unit time. Önder (1998) defined the fluid transfer rate as:

$$v_d = \varepsilon T_b (h_f - h_b) \tag{2.42}$$

where $\xi = \frac{\varepsilon T_b}{\gamma_s}$, ε is the fluid transfer parameter and T_b is the transmissivity of blocks

which can be defined as:

$$T_b = BK_b \quad 2.43$$

Note that there is no specific reference to fracture and block geometries in *equation 2.42*, therefore this equation is consistent with the continuum theory that assumes no specific knowledge at the sub-continuum level.

On the other hand, several researchers have suggested various fluid transfer parameters considering the geometry block and fracture geometries. For example, Warren and Root (1963) suggested:

$$\xi = \frac{\alpha_T k_b}{\mu} \quad 2.44$$

where α_T is the shape factor, μ is the dynamic viscosity of the fluid and k_b is the permeability of the matrix. For a rectangular matrix, the shape factor can be described as:

$$\alpha_T = 8 \left(\frac{1}{L_x^2} + \frac{1}{L_y^2} + \frac{1}{L_z^2} \right) \quad 2.45$$

where L_x , L_y and L_z are the dimensions of the rectangular matrix in the x , y , and z -directions respectively.

James and Lee (1977) also suggested:

$$\xi = \frac{\alpha_T}{\mu} \quad 2.46$$

and

$$\alpha_T = 4 \frac{k_b n_f \rho}{\pi c l} \quad 2.47$$

where k_b is the permeability of the blocks, n_f is the porosity of the fractures, ρ is the density of the fluid, c is the half length of the fracture width and l is the half length of the fractures and blocks in contact.

In this study, *equation 2.42* is used to calculate the fluid transfer rate between fractures and blocks.

2.10 Initial and Boundary Conditions

The idealized version of the flow system depicted in *Figure 1.1* is shown in *Figure 2.8*.

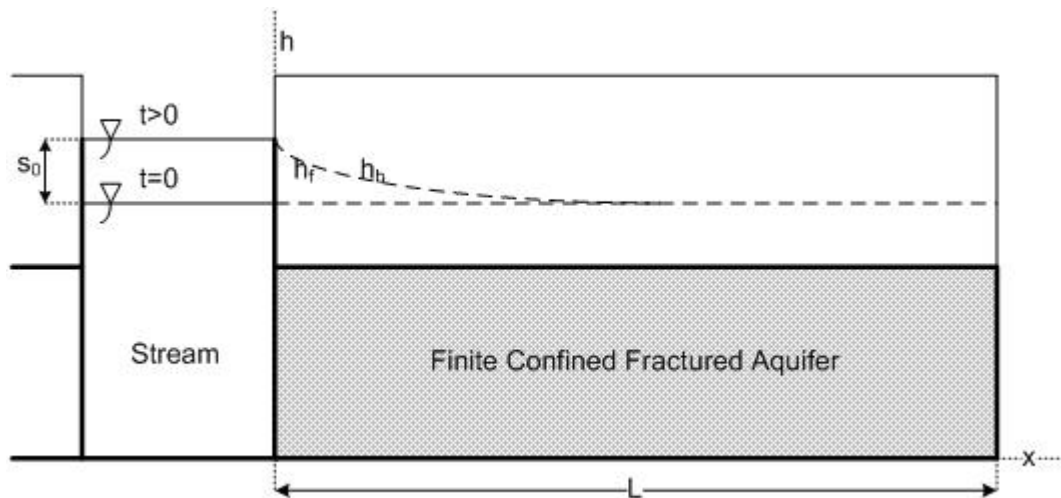


Figure 2.8: Idealized flow system (Önder, 1998).

The stream boundary condition is arranged for a sudden rise in the stream level. The stage hydrograph which represents this special case is also presented in *Figure 2.9*.



Figure 2.9: Stage hydrograph for a sudden rise in the stream level.

The initial and boundary conditions to be satisfied by the piezometric head for the fractures and the piezometric head for the blocks are:

$$h_b = h_0 \quad 0 \leq x \leq L \quad t = 0 \quad 2.48$$

$$h_f = h_0 \quad 0 \leq x \leq L \quad t = 0 \quad 2.49$$

$$h_b = h_0 + s_0 \quad x = 0 \quad t > 0 \quad 2.50$$

$$h_f = h_0 + s_0 \quad x = 0 \quad t > 0 \quad 2.51$$

$$\frac{\partial h_b}{\partial x} = 0 \quad x = L \quad t > 0 \quad 2.52$$

$$\frac{\partial h_f}{\partial x} = 0 \quad x = L \quad t > 0 \quad 2.53$$

where h_o is the initial piezometric head, s_o is the change in the stream stage and L is the length of the aquifer.

2.11 Governing Equations Presented by Önder (1998) for the Same Problem

Önder (1998) studied the same problem. Assuming that Darcy's law is valid for the flow in blocks as well as in fractures, he derived governing equations for the fracture and block flows as follows:

$$BK_b \frac{\partial^2 h_b}{\partial x^2} = S_b \frac{\partial h_b}{\partial t} - v_d \quad 2.54$$

$$BK_f \frac{\partial^2 h_f}{\partial x^2} = S_f \frac{\partial h_f}{\partial t} + v_d \quad 2.55$$

Notice that *equation 2.54* is the same as *equation 2.38*.

Based on the previous studies of Barenblatt *et al.* (1960) and Warren and Root (1963), Önder (1998) stated that the conducting capability of the blocks is much less important than their storage capability in general. The aquifer data presented in the literature show that fracture conductivity is much greater (10^3 times or more) than the block conductivity and the storage coefficient of blocks is usually equal or ten times greater than the storage coefficient of fractures. Therefore, the term $BK_b \frac{\partial^2 h_b}{\partial x^2}$ can be neglected compared to the term $S_b \frac{\partial h_b}{\partial t}$ in *equation 2.54*.

Then:

$$v_d = S_b \frac{\partial h_b}{\partial t} \quad 2.56$$

When *equation 2.56* is inserted into *equation 2.55*, a partial differential equation governing the flow in the fractured aquifer is obtained:

$$BK_f \frac{\partial^2 h_f}{\partial x^2} = S_f \frac{\partial h_f}{\partial t} + S_b \frac{\partial h_b}{\partial t} \quad 2.57$$

or

$$T_f \frac{\partial^2 h_f}{\partial x^2} = S_f \frac{\partial h_f}{\partial t} + S_b \frac{\partial h_b}{\partial t} \quad 2.58$$

where

$$T_b = BK_b \quad 2.43$$

Furthermore, Önder (1998) calculated the groundwater flow per unit length of the stream into the aquifer using Darcy's law as follows:

$$q = KJ = K \frac{dh}{dx} \quad 2.2$$

$$Q = Aq \quad 2.3$$

$$A = B \cdot 1 \quad 2.59$$

$$Q = B \cdot 1 \cdot K \frac{dh}{dx} \Big|_{x=0} \quad 2.60$$

$$T = BK \quad 2.61$$

$$Q = T \frac{dh}{dx} \Big|_{x=0} \quad 2.62$$

where Q is the time dependent flow rate, q is the specific discharge, B is the thickness of the aquifer, K is the conductivity and T is the transmissivity.

Flow from the stream into the blocks is:

$$Q_b = T_b \left. \frac{dh_b}{dx} \right|_{x=0} \quad 2.63$$

Flow from the stream into the fractures is:

$$Q_f = T_f \left. \frac{dh_f}{dx} \right|_{x=0} \quad 2.64$$

Then, the total flow is:

$$Q = T_b \left. \frac{dh_b}{dx} \right|_{x=0} + T_f \left. \frac{dh_f}{dx} \right|_{x=0} \quad 2.65$$

In *equation 2.65*, the flow from the stream into the blocks can be ignored. In view of the fact that the conducting capability of blocks as compared to that of fractures is negligibly small, this may be considered as a reasonable approximation. Therefore:

$$Q = T_f \left. \frac{dh}{dx} \right|_{x=0} \quad 2.66$$

Önder (1998) solved *equations 2.58* and *2.66* analytically by applying integral transformations successively with regard to the space and time variables. Finite Fourier sine transformation was used to replace the space derivative, while the time derivative was replaced through the application of the Laplace transformation.

CHAPTER 3

NUMERICAL SOLUTION OF THE PROBLEM

3.1 Non-Dimensionalization of the Governing Equations and Boundary Conditions

In order to non-dimensionalize the governing partial differential equations and the related initial and boundary conditions, the following dimensionless variables, which are similar to the variables presented by Streltsova (1975) and Önder (1998), may be defined as:

$$z_b = \frac{h_b - h_0}{s_0} \quad 3.1$$

$$z_f = \frac{h_f - h_0}{s_0} \quad 3.2$$

$$\lambda = \frac{x}{L} \quad 3.3$$

$$\theta = \frac{T_f t}{S_f L^2} \quad 3.4$$

The derivatives of these variables should be taken with respect to time and space for non-dimensionalization.

The space derivative of the dimensionless variable z_b is taken as:

$$z_b = \frac{h_b - h_0}{s_0} \quad 3.1$$

$$h_b = s_0 z_b + h_0 \quad 3.1.1$$

$$\partial h_b = s_0 \partial z_b \quad 3.1.2$$

$$\partial^2 h_b = s_0 \partial^2 z_b \quad 3.1.3$$

The space derivative of the dimensionless variable z_f is taken as:

$$z_f = \frac{h_f - h_0}{s_0} \quad 3.2$$

$$h_f = s_0 z_f + h_0 \quad 3.2.1$$

$$\partial h_f = s_0 \partial z_f \quad 3.2.2$$

$$\partial^2 h_f = s_0 \partial^2 z_f \quad 3.2.3$$

The space derivative of the dimensionless variable λ is taken as:

$$\lambda = \frac{x}{L} \quad 3.3$$

$$x = L\lambda \quad 3.3.1$$

$$\partial x = L\partial\lambda \quad 3.3.2$$

$$\partial^2 x = L\partial^2\lambda \quad 3.3.3$$

Finally, the time derivative of the dimensionless variable θ is taken as:

$$\theta = \frac{T_f t}{S_f L^2} \quad 3.4$$

$$t = \frac{S_f L^2 \theta}{T_f} \quad 3.4.1$$

$$\partial t = \frac{S_f L^2}{T_f} \partial \theta \quad 3.4.2$$

$$\partial^2 t = \frac{S_f L^2}{T_f} \partial^2 \theta \quad 3.4.3$$

When these derivative terms are inserted, the governing equations for the blocks and the fractures are transformed into non-dimensional form as follows:

For the blocks,

$$\frac{\partial^2 h_b}{\partial x^2} = \frac{\partial}{\partial x} \left(\frac{\partial h_b}{\partial x} \right) \quad 3.5$$

$$\frac{\partial^2 h_b}{\partial x^2} = \frac{\partial}{L \partial \lambda} \left(\frac{s_0 \partial z_b}{L \partial \lambda} \right) \quad 3.6$$

$$\frac{\partial^2 h_b}{\partial x^2} = \frac{s_0}{L^2} \frac{\partial^2 z_b}{\partial \lambda^2} \quad 3.7$$

$$\frac{\partial h_b}{\partial t} = \frac{s_0 \partial z_b}{\frac{S_f L^2}{T_f} \partial \theta} \quad 3.8$$

$$\frac{\partial h_b}{\partial t} = \frac{s_0 T_f}{S_f L^2} \frac{\partial z_b}{\partial \theta} \quad 3.9$$

$$BK_b \frac{\partial^2 h_b}{\partial x^2} = S_b \frac{\partial h_b}{\partial t} - \varepsilon T_b (h_f - h_b) \quad 2.38$$

$$BK_b \frac{s_0}{L^2} \frac{\partial^2 z_b}{\partial \lambda^2} = S_b \frac{s_0 T_f}{S_f L^2} \frac{\partial z_b}{\partial \theta} - \varepsilon T_b (z_f s_0 + h_0 - z_b s_0 - h_0) \quad 3.10$$

$$\frac{T_b}{L^2} s_0 \frac{\partial^2 z_b}{\partial \lambda^2} = \frac{S_b}{S_f} \frac{T_f}{L^2} s_0 \frac{\partial z_b}{\partial \theta} - \varepsilon T_b s_0 (z_f - z_b) \quad 3.11$$

$$\frac{T_b}{L^2} \frac{\partial^2 z_b}{\partial \lambda^2} = \frac{S_b}{S_f} \frac{T_f}{L^2} \frac{\partial z_b}{\partial \theta} - \varepsilon T_b (z_f - z_b) \quad 3.12$$

$$\frac{\partial^2 z_b}{\partial \lambda^2} = \frac{L^2}{T_b} \frac{S_b}{S_f} \frac{T_f}{L^2} \frac{\partial z_b}{\partial \theta} - \frac{L^2}{T_b} \varepsilon T_b (z_f - z_b) \quad 3.13$$

$$\frac{\partial^2 z_b}{\partial \lambda^2} = \frac{S_b}{S_f} \frac{T_f}{T_b} \frac{\partial z_b}{\partial \theta} - L^2 \varepsilon (z_f - z_b) \quad 3.14$$

For the fractures,

$$\frac{\partial^2 h_f}{\partial x^2} = \frac{\partial}{\partial x} \left(\frac{\partial h_f}{\partial x} \right) \quad 3.15$$

$$\frac{\partial^2 h_f}{\partial x^2} = \frac{\partial}{L \partial \lambda} \left(\frac{s_0 \partial z_f}{L \partial \lambda} \right) \quad 3.16$$

$$\frac{\partial^2 h_f}{\partial x^2} = \frac{s_0}{L^2} \frac{\partial^2 z_f}{\partial \lambda^2} \quad 3.17$$

$$\frac{\partial h_f}{\partial t} = \frac{s_0 \partial z_f}{S_f L^2} \frac{\partial \theta}{T_f} \quad 3.18$$

$$\frac{\partial h_f}{\partial t} = \frac{s_0 T_f}{S_f L^2} \frac{\partial z_f}{\partial \theta} \quad 3.19$$

$$\frac{B}{F(q)} \frac{\partial^2 h_f}{\partial x^2} = S_f \frac{\partial h_f}{\partial t} + \varepsilon T_b (h_f - h_b) \quad 2.39$$

$$\frac{B}{F(q)} \frac{s_0}{L^2} \frac{\partial^2 z_f}{\partial \lambda^2} = S_f \frac{s_0 T_f}{S_f L^2} \frac{\partial z_f}{\partial \theta} + \varepsilon T_b (z_f s_0 + h_0 - z_b s_0 - h_0) \quad 3.20$$

$$\frac{B}{F(q)} \frac{1}{L^2} s_0 \frac{\partial^2 z_f}{\partial \lambda^2} = \frac{T_f}{L^2} \frac{\partial z_f}{\partial \theta} s_0 + \varepsilon T_b s_0 (z_f - z_b) \quad 3.21$$

$$\frac{B}{F(q)} \frac{1}{L^2} \frac{\partial^2 z_f}{\partial \lambda^2} = \frac{T_f}{L^2} \frac{\partial z_f}{\partial \theta} + \varepsilon T_b (z_f - z_b) \quad 3.22$$

$$\frac{\partial^2 z_f}{\partial \lambda^2} = \frac{F(q)}{B} L^2 \frac{T_f}{L^2} \frac{\partial z_f}{\partial \theta} + \frac{F(q)}{B} L^2 \varepsilon T_b (z_f - z_b) \quad 3.23$$

$$\frac{\partial^2 z_f}{\partial \lambda^2} = \frac{F(q)}{B} T_f \frac{\partial z_f}{\partial \theta} + \frac{F(q)}{B} L^2 \varepsilon T_b (z_f - z_b) \quad 3.24$$

Non-dimensionalization of the initial and boundary conditions is simpler and as follows:

Initial conditions:

$$z_b(\lambda, 0) = 0 \quad 3.25$$

$$z_f(\lambda, 0) = 0 \quad 3.26$$

Boundary conditions at the stream side:

$$z_b(0, \theta) = 1 \quad 3.27$$

$$z_f(0, \theta) = 1 \quad 3.28$$

Boundary conditions at the impervious side:

$$\frac{\partial h_b}{\partial x} = 0 \quad 2.52$$

$$\frac{s_0 \partial z_b}{L \partial \lambda} = 0 \quad 3.29$$

$$\frac{\partial z_b}{\partial y} = 0 \quad 3.30$$

$$\frac{\partial h_f}{\partial x} = 0 \quad 2.53$$

$$\frac{s_0 \partial z_f}{L \partial \lambda} = 0 \quad 3.31$$

$$\frac{\partial z_f}{\partial \lambda} = 0 \quad 3.32$$

The dimensionless flow rate, Q_d , is defined similar to Önder (1998) as:

$$Q_d = \frac{QL}{s_0 T_f} \quad 3.33$$

3.2 Introductory Remarks for Numerical Solution

The non-dimensionalized partial differential *equations 3.14 and 3.24* correspond to the one-dimensional parabolic model *equation 3.34* except for the additional coupling term v_d . In the model equation, $u = u(x, t)$ is the dependent variable and ψ is a constant coefficient.

$$\frac{\partial u}{\partial t} = \psi \frac{\partial^2 u}{\partial x^2} \quad 3.34$$

The model equation may be solved numerically by the Generalized Trapezoidal method (Hirsch, 1989), in other words the Combined method. This method provides an implicit scheme which is second order accurate both in space and time, i.e. it has a temporal truncation error that is $O(\Delta t^2)$. To provide this accuracy, difference approximations are developed at the midpoint of the time increment. The computational molecule for this method is given in *Figure 3.1*.

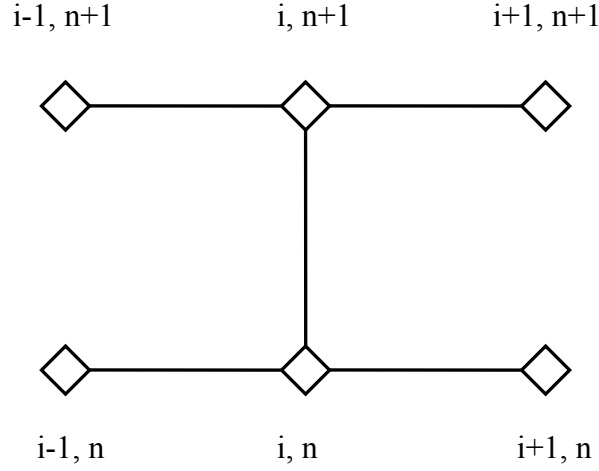


Figure 3.1: Computational molecule for Combined method.

In the model equation, the temporal first derivative on the left hand side can be approximated by first-order differencing as:

$$\frac{\partial u}{\partial t} = \frac{u_i^{n+1} - u_i^n}{\Delta t} \quad 3.35$$

The right hand side of the model equation is approximated with the average of central difference scheme evaluated at the current and the next time step.

$$\frac{\partial^2 u}{\partial x^2} = \left[\gamma \left(\frac{u_{i+1}^{n+1} - 2u_i^{n+1} + u_{i-1}^{n+1}}{\Delta x^2} \right) + (1 - \gamma) \left(\frac{u_{i+1}^n - 2u_i^n + u_{i-1}^n}{\Delta x^2} \right) \right] \quad 3.36$$

When these approximations are inserted into the model equation, the discretized form of the model equation is obtained.

$$\frac{u_i^{n+1} - u_i^n}{\Delta t} = \psi \left[\gamma \left(\frac{u_{i+1}^{n+1} - 2u_i^{n+1} + u_{i-1}^{n+1}}{\Delta x^2} \right) + (1 - \gamma) \left(\frac{u_{i+1}^n - 2u_i^n + u_{i-1}^n}{\Delta x^2} \right) \right] \quad 3.37$$

The Combined method is equivalent to:

- the simple explicit method when $\gamma = 0$
- the simple implicit method when $\gamma = 1$
- the Crank-Nicolson method when $\gamma = \frac{1}{2}$

The Combined method is convergent and unconditionally stable provided that $\frac{1}{2} < \gamma < 1$.

When $\gamma = \frac{1}{2}$ is inserted in *equation 3.37*, the Crank-Nicolson implicit scheme is obtained.

$$\frac{u_i^{n+1} - u_i^n}{\Delta t} = \psi \left[\frac{1}{2} \left(\frac{u_{i+1}^{n+1} - 2u_i^{n+1} + u_{i-1}^{n+1}}{\Delta x^2} \right) + \frac{1}{2} \left(\frac{u_{i+1}^n - 2u_i^n + u_{i-1}^n}{\Delta x^2} \right) \right] \quad 3.38$$

Notice that the dependent variable u from time step $n+1$ and time step n appear on the right hand side. *Equation 3.38* is used to predict the values of u at time $n+1$, so that all values of u at time n are assumed to be known.

If there are N internal mesh points along each time row, then *equation 3.38* gives N simultaneous equations for N unknown values of u along the first time row in terms of known initial and boundary conditions. Similarly, $n=2$ expresses N unknown values of u along the second time row in terms of the calculated values along the first row and so on. Therefore, the Crank-Nicolson scheme necessitates the solution of a set of N simultaneous equations.

The modified equation of the Crank-Nicolson implicit scheme is (Neta, 2003):

$$u_t + \psi u_{xx} = \frac{\psi \Delta x^2}{12} u_{xxxx} + \left[\frac{1}{12} \psi^3 \Delta t^2 + \frac{1}{360} \psi \Delta x^4 \right] u_{xxxxx} + \dots \quad 3.39$$

The Crank-Nicolson scheme has purely dispersion error so that it is prone to oscillations.

3.3 Discretization of the Governing Equations

The non-dimensionalized partial differential *equation 3.14* governing the flow through the blocks is discretized by the Combined method as follows:

$$\frac{\partial^2 z_b}{\partial \lambda^2} = \frac{S_b}{S_f} \frac{T_f}{T_b} \frac{\partial z_b}{\partial \theta} - L^2 \varepsilon(z_f - z_b) \quad 3.14$$

$$\frac{\partial z_b}{\partial \theta} = \frac{S_f}{S_b} \frac{T_b}{T_f} \frac{\partial^2 z_b}{\partial \lambda^2} + \frac{S_f}{S_b} \frac{T_b}{T_f} L^2 \varepsilon(z_f - z_b) \quad 3.40$$

$$\begin{aligned} \frac{zb_i^{n+1} - zb_i^n}{\Delta \theta} &= \frac{S_f}{S_b} \frac{T_b}{T_f} \frac{1}{\Delta \lambda^2} \left[\gamma (zb_{i+1}^{n+1} - 2zb_i^{n+1} + zb_{i-1}^{n+1}) \right. \\ &\quad \left. + (1-\gamma)(zb_{i+1}^n - 2zb_i^n + zb_{i-1}^n) \right] \\ &+ \frac{S_f}{S_b} \frac{T_b}{T_f} L^2 \varepsilon(zf_i^n - zb_i^n) \end{aligned} \quad 3.41$$

$$\begin{aligned} zb_i^{n+1} - zb_i^n &= \frac{S_f}{S_b} \frac{T_b}{T_f} \frac{\Delta \theta}{\Delta \lambda^2} \left[\gamma (zb_{i+1}^{n+1} - 2zb_i^{n+1} + zb_{i-1}^{n+1}) \right. \\ &\quad \left. + (1-\gamma)(zb_{i+1}^n - 2zb_i^n + zb_{i-1}^n) \right] \\ &+ \Delta \theta \frac{S_f}{S_b} \frac{T_b}{T_f} L^2 \varepsilon(zf_i^n - zb_i^n) \end{aligned} \quad 3.42$$

$$\begin{aligned} zb_i^{n+1} - \frac{S_f}{S_b} \frac{T_b}{T_f} \frac{\Delta \theta}{\Delta \lambda^2} \gamma (zb_{i+1}^{n+1} - 2zb_i^{n+1} + zb_{i-1}^{n+1}) &= \\ zb_i^n + \frac{S_f}{S_b} \frac{T_b}{T_f} \frac{\Delta \theta}{\Delta \lambda^2} (1-\gamma)(zb_{i+1}^n - 2zb_i^n + zb_{i-1}^n) & \\ + \Delta \theta \frac{S_f}{S_b} \frac{T_b}{T_f} L^2 \varepsilon(zf_i^n - zb_i^n) & \end{aligned} \quad 3.43$$

$$\begin{aligned}
& - \left(\frac{S_f T_b \Delta \theta}{S_b T_f \Delta \lambda^2} \gamma \right) z b_{i+1}^{n+1} + \left(1 + \frac{S_f T_b \Delta \theta}{S_b T_f \Delta \lambda^2} 2\gamma \right) z b_i^{n+1} \\
& - \left(\frac{S_f T_b \Delta \theta}{S_b T_f \Delta \lambda^2} \gamma \right) z b_{i-1}^{n+1} \\
& = z b_i^n + \frac{S_f T_b \Delta \theta}{S_b T_f \Delta \lambda^2} (1 - \gamma) (z b_{i+1}^n - 2z b_i^n + z b_{i-1}^n) \\
& + \Delta \theta \frac{S_f T_b}{S_b T_f} L^2 \varepsilon (z f_i^n - z b_i^n)
\end{aligned} \tag{3.44}$$

Equation 3.44 can be expressed in the form of equation 3.45:

$$- A_i^n z b_{i+1}^{n+1} + B_i^n z b_i^{n+1} - C_i^n z b_{i-1}^{n+1} = D_i^n \tag{3.45}$$

$$A_i^n = \left(\frac{S_f T_b \Delta \theta}{S_b T_f \Delta \lambda^2} \gamma \right) \tag{3.46}$$

$$B_i^n = \left(1 + \frac{S_f T_b \Delta \theta}{S_b T_f \Delta \lambda^2} 2\gamma \right) \tag{3.47}$$

$$C_i^n = \left(\frac{S_f T_b \Delta \theta}{S_b T_f \Delta \lambda^2} \gamma \right) \tag{3.48}$$

$$\begin{aligned}
D_i^n & = z b_i^n + \frac{S_f T_b \Delta \theta}{S_b T_f \Delta \lambda^2} (1 - \gamma) (z b_{i+1}^n - 2z b_i^n + z b_{i-1}^n) \\
& + \Delta \theta \frac{S_f T_b}{S_b T_f} L^2 \varepsilon (z f_i^n - z b_i^n)
\end{aligned} \tag{3.49}$$

The non-dimensionalized partial differential equation 3.24 governing non-Darcian flow through the fractures is discretized by the Combined method as follows:

$$\frac{\partial^2 z_f}{\partial \lambda^2} = \frac{F(q)}{B} T_f \frac{\partial z_f}{\partial \theta} + \frac{F(q)}{B} L^2 \varepsilon T_b (z_f - z_b) \quad 3.24$$

$$\frac{\partial z_f}{\partial \theta} = \frac{B}{F(q)} \frac{1}{T_f} \frac{\partial^2 z_f}{\partial \lambda^2} + \frac{L^2 \varepsilon T_b}{T_f} (z_b - z_f) \quad 3.50$$

$$\begin{aligned} \frac{z_f^{n+1} - z_f^n}{\Delta \theta} &= \frac{B}{F(q)_i^n} \frac{1}{T_f} \frac{1}{\Delta \lambda^2} \left[\gamma (z_{i+1}^{n+1} - 2z_i^{n+1} + z_{i-1}^{n+1}) \right. \\ &\quad \left. + (1-\gamma)(z_{i+1}^n - 2z_i^n + z_{i-1}^n) \right] \\ &\quad - \frac{L^2 \varepsilon T_b}{T_f} (z_i^n - z b_i^n) \end{aligned} \quad 3.51$$

$$\begin{aligned} z_f^{n+1} - z_f^n &= \frac{B}{F(q)_i^n} \frac{1}{T_f} \frac{\Delta \theta}{\Delta \lambda^2} \left[\gamma (z_{i+1}^{n+1} - 2z_i^{n+1} + z_{i-1}^{n+1}) \right. \\ &\quad \left. + (1-\gamma)(z_{i+1}^n - 2z_i^n + z_{i-1}^n) \right] \\ &\quad - \frac{L^2 \varepsilon T_b}{T_f} \Delta \theta (z_i^n - z b_i^n) \end{aligned} \quad 3.52$$

$$\begin{aligned} z_f^{n+1} - \frac{B}{F(q)_i^n} \frac{1}{T_f} \frac{\Delta \theta}{\Delta \lambda^2} \gamma (z_{i+1}^{n+1} - 2z_i^{n+1} + z_{i-1}^{n+1}) &= \\ z_f^n + \frac{B}{F(q)_i^n} \frac{1}{T_f} \frac{\Delta \theta}{\Delta \lambda^2} (1-\gamma)(z_{i+1}^n - 2z_i^n + z_{i-1}^n) & \\ - \frac{L^2 \varepsilon T_b}{T_f} \Delta \theta (z_i^n - z b_i^n) & \end{aligned} \quad 3.53$$

$$\begin{aligned} & - \left(\frac{B}{F(q)_i^n} \frac{1}{T_f} \frac{\Delta \theta}{\Delta \lambda^2} \gamma \right) z_{i+1}^{n+1} + \left(1 + \frac{B}{F(q)_i^n} \frac{1}{T_f} \frac{\Delta \theta}{\Delta \lambda^2} 2\gamma \right) z_i^{n+1} \\ & - \left(\frac{B}{F(q)_i^n} \frac{1}{T_f} \frac{\Delta \theta}{\Delta \lambda^2} \gamma \right) z_{i-1}^{n+1} \\ & = z_i^n + \frac{B}{F(q)_i^n} \frac{1}{T_f} \frac{\Delta \theta}{\Delta \lambda^2} (1-\gamma)(z_{i+1}^n - 2z_i^n + z_{i-1}^n) \\ & - \frac{L^2 \varepsilon T_b}{T_f} \Delta \theta (z_i^n - z b_i^n) \end{aligned} \quad 3.54$$

Note that in *equation 3.54*, z_f values at time step $n+1$ are calculated using the z_f values at time step n . Also, the scalar function $F(q)$ of Forcheimer's equation is evaluated at time step n . In this way, the non-linear *equation 3.24* is linearized.

Equation 3.54 can be expressed in the form of *equation 3.55*:

$$-A_i^n z_{f_{i+1}}^{n+1} + B_i^n z_{f_i}^{n+1} - C_i^n z_{f_{i-1}}^n = D_i^n \quad 3.55$$

$$A_i^n = \left(\frac{B}{F(q)_i^n} \frac{1}{T_f} \frac{\Delta\theta}{\Delta\lambda^2} \gamma \right) \quad 3.56$$

$$B_i^n = \left(1 + \frac{B}{F(q)_i^n} \frac{1}{T_f} \frac{\Delta\theta}{\Delta\lambda^2} 2\gamma \right) \quad 3.57$$

$$C_i^n = \left(\frac{B}{F(q)_i^n} \frac{1}{T_f} \frac{\Delta\theta}{\Delta\lambda^2} \gamma \right) \quad 3.58$$

$$D_i^n = z_{f_i}^n + \frac{B}{F(q)_i^n} \frac{1}{T_f} \frac{\Delta\theta}{\Delta\lambda^2} (1-\gamma)(z_{f_{i+1}}^n - 2z_{f_i}^n + z_{f_{i-1}}^n) - \frac{L^2 \varepsilon T_b}{T_f} \Delta\theta (z_{f_i}^n - z_{b_i}^n) \quad 3.59$$

Recall that when $\gamma = 1/2$, the Combined method is equivalent to the Crank-Nicolson scheme.

3.4 Calculation of the Scalar Function $F(q)$

Calculation of the scalar function $F(q)$ requires the calculation of the specific discharge q at all points in the solution domain. The specific discharge can be

defined by the Darcy's equation. In this regard, the procedure for the calculation of $F(q)$ is as follows:

$$-\frac{dh}{dx} = F(q)q \quad 2.20$$

$$F(q) = a + bq \quad 2.17$$

$$q = \sqrt{q_x^2 + q_y^2} \quad 2.18$$

$$q_y = 0 \quad 3.60$$

$$q = q_x \quad 3.61$$

$$q_x = -K \frac{dh}{dx} \quad 2.10$$

The spatial derivative in *equation 2.10* is replaced by the central finite difference approximation:

$$q_{xi}^n = -K \frac{h_{i+1}^n - h_{i-1}^n}{2\Delta x} \quad 3.62$$

The scalar function $F(q)$ at any point i in the solution domain at the current time step n can be written as:

$$F(q)_i^n = a + bq_{xi}^n \quad 3.63$$

The specific discharge should be calculated by using piezometric heads in fractures h_f , because non-Darcian flow takes place through the fractures.

$$F(q)_i^n = a - \frac{bK}{2\Delta x} (h_{f_{i+1}}^n - h_{f_{i-1}}^n) \quad 3.64$$

Since a is the reciprocal of the hydraulic conductivity, K :

$$K = \frac{1}{a} \quad 2.22$$

Thus, the discretized form of the Forcheimer's equation is:

$$F(q)_i^n = a - \frac{b}{2a\Delta x} (h_{f_{i+1}}^n - h_{f_{i-1}}^n) \quad 3.65$$

An alternative procedure for the calculation of the specific discharge, q , is as follows:

$$-\frac{dh}{dx} = aq + bq^2 \quad 2.19$$

where $q = q_x$.

Equation 2.19 can be written in the form of a quadratic equation as:

$$bq_x^2 + aq_x + \frac{dh}{dx} = 0 \quad 3.66$$

The roots of equation 3.66 are:

$$q_{x1,2} = \frac{-a \mp \sqrt{a^2 - 4b \frac{dh}{dx}}}{2b} \quad 3.67$$

The positive root gives the specific discharge:

$$q_x = \frac{-a + \sqrt{a^2 - 4b \frac{dh}{dx}}}{2b} \quad 3.68$$

The spatial derivative in *equation 3.68* can be replaced by the central finite difference approximation. Then,

$$q_{x,i} = \frac{-a + \sqrt{a^2 - 4b \frac{h_{i+1}^n - h_{i-1}^n}{2\Delta x}}}{2b} \quad 3.69$$

When *equation 3.69* is inserted into *equation 3.63*:

$$F(q)_i^n = a + b \frac{-a + \sqrt{a^2 - 2b \frac{h_{i+1}^n - h_{i-1}^n}{\Delta x}}}{2b} \quad 3.70$$

Then,

$$F(q)_i^n = \frac{1}{2} \left(a + \sqrt{a^2 - 2b \frac{h_{i+1}^n - h_{i-1}^n}{\Delta x}} \right) \quad 3.71$$

3.5 Discretization of the Boundary Conditions

The derivative boundary conditions at the impervious boundary, that are *equations 3.30* and *3.32*, are discretized by the backward finite difference approximation as follows:

For the blocks,

$$\frac{\partial z_b}{\partial \lambda} = 0 \quad 3.30$$

$$\frac{\partial z_b}{\partial \lambda} = \frac{zb_N^n - zb_{N-1}^n}{\Delta \lambda} = 0 \quad 3.72$$

$$zb_N^n = zb_{N-1}^n \quad 3.73$$

For the fractures,

$$\frac{\partial z_f}{\partial \lambda} = 0 \quad 3.32$$

$$\frac{\partial z_f}{\partial \lambda} = \frac{zf_N^n - zf_{N-1}^n}{\Delta \lambda} = 0 \quad 3.74$$

$$zf_N^n = zf_{N-1}^n \quad 3.75$$

3.6 Calculation of the Flow Rate from the Stream to the Aquifer

The rate of the flow per unit width from the stream to the aquifer can be calculated using Darcy's law.

$$q = -K \frac{dh}{dx} \quad 2.10$$

In a fractured aquifer whose depth is B , the total flow from the stream to the aquifer is:

$$Q = -BK \frac{dh}{dx} \quad 3.76$$

Equation 3.76 could be discretized using the forward difference approximation.

$$Q = -BK \frac{h_1^n - h_0^n}{\Delta x} \quad 3.77$$

where h_0 is the piezometric head at the stream boundary and h_1 is the piezometric head at the first internal mesh point.

Given that the rate of the flow in the fractures is much higher than in the blocks, it would be reasonable to assume that the flow rate into the aquifer is almost equal to the flow rate through the fractures. Therefore, in equation 3.77, $K = K_f$, or:

$$Q = -BK_f \frac{h_1^n - h_0^n}{\Delta x} \quad 3.78$$

Then,

$$Q = -T_f \frac{h_1^n - h_0^n}{\Delta x} \quad 3.79$$

3.7 Stability, Consistency and Convergence

This section and the following section shortly summarize the information on the basic concepts concerning numerical methods presented by Smith (1975), Andersen (1995), Hoffmann and Chiang (1993), Hirsch (1989) and Fletcher (1991).

The conditions that must be satisfied to ensure the solution of finite difference equations is reasonably accurate are the convergence of the exact solution of the approximating difference equations to the solution of the differential equation and the unbounded growth or uncontrolled decay of any errors associated with the solution of the finite difference equations.

Therefore, the convergence of finite difference equations approximating linear parabolic and hyperbolic equations can be investigated in terms of stability and consistency.

Stability is related to convergence through the concept of consistency and they together guarantee convergence.

A finite difference scheme is stable when the error remains bounded as time increases indefinitely. Given that the propagation of errors is the same as that of calculation of variables, the most fruitful way to define stability is in terms of the boundedness of the exact solution of the difference equations. For a stable finite difference scheme, local rounding errors and local truncation errors should not increase unboundedly with increasing time-levels of calculations.

If the local truncation error at any mesh point in the solution domain tends to zero as the mesh lengths tend to zero, the difference equation is said to be consistent with the partial differential equation. The real importance of the concept of consistency lies in a theorem by Lax which states that if a linear finite difference equation is consistent with a properly posed initial value problem, then stability guarantees convergence. A problem is posed if the solution is unique when it exists and depends continuously on the initial data.

Unique solution means having only one solution which is continuous throughout the solution domain and its boundary and has continuous partial derivatives in time and space.

If the solution of a partial differential equation exists and is unique, and if the solution depends continuously upon the initial and boundary conditions, then the problem is called well-posed. It is sometimes easy to attempt a solution using incorrect or insufficient initial and boundary conditions. Whether the solution being attempted analytically or numerically, such an ill-posed problem will usually lead to spurious results.

For initial value problems, any perturbation introduced in the solution domain at time $t=T$ will only be felt for times $t>T$. The future cannot influence the past. As a consequence, no boundary conditions may be imposed at time T . On the other hand, it is necessary to prescribe boundary conditions at $t=0$, i.e. the initial data. Because of the restricted zone of influence of perturbations, points in the solution domain are only coupled to the set of points which can influence them. This implies that the solution can be computed by advancing progressively (marching) in the domain. This is the characteristic of parabolic differential equations. All unsteady flows are described by initial value problems.

It is sometimes possible to approximate a parabolic or hyperbolic equation by a finite difference scheme that is stable but which has a solution that converges to the solution of a differential equation as the mesh lengths tend to zero. Such a difference scheme is said to be inconsistent or incompatible with the partial differential equation.

Given a properly posed linear initial value problem and a linear finite difference approximation to it that satisfies the consistency conditions, stability is the necessary and sufficient condition for convergence.

There are three standard methods for investigating the stability of the solution of the finite difference equations. In the first method, the equations are expressed in matrix form and eigen values of associated matrix are investigated. The second method, namely von Neuman method uses finite Fourier series and the third method is the discrete perturbation analysis.

3.8 Accuracy

Stability, consistency and convergence has been concerned with the behaviour of the approximate solution in the limit $\Delta t, \Delta x \rightarrow 0$. However, allowing the grid to converge to zero size may not be realizable in practice so that approximate solutions for real flow problems are obtained on a finite grid and the corresponding accuracy is of considerable importance. In this context, an important question concerning numerical solutions is under what circumstances they would coincide with the exact solution.

Stability analysis of finite difference equations provides insight into the limitation on grid size that is needed to obtain stable and accurate solutions. However, it would not be solely sufficient to determine the accuracy of the numerical solution of real problems.

One way of determining the accuracy of a particular algorithm on a finite grid is to apply it to a related but simplified problem, which possesses an exact solution. However, accuracy is also problem dependent, and an algorithm which is accurate for a model problem may not be so accurate for the (more complicated) problem of interest.

A second technique of accessing accuracy is to obtain solutions on successively refined grids (assuming the computing capacity is available) and to check that, with successive refinement, the solution is not changing to some predetermined accuracy. This assumes that the approximate solution will converge to the exact solution in the limit $\Delta t, \Delta x \rightarrow 0$ and that the approximate solution on the finest grid can be used in place of the exact solution. Since this is usually impossible to guarantee for real problems, it is useful to compare the computational solutions with reliable experimental data of known accuracy or available analytical solutions of the same problem. However, experimental data are usually not available in

sufficient detail to permit an evaluation of the global error of the solution Hoffmann and Chiang (1993).

Assuming that the accuracy of the approximate solution can be assessed, it is important to consider the related question of how the accuracy may be improved. At the broadest level, the answer to this question may lie in making a different choice for the dependent variables, e.g. vorticity and stream function instead of velocity and pressure. Alternatively, a different choice of independent variables may be appropriate. For example polar coordinates will produce more accurate solutions for pipe flow than Cartesian coordinates for the same number of grid points (Fletcher, 1991).

For explicit schemes, selection of step size is limited for stability requirement. On the other hand, implicit methods, which are unconditionally stable allow larger time steps. However, the accuracy requirement limits the use of large time steps, since an increase in time steps will increase the truncation errors introduced in the approximation process. It should also be noted that selecting very small step size ought to be avoided since the accuracy of the solution is dominated by round-off errors.

It should also be stressed that larger Δt means larger truncation error and the use of implicit methods to follow exact transients may not attain desired accuracy. However, for a time-dependent solution in which steady state is the desired result as in our problem, this relative time-wise accuracy is not important.

3.9 Discrete Perturbation Stability Analysis

Discrete perturbation stability analysis is a commonly used procedure for determining the stability requirements of finite difference equations. In this method, a disturbance is introduced at a point and its effect on neighbouring points is investigated. If the disturbance dies out as the solution proceeds, then the numerical

technique used is indeed stable. However, if the disturbance grows with the solution, the method is unstable (Hoffmann and Chiang, 1993).

To illustrate this analysis, the parabolic model equation (*equation 3.34*) is considered:

$$\frac{\partial u}{\partial t} = \psi \frac{\partial^2 u}{\partial x^2} \quad 3.34$$

where $u = u(x, t)$ is the dependent variable and ψ is a constant coefficient. An explicit finite difference equation discretized using second-order central differencing for the space derivative and first-order differencing for the time derivative as:

$$\frac{u_i^{n+1} - u_i^n}{\Delta t} = \psi \frac{u_{i+1}^n - 2u_i^n + u_{i-1}^n}{\Delta x^2} \quad 3.80$$

Assuming that a solution $u_i^n = 0$ at all i nodes obtained, a disturbance e_i^n is introduced at node i at time level n and the disturbance at time level $n+1$ at the node i is sought. Therefore,

$$\frac{(u_i^{n+1} + e_i^{n+1}) - (u_i^n + e_i^n)}{\Delta t} = \psi \frac{u_{i+1}^n - 2(u_i^n + e_i^n) + u_{i-1}^n}{\Delta x^2} \quad 3.81$$

Subtracting *equation 3.80* from *equation 3.81* produces:

$$\frac{e_i^{n+1} - e_i^n}{\Delta t} = \psi \frac{-2e_i^n}{\Delta x^2} \quad 3.82$$

Then,

$$e_i^{n+1} = e_i^n - 2\psi \frac{\Delta t}{\Delta x^2} e_i^n \quad 3.83$$

Hence,

$$\frac{e_i^{n+1}}{e_i^n} = 1 - 2\psi \frac{\Delta t}{\Delta x^2} \quad 3.84$$

In order to prevent its growing with the solution, the error must be bounded. For this purpose, the absolute value of error propagation is set to be less than or equal to 1 Hoffmann and Chiang (1993).

$$\left| \frac{e_i^{n+1}}{e_i^n} \right| \leq 1 \quad 3.85$$

Discrete perturbation stability analysis would also give an indication for selection of appropriate time step and grid size for numerical solutions to ensure accuracy.

CHAPTER 4

SOLUTION AND RESULTS

4.1 Basic Data and Solution Procedure

The finite difference equations for the fractures and the blocks were solved by a FORTRAN program according to initial and boundary conditions as well as the basic aquifer data taken from Önder (1998). The aquifer parameters are given in *Table 4.1*. These are also shown schematically in *Figure 4.1*. The flow chart of the FORTRAN program is presented in *Figure 4.2*. Furthermore, the text of the program is given in *Appendix A*.

Table 4.1: Aquifer parameters (Önder, 1998)

Width of aquifer, L	800 m
Thickness of aquifer, B	60 m
Initial piezometric head, h_0	65 m
Constant drawdown in stream, s_0	2 m
Transmissivity of fractures, T_f	280 m² /day
Transmissivity of blocks, T_b	1.75x10⁻² m² /day
Storage coefficient of fractures, S_f	1.4x10⁻⁷
Storage coefficient of blocks, S_b	1.4x10⁻⁶
Fluid transfer rate, ε	6.25x10⁻³ m⁻²

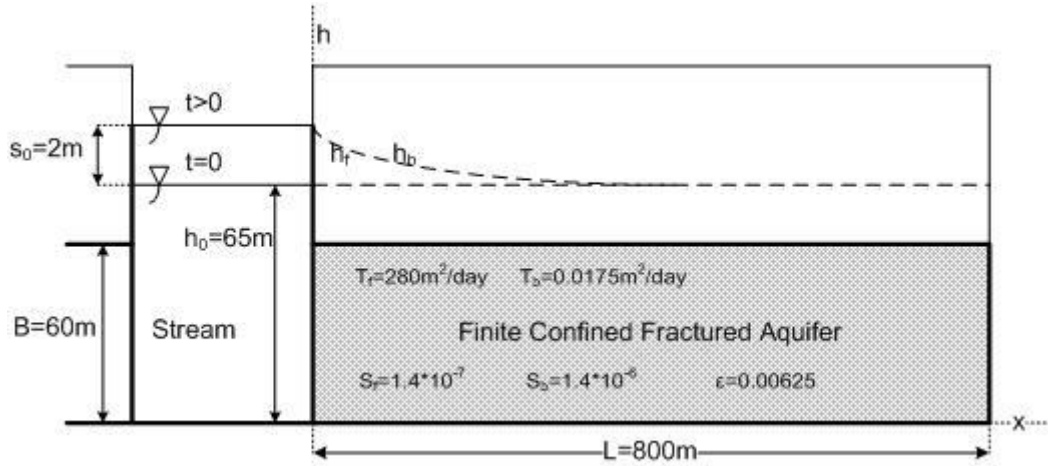


Figure 4.1: Schematic demonstration of the aquifer parameters.

It is assumed that the aquifer starts 5m below the average stream level.

Three dimensionless parameters, namely storativity contrast, conductivity contrast and diffusivity contrast were defined in order to evaluate better the effect of the aquifer parameters on the flow in the aquifer. These parameters were altered by changing the aquifer parameters in the calculations.

$$\text{Storativity contrast} \quad \eta = \frac{S_b}{S_f} \quad 4.1$$

$$\text{Conductivity contrast} \quad \kappa = \frac{T_b}{T_f} \quad 4.2$$

$$\text{Diffusivity contrast} \quad \delta = \frac{4\epsilon T_b S_f L^2}{T_f S_b} = 4\epsilon L^2 \frac{\kappa}{\eta} \quad 4.3$$

The dimensionless parameters as well as corresponding aquifer parameters on which computations were based are listed in *Table 4.2*.

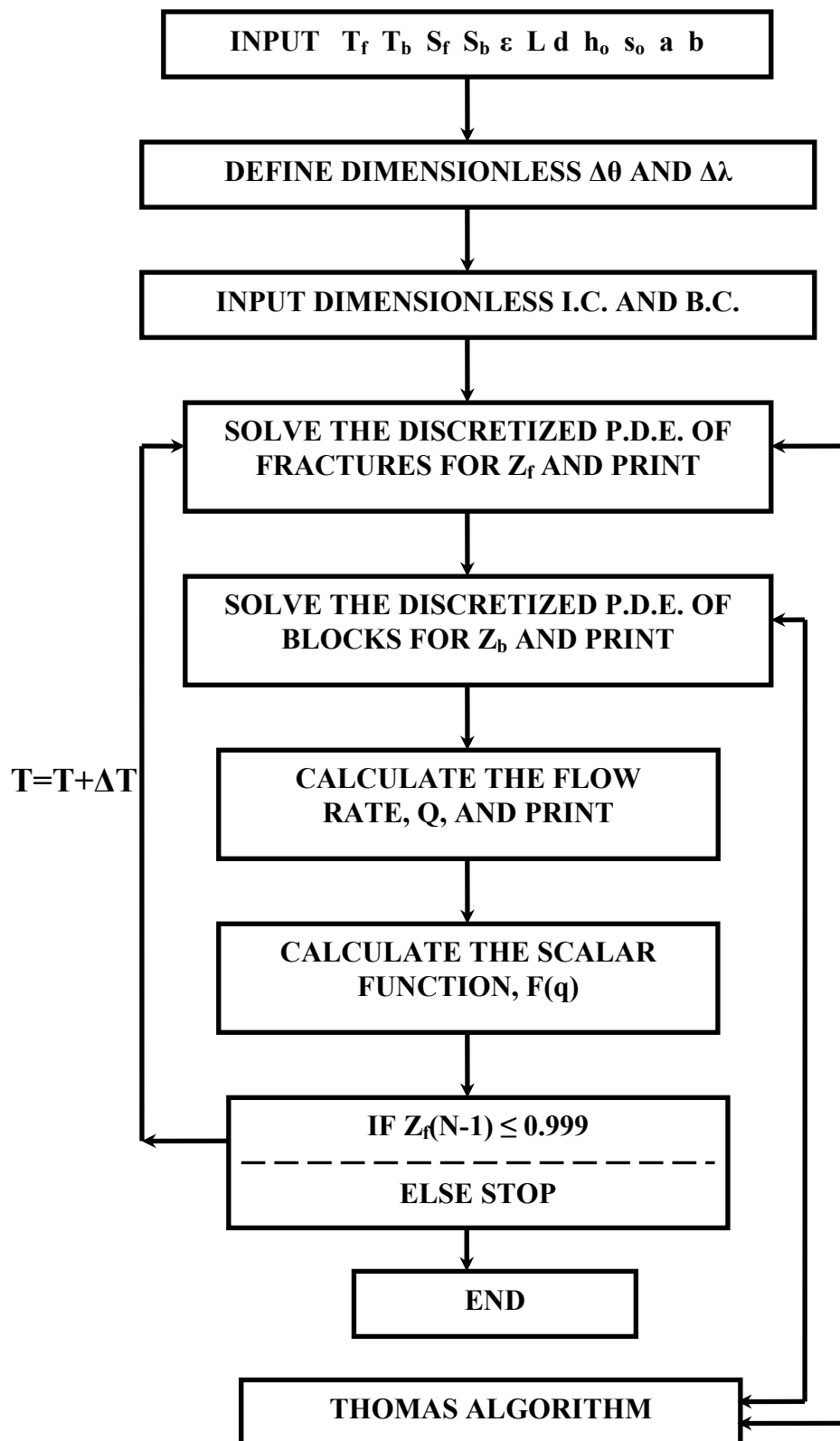


Figure 4.2: Flow chart of the computer program.

Another dimensionless parameter that accounts for the non-Darcian flow can also be defined. Wu (2002a) presented a dimensionless non-Darcy flow parameter β for fractured reservoirs. An analogous non-dimensional parameter β is derived for a strip fractured aquifer as the coefficient of $\frac{\partial z_f}{\partial \theta}$ in *equation 3.24*, i.e., $\frac{F(q)T_f}{B}$ is modified to a dimensionless non-Darcy flow parameter as:

$$\beta = \frac{F(q)T_f}{B} = 1 + \frac{b}{a}q \quad 4.4$$

As the specific discharge, q , in *equation 4.4* is a function of space and time (x and t), β is also a function of space and time. In order to define a representative dimensionless non-Darcian flow parameter which is independent of space and time, q in *equation 4.4* is arbitrarily replaced by a constant value given by $q_0 = K_f \frac{s_0}{L}$. Thus, the following expression is obtained:

$$\beta_0 = 1 + \frac{bs_0}{a^2L} \quad 4.5$$

In the solution of the governing equations, the actual value of β is used. In the presentation of the results where the objective was to explore the influence of non-Darcian flow, i.e., the influence of b , β_0 is used.

The linear parameter a of Forcheimer's equation, which is the reciprocal of hydraulic conductivity of the fractures, K_f , is obtained using *equation 2.22*.

In the numerical calculations, firstly the aquifer parameters are specified. Initially, there is no flow in the aquifer and the water levels in the stream and in the aquifer were assumed to be horizontal.

Table 4.2: Examples to the dimensionless parameters and related aquifer parameters which were used in the calculations

η	δ	κ	T_f <i>m²/day</i>	T_b <i>m²/day</i>	S_f	S_b	$a=1/K_f$ <i>day/ m</i>	ε <i>m⁻²</i>
1	10	$6.25*10^{-5}$	280	0.0175	$1.4*10^{-6}$	$1.4*10^{-6}$	0.215	0.0625
10	0	0	280	0	$1.4*10^{-7}$	$1.4*10^{-6}$	0.215	0.0625
10	1	$6.25*10^{-5}$	280	0.0175	$1.4*10^{-7}$	$1.4*10^{-6}$	0.215	0.0625
10	10	$6.25*10^{-5}$	280	0.0175	$1.4*10^{-7}$	$1.4*10^{-6}$	0.215	0.625
10	50	$3.125*10^{-4}$	56	0.175	$1.4*10^{-7}$	$1.4*10^{-6}$	0.86	0.0625
10	5	$3.125*10^{-5}$	56	0.0175	$1.4*10^{-7}$	$1.4*10^{-6}$	0.86	0.0625
10	100	$6.25*10^{-4}$	280	0.175	$1.4*10^{-7}$	$1.4*10^{-6}$	0.215	0.625
100	1	$6.25*10^{-4}$	280	0.175	$1.4*10^{-7}$	$1.4*10^{-5}$	0.215	0.625

The fluid transfer rate and the non-linear parameter b of the Forcheimer's equation are assumed as θ for calculations at the initial stage.

Then, a step rise is imposed as a boundary condition in the stream and the set of algebraic equations for the fractures and the blocks are solved successively by backward substitution, i.e. the Thomas algorithm. Therefore, dimensionless drawdowns for the fractures and the blocks with respect to dimensionless time and space are obtained and printed.

Calculation of the scalar function $F(q)$ requires the computation of the flow rate through the fractures. Dimensionless drawdowns in the fractures and in the blocks are converted to dimensional drawdowns in order to calculate the flow rate at all mesh points.

Given that *Equation 3.71* creates instability and gives inadequate results in calculation of the specific discharge, q , due to the step rise in the stream level which leads to very high hydraulic gradients at the initial stages of the computations, *equation 3.65*, which is based on Darcy's law, is used to calculate q in numerical simulations.

Having calculated the specific discharge, the scalar function $F(q)$ is evaluated at all mesh points and updated for the next step calculations. Finally, the rate of the flow from the stream to the aquifer and Reynold's number are calculated.

Simulations are terminated when the dimensionless drawdown in the fractures and in the blocks are very close to 1 (drawdown never exceeds 1) at all mesh points which indicates that a new steady-state condition is reached.

Solution of the dimensionless governing equations yields dimensionless drawdown in the fractures and in the blocks with respect to dimensionless time and space. Drawdown versus time and drawdown versus space curves can be constructed for various combinations of storativity, conductivity and diffusivity contrasts at certain dimensionless locations and times.

It is reasonable to assume that an observation well, screened over the depth of the formation, would intersect several fractures, so the observed drawdown in the aquifer would be that of the fractures (Barker, 1985 and Önder, 1998). Therefore, the drawdown in the matrix is unlikely to be of interest and the drawdown response of the aquifer is primarily analyzed and presented by the drawdown in the fractures.

In addition, the solution gives the dimensionless flow rate from the stream to the aquifer with respect to dimensionless time. Flow rate versus time curves can also be drawn for various combinations of storativity, conductivity and diffusivity contrasts.

4.2 Stability of the Finite Difference Equations of the Fractures and the Blocks

The discrete perturbation stability analysis was applied to the finite difference equations of the fractures and the blocks. The basic theory of this analysis is summarized in *Section 3.9* and the mathematical procedure for application is given in *Appendix B*.

A disturbance was introduced at a point i and its effect on neighbouring points have been investigated using a computer program. Calculations were based on the aquifer parameters presented in *Table 4.2* and carried out by the 80^{th} time step ($n=80$).

In order to evaluate the effect of time step and grid size on the stability and the accuracy of the numerical solution, calculations have been carried out for six different values α ($0.028, 0.5, 1, 2.09, 6.4$ and 25.6) which is defined as:

$$\alpha = \frac{\Delta\theta}{\Delta\lambda^2} \tag{4.6}$$

Figure 4.3 shows graphically the propagation of disturbance for the fractures when $\alpha=2.09$. It is apparent from the figure that the disturbance, e , is very close to 0 at all points except for the node i . The disturbance level at the node i is very close to 1 and dies out at the neighbouring points immediately. This situation does not change in time. The disturbance level decreases in time although it very small. Therefore, the stability condition which is *equation 3.85* is ensured.

Figure 4.4 gives the propagation of disturbance, e , for the blocks when $\alpha=0.5$. In this case, the disturbance at the node i is again very close to 1 and the disturbance at the nodes $i+1$ and $i-1$ is -0.447 . Then, the disturbance dies out at the neighbouring points similar to the fractures and this situation does not change in time.

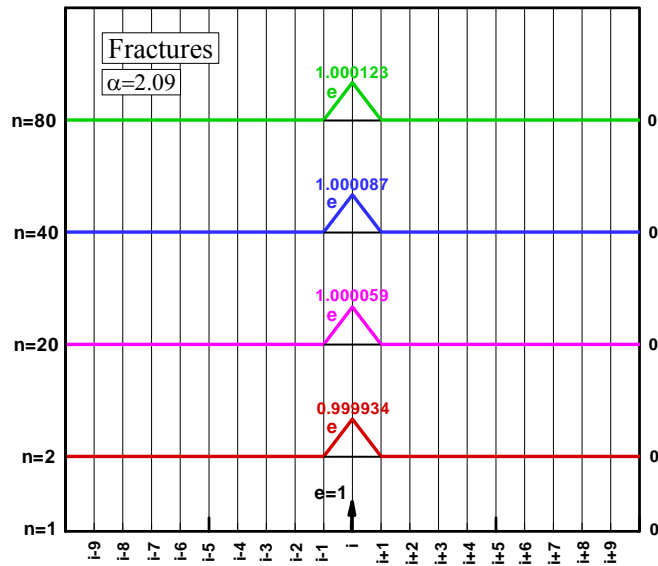


Figure 4.3: Graphical presentation of the results of the discrete perturbation stability analysis for the fractures when $\alpha=2.09$.

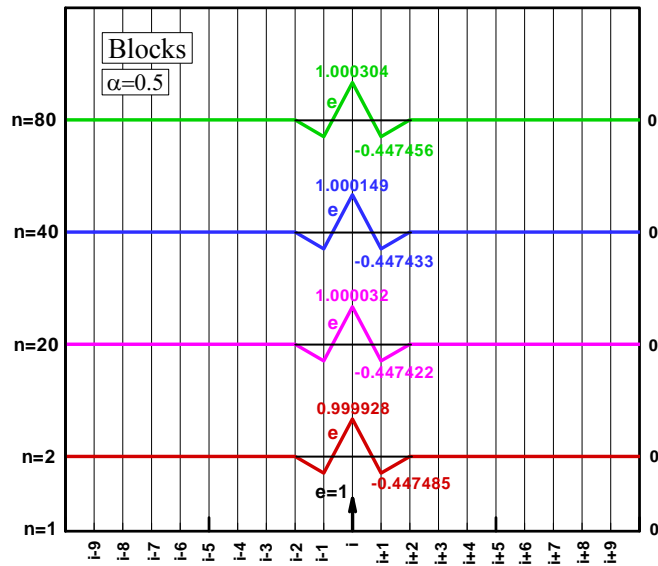


Figure 4.4: Graphical presentation of the results of the discrete perturbation stability analysis for the blocks when $\alpha=0.5$.

In addition, changing the aquifer parameters in the calculations does not affect significantly the disturbance level in the solution domain.

Two examples to the results of the discrete perturbation stability analysis, one for the fractures when $\alpha=1$ and the other for the blocks when $\alpha=0.028$, are presented in *Appendix F*.

The results of the discrete perturbation stability analysis show that the static stability is assured for the solution of the finite difference equations of the blocks and the fractures. However, the analysis has not given any indication for which value of α the numerical solution gives accurate results.

4.3 Comparison of the Numerical Solution with the Analytical Solution - Determination of Appropriate Step Size and Mesh Size

The discrete perturbation stability analysis showed that the numerical solution of the finite difference equations for the fractures and blocks are unconditionally stable for all values of $\Delta\theta$ and $\Delta\lambda$. Therefore, it is possible to solve the aforementioned equations by infinite number of α values without facing any stability problem and to obtain an infinite number of solutions.

In this regard, the accuracy of the solution is investigated by successive refinement of the mesh while fixing the time step. Changing α by successively decreasing $\Delta\lambda$ altered the results significantly and proved that this technique for determining accuracy is not applicable to the problem.

Following that, the accuracy of the numerical solution is elaborated by comparing its results against the results of the analytical solution to the same problem given by Önder (1998). In this comparison, two points are to be noted:

- The flow in the fractures is in non-Darcian regime in the present study.

- Based on the previous studies of Barenblatt *et al.* (1960), Warren and Root (1963), Streltsova and Adams (1978); Önder (1998) assumed that the conducting capability of the blocks is much less important than their storage capability, therefore the term $BK_b \frac{\partial^2 h_b}{\partial x^2}$ in equation 2.54 was neglected compared to term $S_b \frac{\partial h_b}{\partial t}$. The same assumption was also used by Wu (2002a) later. In the present study, this assumption is not used.

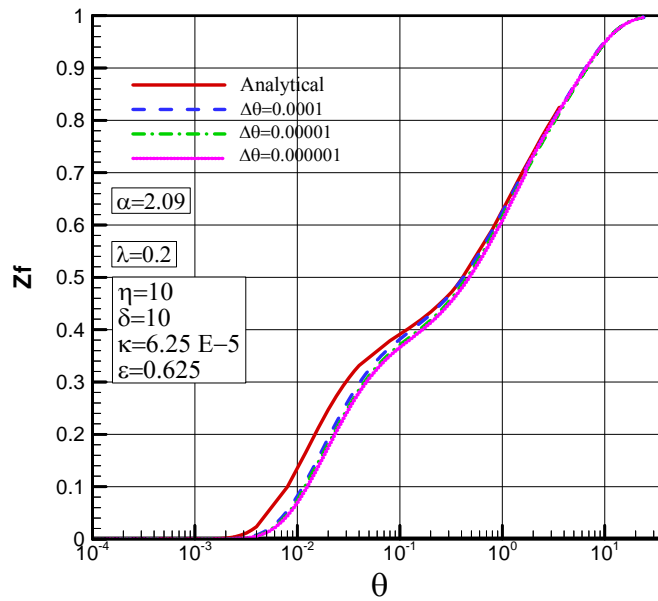


Figure 4.5: Z_f versus θ curves at $\lambda=0.2$ for $\alpha=2.09$ for different values of $\Delta\theta$ when $\alpha = 0.0022$, $\eta=10$, $\delta=5$ and $\kappa=6.25 \cdot 10^{-5}$.

Numerical calculations have been carried out for different values of $\Delta\theta$ and $\Delta\lambda$ for various storativity, conductivity and diffusivity contrasts. Then, dimensionless drawdown versus dimensionless time curves for the fractures were plotted at a dimensionless locations $\lambda = 0.2$, $\lambda = 0.4$ and $\lambda = 0.8$, and compared to the curves plotted using the available data from the analytical solution. In numerical calculations, the flow in the fractures assumed Darcian as in the analytical solution and, thus, the non-linear term of Forcheimer's equation, b , was taken as 0.

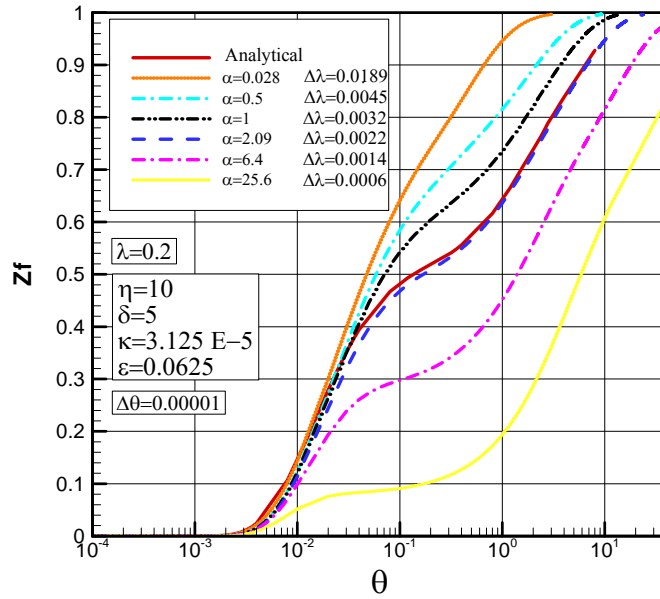


Figure 4.6: Z_f versus θ curves at $\lambda=0.2$ for different α values when $\eta=10$, $\delta=5$ and $\kappa=3.125*10^{-5}$.

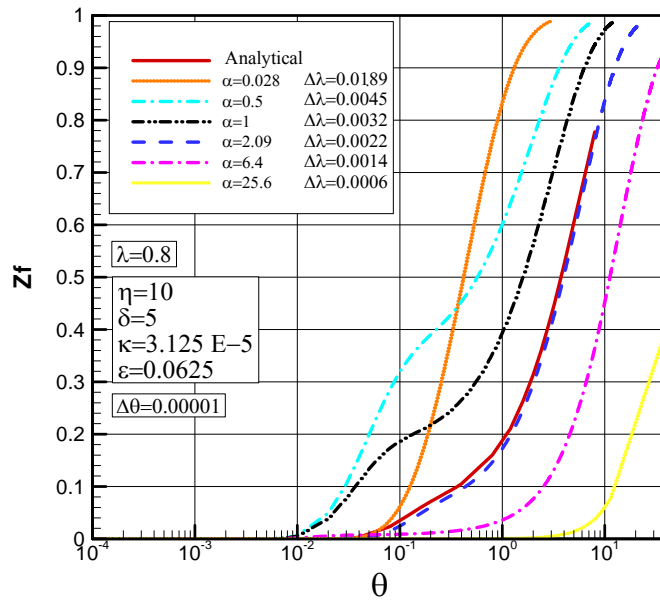


Figure 4.7: Z_f versus θ curves at $\lambda=0.8$ for different α values when $\eta=10$, $\delta=5$ and $\kappa=3.125*10^{-5}$.

Firstly, the effect of the time step on the solution is investigated considering that the stability and accuracy may be maintained over larger values of $\Delta\theta$ in implicit methods as explained in *Section 3.7*. To this end, numerical calculations were carried out for three different time steps, i.e. $\Delta\theta = 1*10^{-4}$, $1*10^{-5}$ and $1*10^{-6}$ while fixing α by playing with $\Delta\lambda$. Then, the results obtained are compared to each other and the analytical solution.

Figure 4.5 shows the effect of $\Delta\theta$ on the solution for the case $\eta=10$, $\delta=10$ and $\kappa=6.25*10^{-5}$. It is obvious from the figure that the change in $\Delta\theta$ has almost no effect on the numerical solution if α is fixed. Therefore, larger values of $\Delta\theta$ could be used to reduce the cost and time of calculations.

Then, the effect of α on the numerical solution has been investigated. For this case, $\Delta\theta$ is fixed to $1*10^{-5}$ and α is changed by changing $\Delta\lambda$. The results have been compared to the results of the analytical solution at dimensionless locations $\lambda = 0.2$, $\lambda = 0.4$ and $\lambda = 0.8$.

Figure 4.6 shows the case $\eta=10$, $\delta=5$ and $\kappa=3.125*10^{-5}$ at $\lambda = 0.2$. It is obvious from the figure that numerical and analytical solutions give similar results when $\alpha=2.09$. For this particular value of α , there is a slight difference between the curves of numerical and analytical solutions at early times, but the curves perfectly overlap at later times. The other values of α give very different results and their curves do not fit the analytical data.

For the same case but at $\lambda = 0.8$, as in *Figure 4.7*, the numerical and analytical solutions give very close results when $\alpha=2.09$. For this particular value of α , the difference between the curves of numerical and analytical solutions is very small even at early times. However, the difference is quite significant for the other values of α .

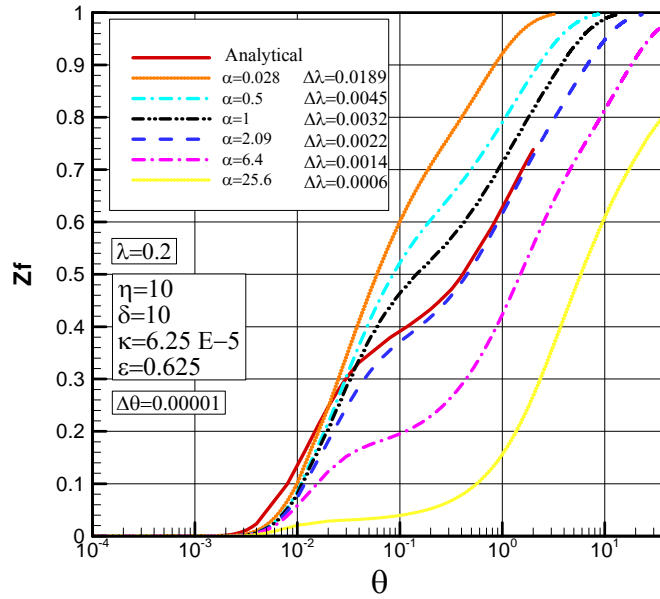


Figure 4.8: Z_f versus θ curves at $\lambda=0.2$ for different α values when $\eta=10$, $\delta=10$ and $\kappa=6.25 \cdot 10^{-5}$.

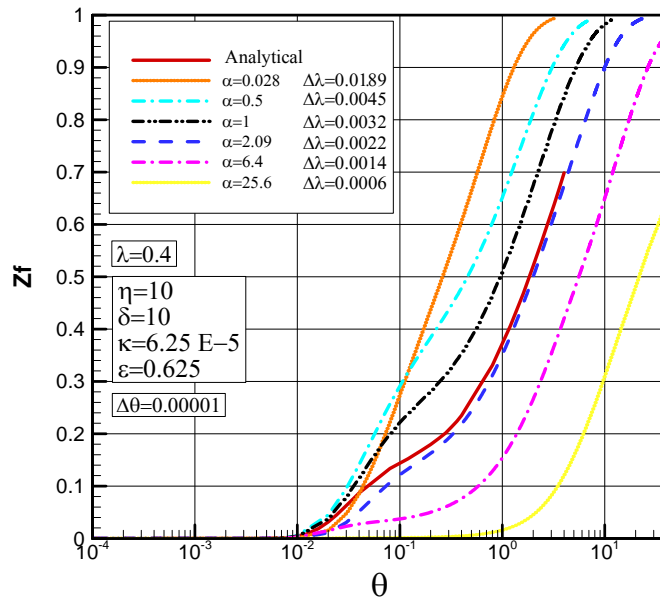


Figure 4.9: Z_f versus θ curves at $\lambda=0.4$ for different α values when $\eta=10$, $\delta=10$ and $\kappa=6.25 \cdot 10^{-5}$.

In *Figure 4.8* where $\eta=10$, $\delta=10$ and $\kappa=6.25*10^{-5}$, the curve of $\alpha=2.09$ again best fits the curve of the analytical data at $\lambda = 0.2$. However, for this case, the difference between these curves is more significant at early times, and the numerical solution gives a small delayed response. On the other hand, the numerical and analytical curves perfectly overlap at later times. Once more the curves for the values of α other than 2.09 are separated from the analytical curve.

For the same case but at $\lambda = 0.4$, as in *Figure 4.9*, the numerical and analytical solutions give closer results when $\alpha=2.09$. Furthermore, the deviation between numerical and analytical results at early times is less at this dimensionless location since the hydraulic gradient is small and, thus, the non-linear effect is less significant.

Figure 4.10 demonstrates the case for $\eta=10$, $\delta=1$ and $\kappa=6.25*10^{-5}$ at $\lambda = 0.2$. The curve of $\alpha=2.09$ is again the most similar curve to the curve of analytical solution. However, there is significant difference between these curves except for the very late times. On the other hand, these curves follow similar patterns.

Figure 4.11 shows the case $\eta=10$, $\delta=10$ and $\kappa=6.25*10^{-5}$ at $\lambda = 0.2$. However, in this case, α is changed by altering $\Delta\theta$ while fixing $\Delta\lambda$ to 0.0022. It can be concluded from the figure that the numerical and analytical solutions give similar results when $\alpha=2.09$. For the numerical solution, it does not matter changing either $\Delta\theta$ or $\Delta\lambda$ as long as α is kept constant.

It should also be stressed that the curvature of the curves is more visible when $\alpha=2.09$. The idea behind this will be explained in the following sections while discussing the transition period.

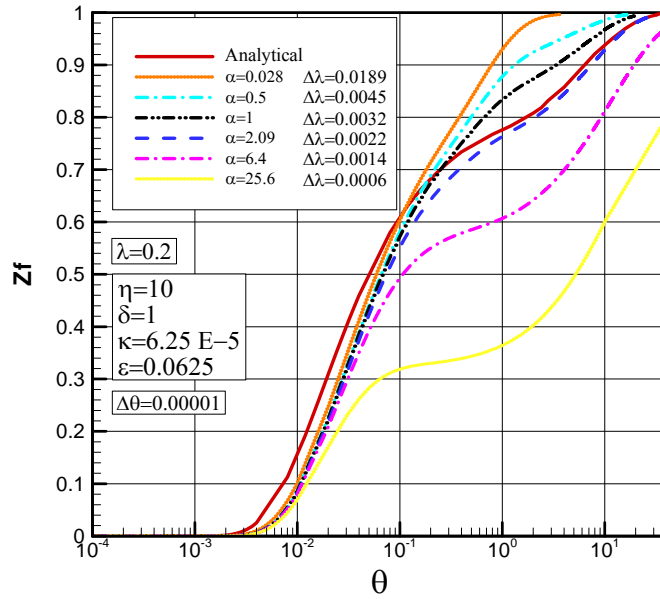


Figure 4.10: Z_f versus θ curves at $\lambda=0.2$ for different α values when $\eta=10$, $\delta=1$ and $\kappa=6.25 \cdot 10^{-5}$.

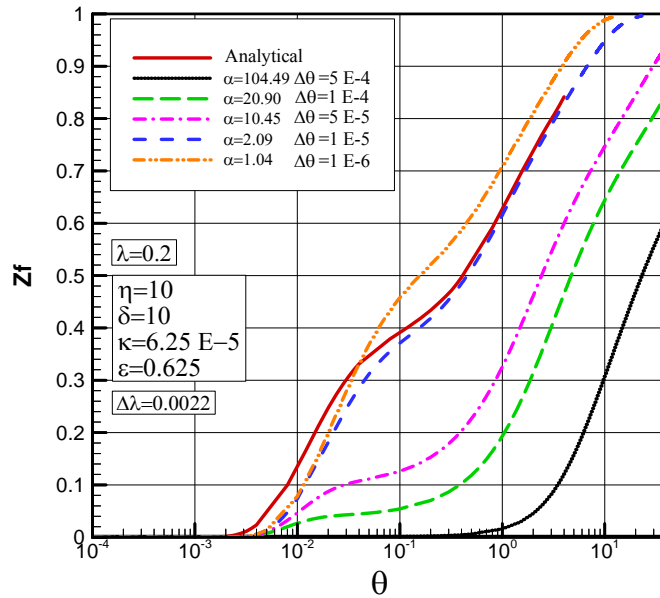


Figure 4.11: Z_f versus θ curves at $\lambda=0.2$ for different α values when $\eta=10$, $\delta=10$ and $\kappa=6.25 \cdot 10^{-5}$.

In order to demonstrate more clearly how the results of numerical solutions fit to the results of the analytical solution, only the curves of the analytical solution and the numerical solution of $\alpha=2.09$ are plotted on same graph for various combinations storativity, conductivity and diffusivity contrasts. These graphs are given in *Appendix C*.

Two graphs are presented in this section for illustration. *Figure 4.12* shows the case $\eta=10$, $\delta=50$ and $\kappa=3.125*10^{-3}$ where the transmissivity of fractures is high. At $\lambda = 0.2$, curves perfectly overlap and numerical and analytical solutions give almost same results.

In *Figure 4.13* where $\eta=10$, $\delta=0$ and $\kappa=0$, the transmissivity of blocks is equal to 0. Therefore, no flow occurs in the blocks and the aquifer acts as a single porosity. For this case, curves show very similar patterns while there is lagging between them.

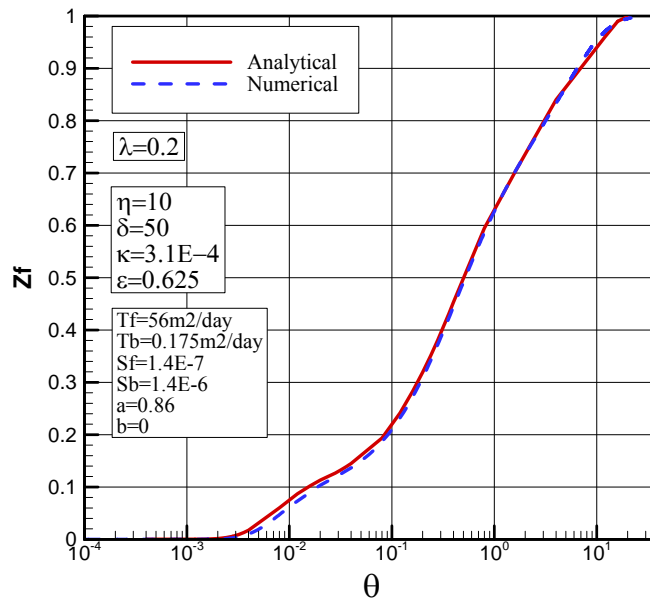


Figure 4.12: Z_f versus θ curves at $\lambda=0.2$ when $\eta=10$, $\delta=50$ and $\kappa=3.1*10^{-4}$.

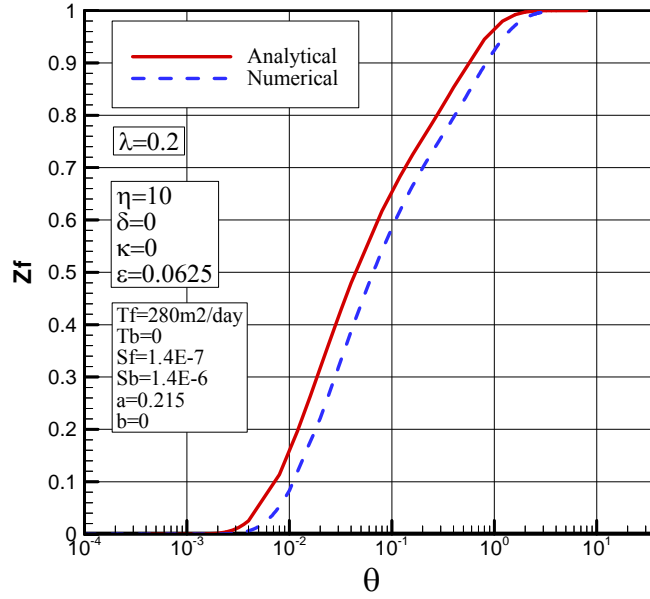


Figure 4.13: Z_f versus θ curves at $\lambda=0.2$ when $\eta=10$, $\delta=0$ and $\kappa=0$.

It is clear that the closest results have been obtained when $\alpha=2.09$, however it would be necessary to prove it quantitatively. To this end, root mean square error for six values α were calculated for three cases, i.e. $\eta=10$, $\delta=5$, $\kappa=3.125*10^{-5}$; $\eta=10$, $\delta=10$, $\kappa=6.25*10^{-5}$; $\eta=10$, $\delta=1$, $\kappa=6.25*10^{-5}$, using *equation 4.7* (Mathews, 1988).

$$RMS \ error = \left[\frac{1}{N} \sum_1^N \left| z_{f \ analytical} - z_{f \ numerical} \right|^2 \right]^{\frac{1}{2}} \quad 4.7$$

where N is the number of points compared.

Table 4.3 shows root mean square errors calculated at the points where the analytical solution is available. It is obvious that minimum errors were obtained when $\alpha=2.09$ for the said three cases. This means the difference between numerical and analytical results is minimum for this particular value of α .

Table 4.3: Root mean square errors

RMS error	$\alpha=0.028$	$\alpha=0.5$	$\alpha=1$	$\alpha=2.09$	$\alpha=6.4$	$\alpha=25.6$
$\eta=10, \delta=5$ $\kappa=3.125*10^{-5}$	0.178	0.112	0.064	0.012	0.145	0.332
$\eta=10, \delta=10$ $\kappa=6.25*10^{-5}$	0.314	0.236	0.184	0.102	0.136	0.195
$\eta=10, \delta=1$ $\kappa=6.25*10^{-5}$	0.170	0.141	0.120	0.088	0.158	0.212

Therefore, it is concluded from the qualitative and quantitative comparison of numerical and analytical solutions that the closest results are obtained when $\alpha=2.09$ ($\Delta\theta=0.00001$ and $\Delta\lambda=0.0022$ which leads 450 mesh points in the solution domain) and that this particular value of α ensures the accuracy of the numerical solution. In this regard, $\alpha=2.09$ is used in the numerical calculations throughout this study.

On the other hand, the deviation between numerical and analytical results at early times persists but at a lesser degree in general. This behaviour is an agreement with the expectation that at early times the hydraulic gradient is high and obviously the non-Darcian flow is more effective. At later times the curves again overlap.

The numerical and the analytical solutions give closer results when the aquifer exhibits normal fractured aquifer characteristics that are the fracture transmissivity is much larger than the block transmissivity and the storage coefficient of the blocks are higher than the storage coefficient of the fractures. However, hand, when $\delta=0$ as in *Figure 4.13* the aquifer acts as a single porosity aquifer and the difference between numerical and analytical solutions is significant.

The reasons for the difference between the results of numerical and analytical solutions are worth discussing. Given that the flow through the blocks is neglected in the analytical solution of Önder (1998) by eliminating the term $BK_b \frac{\partial^2 h_b}{\partial x^2}$ in *equation 2.54*, a difference may be expected between the analytical and numerical solutions.

4.4 Drawdown in the Aquifer

Dimensionless drawdown versus dimensionless time and dimensionless drawdown versus dimensionless space curves are constructed for various combinations of the storativity, conductivity and diffusivity contrasts and presented in *Appendix E*.

As an example, the case $\eta=10$, $\delta=10$ and $\kappa=6.25*10^{-5}$ is discussed in this section. *Figure 4.14* shows the dimensionless drawdown versus dimensionless space curves for the fractures and the blocks at different times along the aquifer. It is apparent from the figure that the drawdown in the fractures increases faster than the drawdown in the blocks at earlier times so that there exists a lagging between them. The drawdown in the blocks and in the fractures approaches to 1 as the time goes to the infinity while the lagging between them decreases.

Dimensionless drawdown versus dimensionless time curves of the fractures and the blocks at four different dimensionless locations, i.e. $\lambda = 0.1, 0.2, 0.4$ and 0.8 , are shown in *Figure 4.15* for the same case. All curves merge very close to 1, which means the steady-state condition is almost established in the aquifer.

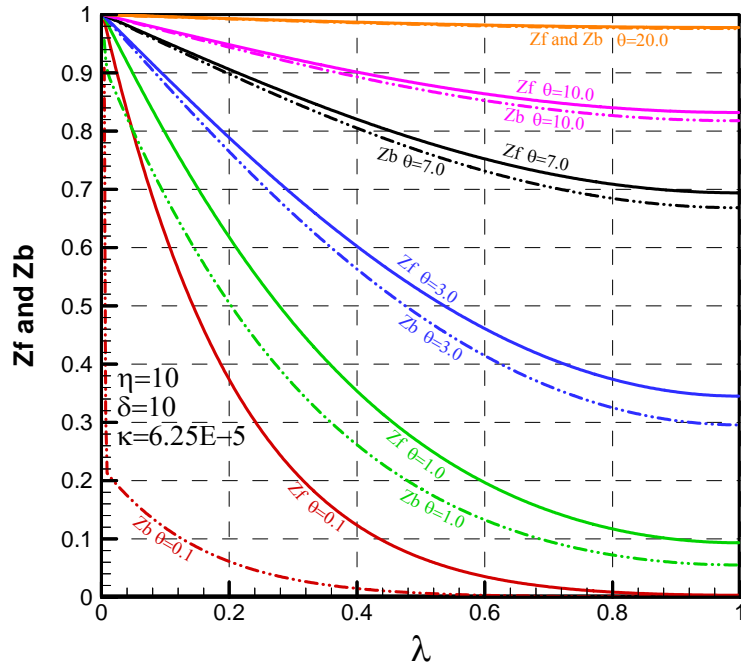


Figure 4.14: Z_f versus λ and Z_b versus λ curves for $\eta=10$, $\delta=10$ and $\kappa=6.25 \cdot 10^{-5}$ at different times θ .

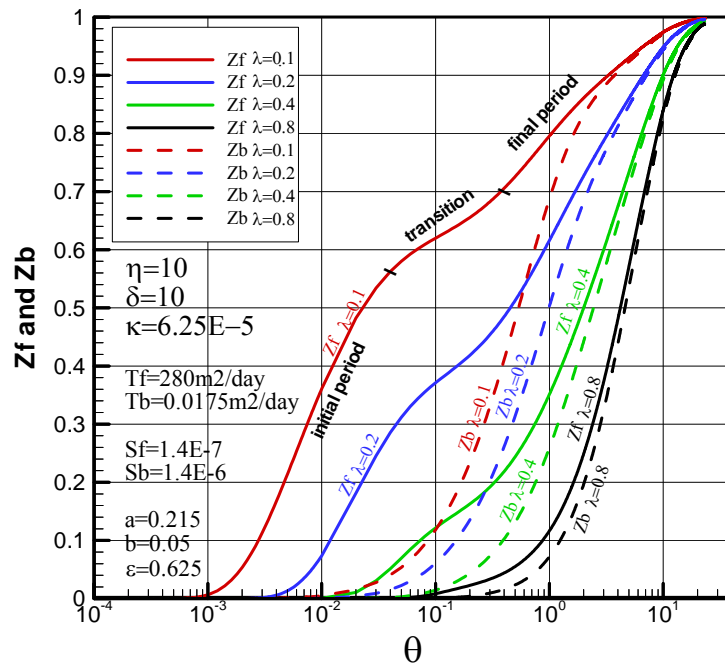


Figure 4.15: Z_f versus θ and Z_b versus θ curves for $\eta=10$, $\delta=10$ and $\kappa=6.25 \cdot 10^{-5}$ at $\lambda=0.1$, 0.2 , 0.4 and 0.8 .

The behaviour of dimensionless drawdown in the aquifer is generally divided into three periods which are demonstrated in *Figure 4.15*. Initially the rate of increase in the drawdown is representative of fracture transmissivity and storage. Therefore, in the initial period, rapid flow takes place in the fractures and the drawdown in the fractures increases sharply. Fracture to block flow develops in the second period where the flow slows down as shown by a decrease of the slope of the drawdown curve. Accordingly, the drawdown response of the aquifer enters into transition and the increase in the drawdown in the fractures is slowed down. More water is stored in the blocks. As a result, the difference between the drawdown in the fractures and in the blocks decreases more rapidly. The transition period basically depends on the aquifer parameters. The third or final period of the drawdown response is homogenous but delayed in time. In this period, the drawdown in the fractures and in the blocks increases gradually to reach the steady-state condition.

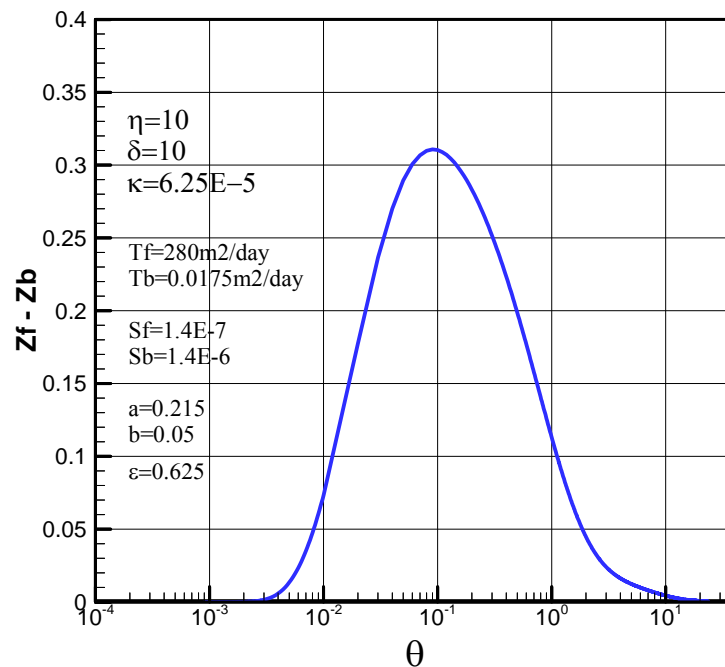


Figure 4.16: $(Z_f - Z_b)$ versus θ curve for $\eta=10$, $\delta=50$ and $\kappa=6.25 \cdot 10^{-5}$ at $\lambda=0.2$.

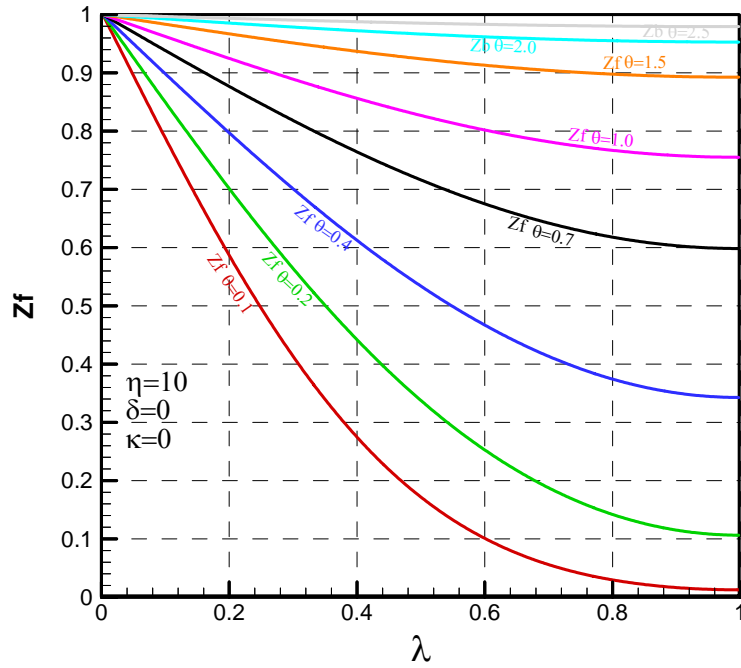


Figure 4.17: Z_f versus λ and Z_b versus λ curves for $\eta=10$, $\delta=10$ and $\kappa=0$ at different times θ .

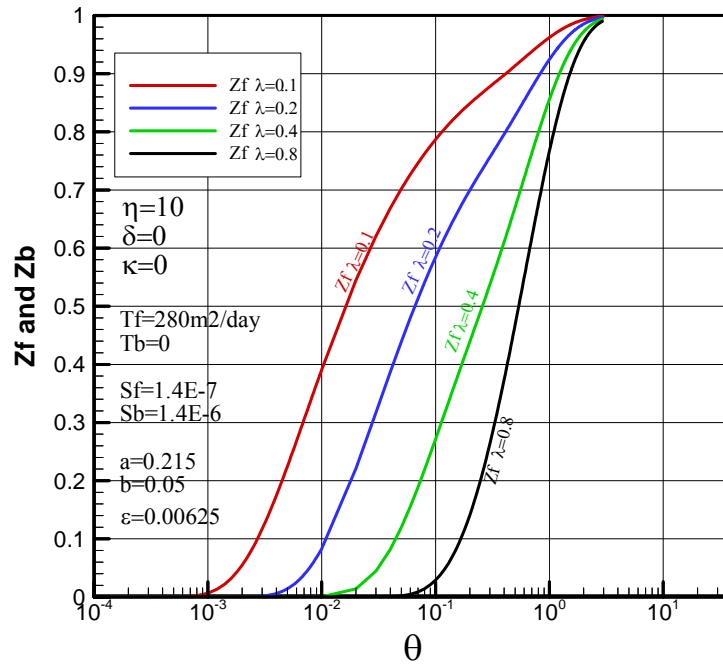


Figure 4.18: Z_f versus θ and Z_b versus θ curves for $\eta=10$, $\delta=0$ and $\kappa=0$ at $\lambda=0.1, 0.2, 0.4$ and 0.8 .

Figure 4.16 shows the change in difference between the drawdown in the fractures and the drawdown in the blocks with respect to time. It could be said that the difference increases at early stages up to $\theta \cong 10^{-1}$, then decreases due to the effect of transition, finally approaches to θ as the time goes to infinity.

When the transmissivity of the blocks is equal to θ , which is the case $\delta=0$ and $\kappa=0$ as in *Figures 4.17* and *4.18*, the aquifer functions as a single porosity aquifer. Flow occurs only through the fractures. Given that the blocks neither transmit nor store water when $T_b=0$, fracture to block flow does not develop. Therefore, the drawdown in the blocks is equal to θ .

Drawdown versus time and drawdown versus space curves can also be plotted for various combinations of the storativity, conductivity and diffusivity contrasts. To this end, the dimensionless drawdown as well as dimensionless time and space variables should be converted to the dimensional ones by arithmetic operations using the relevant non-dimensionalization parameters.

Figures 4.19 and *4.20* give drawdown versus space and drawdown versus time curves respectively for the case $\eta=10$, $\delta=10$ and $\kappa=6.25*10^{-5}$.

4.5 Effect of the Non-Linear Forcheimer Parameter, b , on the Drawdown in the Fractures

The main objective of this study is to investigate the non-Darcian flow behaviour in the aquifer, particularly in the fractures. The non-Darcian flow in the fractures is primarily governed by the non-linear parameter b in Forcheimer's equation. Therefore, the effect of this on the drawdown response of the aquifer was investigated by changing it while fixing the other aquifer parameters in the numerical calculations.

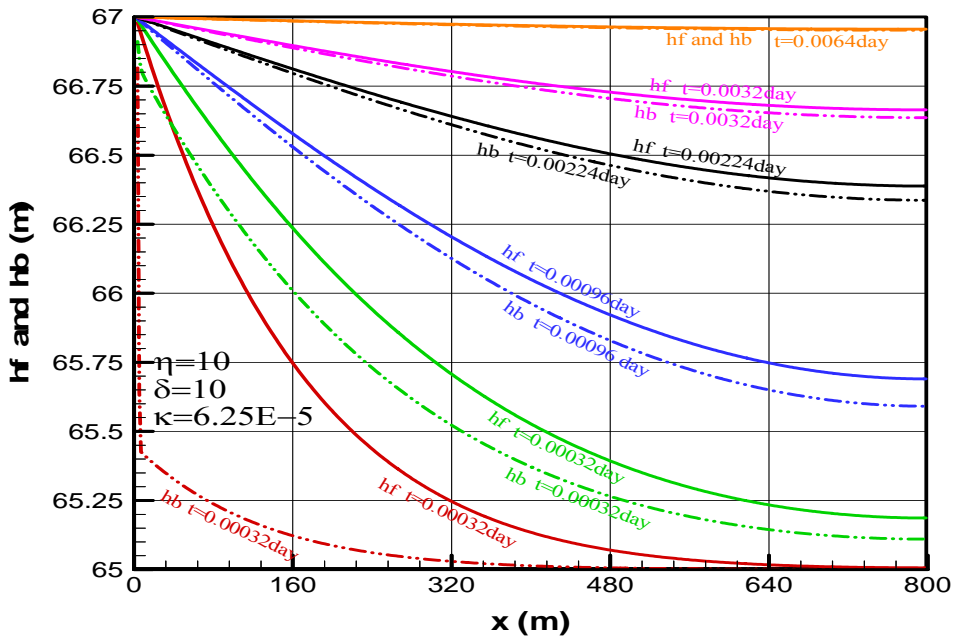


Figure 4.19: h_f versus x and h_b versus x curves for $\eta=10$, $\delta=10$ and $\kappa=6.25 \cdot 10^{-5}$ at different times t .

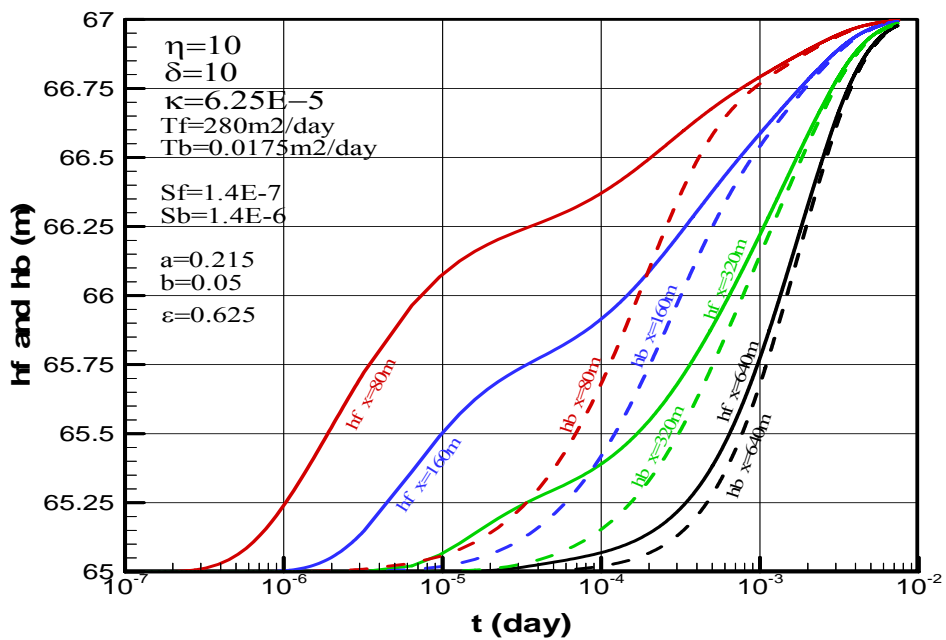


Figure 4.20: h_f versus t and h_b versus t curves for $\eta=10$, $\delta=10$ and $\kappa=6.25 \cdot 10^{-5}$ at $x=80, 160, 320$ and 640m .

Numerical runs were carried out for five different values for b , i.e. 0 , 0.005 , 0.05 , 0.1 and 0.5 . *Figures 4.21, 4.22, 4.23 and 4.24* show dimensionless drawdown versus dimensionless time curves for the fractures at a dimensionless location $\lambda=0.2$ for $T_f=280m^2/day$, $T_f=1400m^2/day$, $T_f=2800m^2/day$ and $T_f=5600m^2/day$ respectively. Recall that changing b naturally changes the dimensionless parameter β_0 .

It was mentioned in *Section 2.5* that when $b=0$, the flow in the fractures is Darcian. On the other hand, it is obvious that $b=0.5$ is a very extreme and unrealistic value compared to the values of b presented in *Table D.1*. However, these values were used in the calculations in order to evaluate the effect of non-linearity on the flow in the aquifer more precisely.

Figure 4.21 gives the dimensionless drawdown versus dimensionless time curves for five different values of non-linear parameter, b , when $T_f=280m^2/day$. It is apparent from the figure that all curves perfectly overlap which means the non-Darcian effect on the flow is negligible, even non-existent. Reynold's number calculated at the initial stages is around $1*10^{-2}$. Furthermore, the results of the numerical solution are identical with that of the analytical solution.

Therefore, it can be concluded that non-linearity has no effect on the flow when $T_f=280m^2/day$ and R_e is quite small, so that Darcian flow takes place both in the fractures and blocks.

When T_f is increased five times to $1400m^2/day$, any difference among the curves of *Figure 4.22* is only slightly detectable except for the extreme value $b=0.5$. In this case, Reynold's number at the initial stages is around 0.1 , and the non-Darcian effect starts to become apparent.

It is evident from *Figure 4.23* that the curves differ considerably when T_f is increased to $2800m^2/day$ where Reynold's number at the initial stages is around 0.3 . Therefore, the effect of the non-linear Forcheimer parameter becomes significant as T_f and R_e increase.

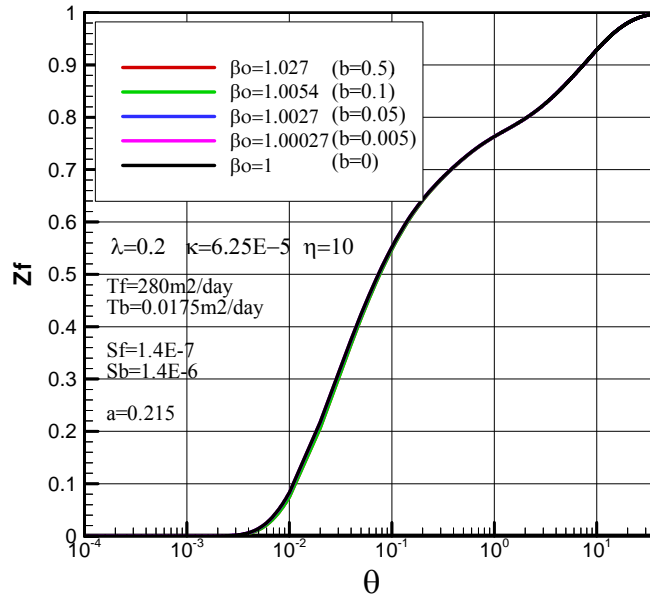


Figure 4.21: Z_f versus θ curves at $\lambda=0.2$ for different non-linear parameter, b , when $T_f=280m^2/day$.

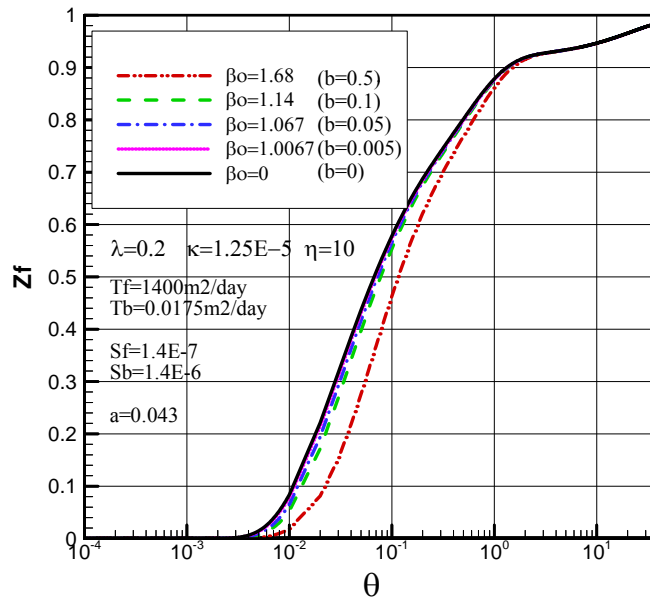


Figure 4.22: Z_f versus θ curves at $\lambda=0.2$ for different non-linear parameter, b , when $T_f=1400m^2/day$.

Furthermore, for the case $T_f=5600\text{m}^2/\text{day}$ as in *Figure 4.24*, the non-Darcian effect is much more significant as the Reynold's number at the initial stages is around 0.8.

It could be concluded that the increase in T_f also increases the specific discharge in fractures as well as the Reynold's number, thus making the non-linear effect on the flow more and more significant.

The specific discharge is the function of the hydraulic gradient, J , and the transmissivity of the fractures. The hydraulic gradient is maximum when x and t approach to 0. As T_f increases, q also increases, and therefore the non-Darcian effect becomes more significant.

It should also be mentioned that the increase in b augments the non-linearity in the flow, the gradient of the drawdown response as well.

The effects of transmissivity of the fractures and Reynold's number on non-Darcian flow are presented in *Table 4.4*. The results obtained are consistent with the ones available in the literature (Beavers and Sparrow, 1969; Ahmed and Sunada, 1969; Cornell and Katz, 1953).

Table 4.4: The effects of transmissivity of the fractures and Reynold's number on non-Darcian flow

$T_f(\text{m}^2/\text{day})$	280	1400	2800	5600
R_e	0.01	0.1	0.3	0.8
Non-Darcian effect	none	slight	significant	very significant

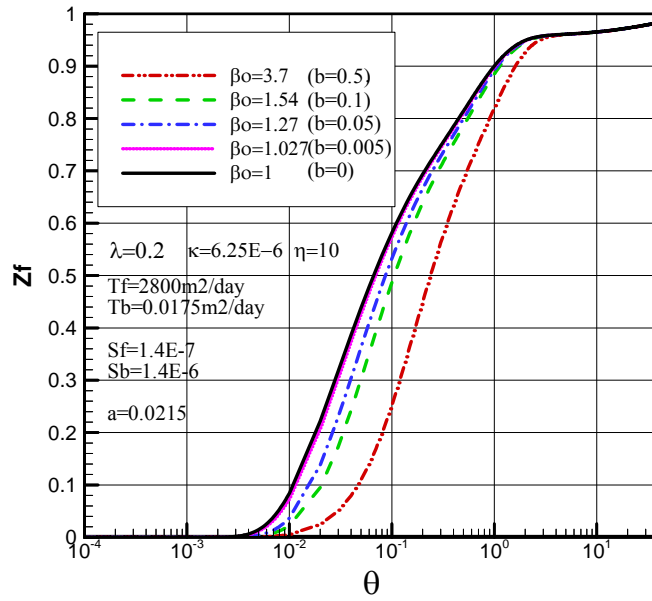


Figure 4.23: Z_f versus θ curves at $\lambda=0.2$ for different non-linear parameter, b , when $T_f=2800m^2/day$.

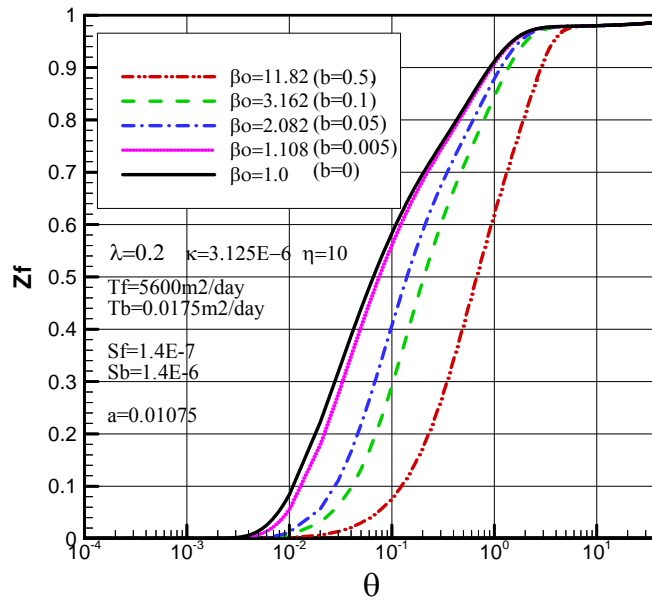


Figure 4.24: Z_f versus θ curves at $\lambda=0.2$ for different non-linear parameter, b , when $T_f=5600m^2/day$.

4.6 Effect of the Storativity Contrast, η , on the Drawdown in the Fractures

Numerical calculations are carried out changing the storativity contrast while fixing the conductivity contrast and the other parameters in order to evaluate the effect of the storage coefficient of the fractures and the blocks on the drawdown response of the aquifer.

Figures 4.25, 4.26, 4.27 and 4.28 give dimensionless drawdown versus dimensionless time curves for different storativity contrasts, η , at a dimensionless location $\lambda=0.2$ for $\kappa=6.25*10^{-4}$, $\kappa=1.25*10^{-4}$, $\kappa=6.25*10^{-5}$ and $\kappa=1.25*10^{-5}$ respectively.

It is apparent from the figures that the transition period becomes longer as η becomes larger. Therefore, the quasi-steady flow from the fractures to the blocks increases. On the other hand, the transition starts later when the transmissivity of fractures gets higher. The reason for this is that the rapid flow in the fractures retards the quasi-steady fracture-block flow to occur.

$\eta=1$ means storage coefficient of the fractures and the blocks are equal. For this case, the aquifer functions almost as a single porosity aquifer and transition period does not occur.

If the storativity contrast is not very large, i.e. $\eta=5$ or $\eta=10$, the transition period takes place in relatively shorter time. However, the transition period is quite long for the case $\eta=50$. It is also worth mentioning that starting points of deviation from the single porosity aquifer is dictated by the conductivity contrast κ . As κ decreases, deviation takes place later. In *Figure 4.25*, where $\kappa=6.25*10^{-4}$, deviation starts when $Z_f=0.25-0.35$ and $\theta=3*10^{-3}$, on the other hand, when $\kappa=1.25*10^{-5}$, as in *Figure 4.28*, deviation takes place later, when $Z_f=0.85-0.90$ and $\theta=10^0$.

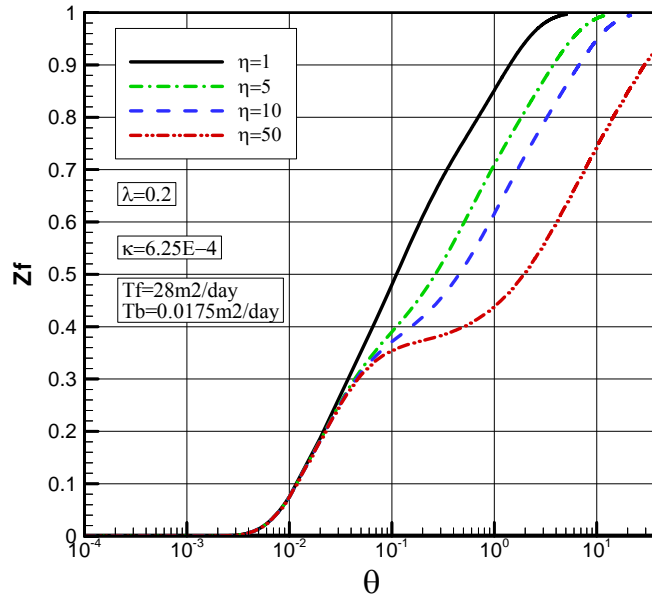


Figure 4.25: Z_f versus θ curves at $\lambda=0.2$ for different storativity contrasts, η , when $\kappa=6.25*10^{-4}$.

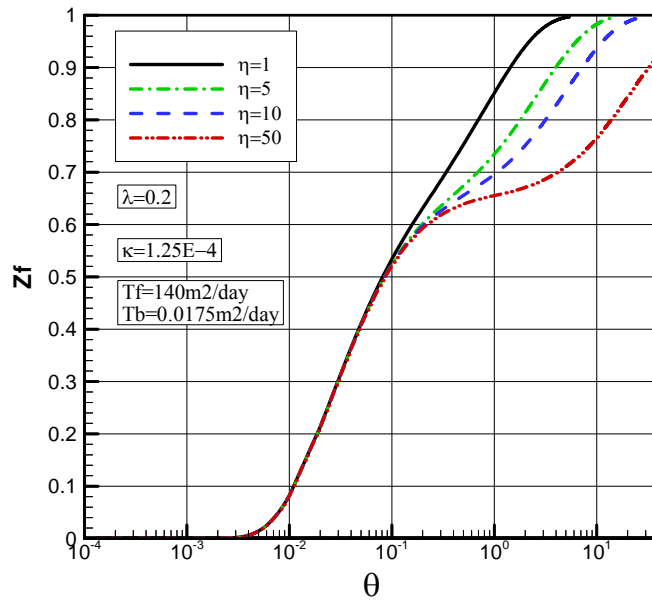


Figure 4.26: Z_f versus θ curves at $\lambda=0.2$ for different storativity contrasts, η , when $\kappa=1.25*10^{-4}$.

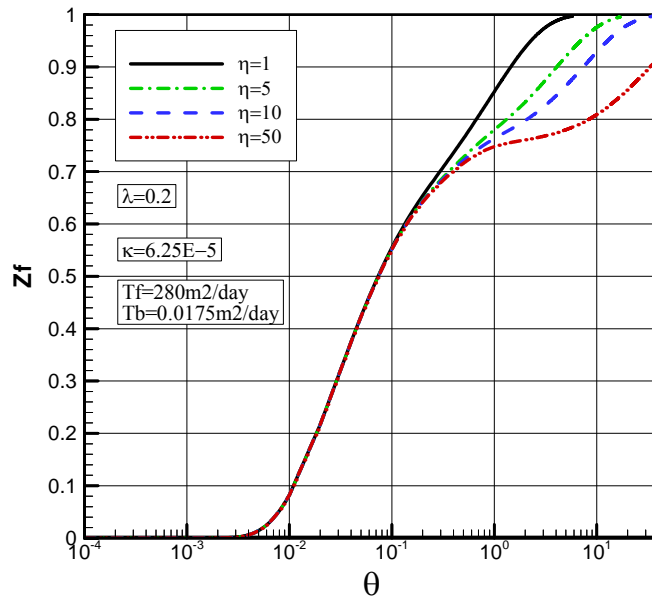


Figure 4.27: Z_f versus θ curves at $\lambda=0.2$ for different storativity contrasts, η , when $\kappa=6.25 \cdot 10^{-5}$.

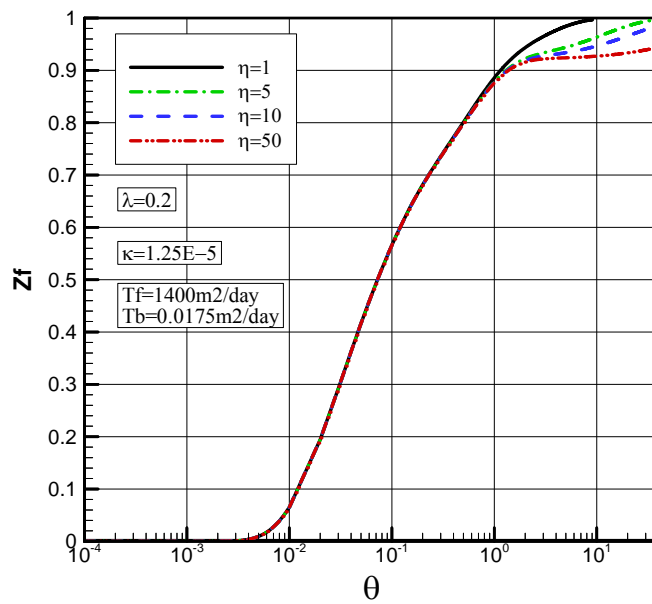


Figure 4.28: Z_f versus θ curves at $\lambda=0.2$ for different storativity contrasts, η , when $\kappa=1.25 \cdot 10^{-5}$.

4.7 Effect of the Conductivity Contrast, κ , on the Drawdown in the Fractures

Effect of the fracture and block transmissivities on the drawdown response of the aquifer is investigated by keeping the storativity contrast and other parameters constant while changing the conductivity contrast in numerical calculations.

Figures 4.29, 4.30 and 4.31 show dimensionless drawdown versus dimensionless time curves of the fractures for different conductivity contrasts κ at a dimensionless location $\lambda=0.2$ for $\eta=1$, $\eta=10$ and $\eta=50$ respectively.

When $\eta=1$, as in *Figure 4.29*, the aquifer acts almost as a single porosity aquifer, therefore the transition period is not clearly apparent. Flow in the aquifer is mainly dictated by the storativity contrast and the effect of the conductivity contrast is not significant.

It is evident from *Figure 4.30* that the transition period is longer when $\eta=10$. Starting time of the transition controlled by κ . As κ decreases, transition takes place later. The reason for this is that, as mentioned in the previous section, if the transmissivity of fractures is much larger than that of the blocks, a rapid flow takes place in the fractures retarding the quasi-steady fracture-block flow to occur. On the other hand, the length of the transition period is the function of the storativity contrast, η .

Figure 4.31 shows the case $\eta=50$ where the storage coefficient of the blocks is much larger than that of the fractures. In this case, the transition period is quite long and large amount of water can be transferred to and stored in the blocks.

Finally, it can be concluded that the length of the transition period is controlled by η and starting time of the transition period is dictated by κ .

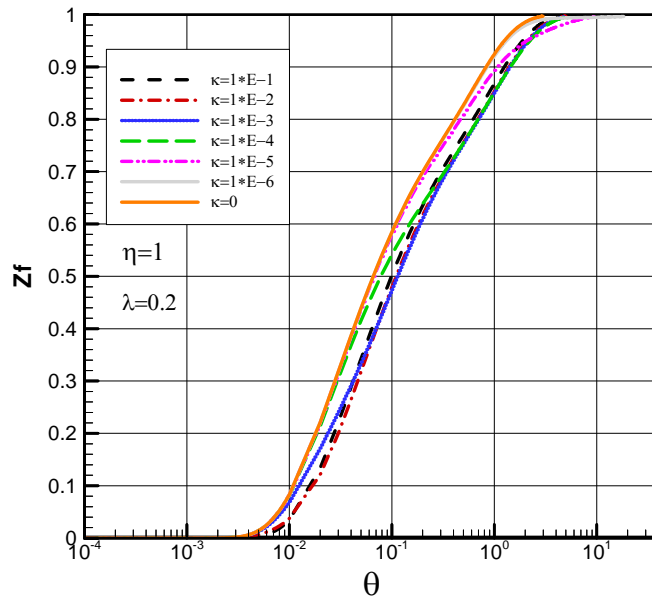


Figure 4.29: Z_f versus θ curves at $\lambda=0.2$ for different conductivity contrasts, κ , when $\eta=1$.

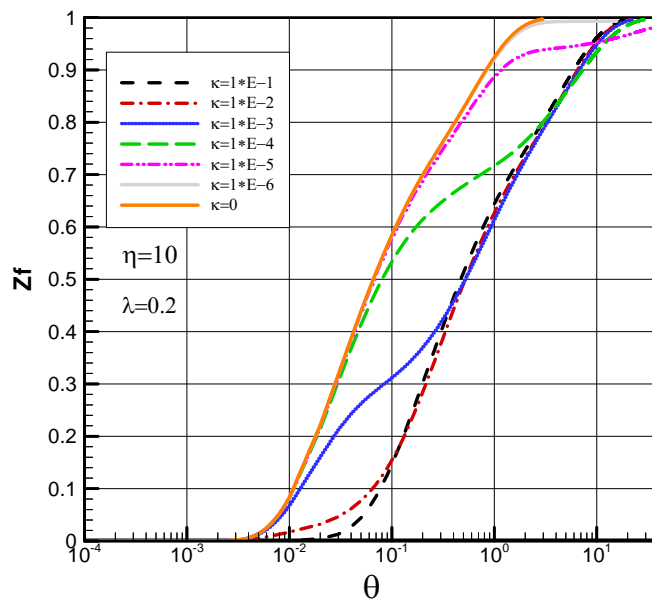


Figure 4.30: Z_f versus θ curves at $y=0.2$ for different conductivity contrasts, κ , when $\lambda=10$.

4.8 Effect of the Fluid Transfer Parameter, ε , on the Drawdown in the Fractures

Effect of the fluid transfer parameter, ε , on the piezometric drawdown response of the aquifer is investigated by changing the said parameter while fixing the others in numerical calculations.

Figure 4.32 shows dimensionless drawdown versus dimensionless time curves of the fractures for different ε values at a dimensionless location $\lambda=0.2$ for $\eta=10$ and $\kappa=6.25*10^{-5}$.

The effect of the fluid transfer parameter on the drawdown response is somehow similar to the effect of conductivity contrast κ . When ε is small, the rate of water transfer between the fractures and the blocks is also small. In this case, flow occurs mainly in the fractures and almost no water is stored in the blocks at early times. Transition period starts lately. As ε increases, more water is transferred to the blocks and water transfer starts relatively earlier.

4.9 Effect of the Non-Linear Forcheimer Parameter, b , on the Flow Rate

The effect of the non-linear parameter, b , on the rate of flow from the stream to the aquifer is investigated by changing the said parameter while keeping the others constant in numerical calculations.

Numerical runs were carried out for five different values for b , i.e. 0 , 0.005 , 0.05 , 0.1 and 0.5 . *Figures 4.33, 4.34, 4.35* and *4.36* demonstrate dimensionless flow rate versus dimensionless time curves for these values of b for $T_f=280m^2/day$, $T_f=1400m^2/day$, $T_f=2800m^2/day$ and $T_f=5600m^2/day$ respectively. Changing b naturally changes the dimensionless parameter β_0 .

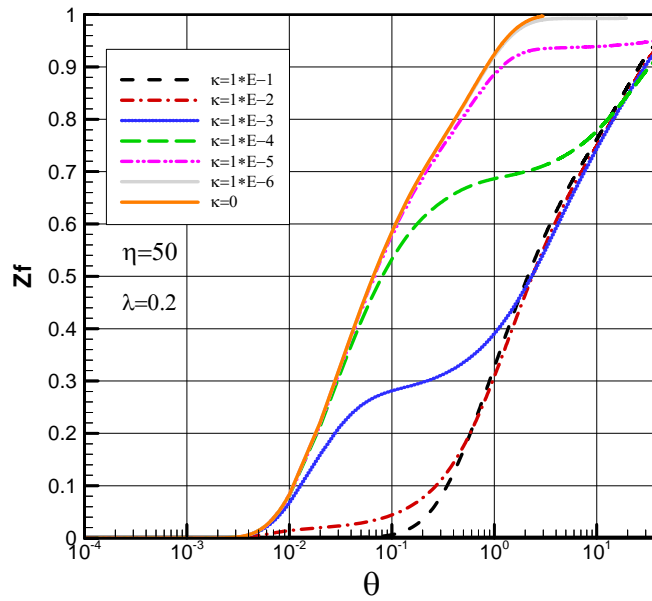


Figure 4.31: Z_f versus θ curves at $\lambda=0.2$ for different conductivity contrasts, κ , when $\eta=50$.

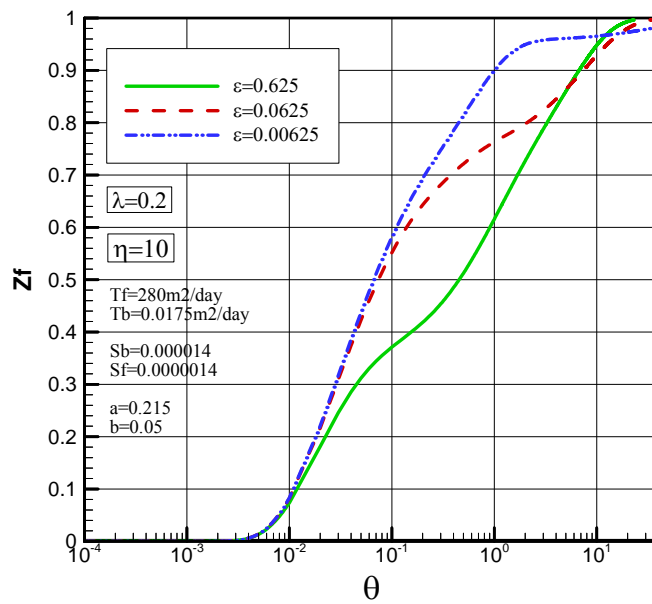


Figure 4.32: Z_f versus θ curves at $\lambda=0.2$ for different fluid transfer parameters, ϵ .

As it was mentioned in *Sections 2.5* and *4.5*, the flow in the fractures is Darcian when b is equal to 0 . On the other hand, 0.5 is a very extreme and unrealistic value for b and it was used in calculations in order to understand better the effect of non-linearity on the flow in the aquifer.

Figure 4.33 shows the dimensionless flow rate versus dimensionless time curves when T_f is $280m^2/day$. All curves perfectly overlaps except for the curve of $b=0.5$. The non-linear effect is slightly visible at early times only for this extreme value. Therefore, the non-linear parameter b has almost no influence on the flow rate when T_f is $280m^2/day$.

Should T_f is increased five times to $1400m^2/day$, the difference between the curves of *Figure 4.34* become visible. Therefore, the non-linearity affects the flow rate significantly.

Furthermore, when T_f is increased to $2800m^2/day$ as in *Figure 4.35*, the influence of non-linearity on the flow rate is quite significant even for the very small value of $b=0.005$. For the case $T_f=5600m^2/day$ as in *Figure 4.36*, the non-Darcian effect is much more significant.

Given that the total flow is the area under each curve, it can be concluded that the rate of the flow from the stream to the aquifer increases as the non-linear term, b , increases.

As the increase in T_f makes the non-Darcian effect more significant it also increases the flow rate.

Flow rate is maximum at early times up to $\theta = 10^{-3} - 10^{-2}$. It stays constant for a while, then decreases almost linearly. All of the curves merge at later stages. That means flow rate is quite small so that the effect of non-linearity is disappeared.

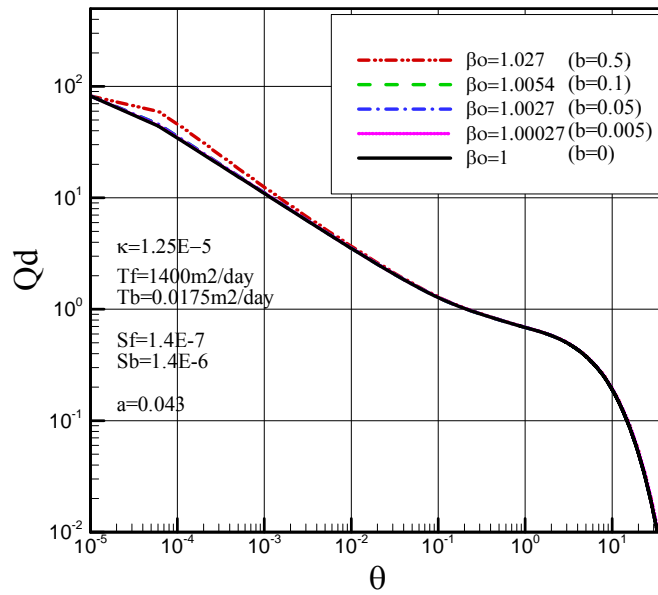


Figure 4.33: Q_d versus θ curves for different non-linear parameters, b , when $T_f=280m^2/day$.

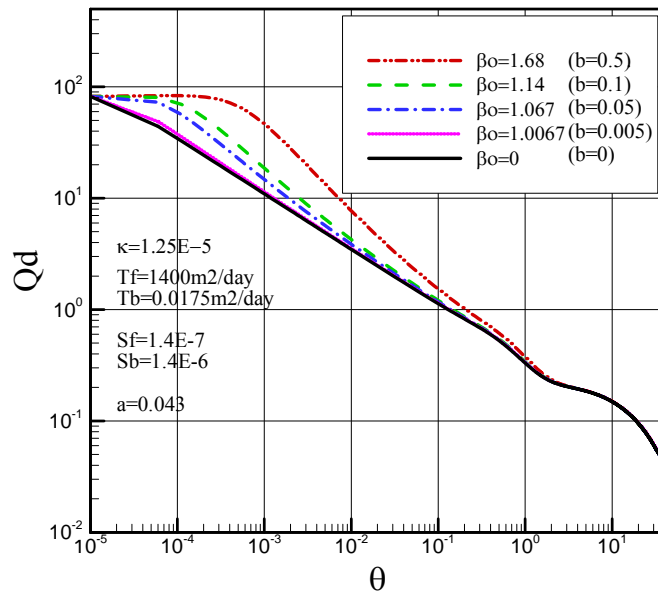


Figure 4.34: Q_d versus θ curves for different non-linear parameters, b , when $T_f=1400m^2/day$.

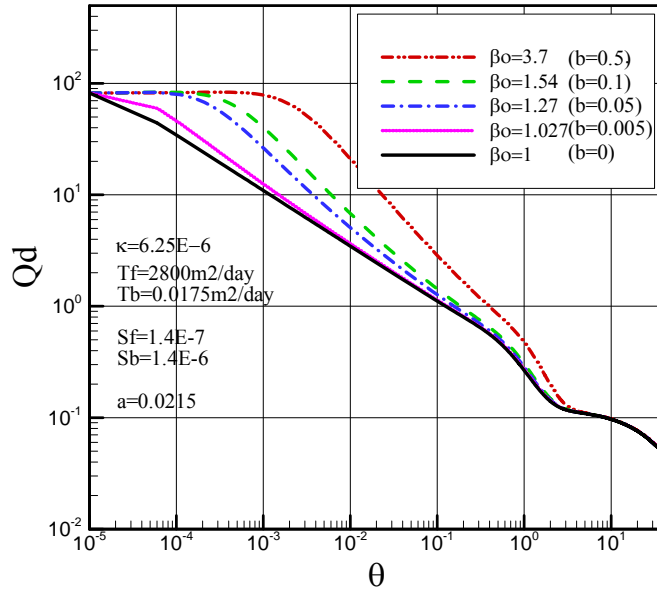


Figure 4.35: Q_d versus θ curves for different non-linear parameters, b , when $T_f=2800m^2/day$.

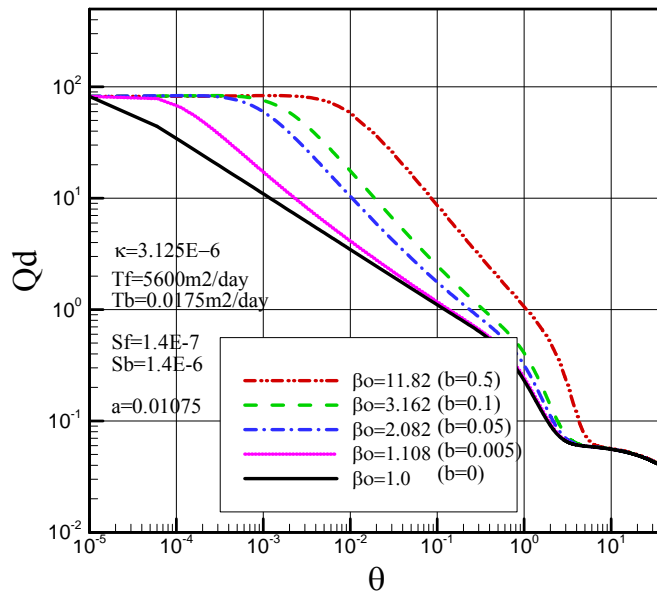


Figure 4.36: Q_d versus θ curves for different non-linear parameters, b , when $T_f=5600m^2/day$.

4.10 Effect of the Storativity Contrast, η , on the Flow Rate

The effect of the fracture and block storage coefficients on the flow rate was investigated by keeping the conductivity contrast and the other parameters constant and changing the storativity contrast in numerical calculations.

Figures 4.37, 4.38, 4.39 and 4.40 show dimensionless flow rate versus dimensionless time curves for different storativity contrasts for $\kappa=6.25 \cdot 10^{-4}$, $\kappa=1.25 \cdot 10^{-4}$, $\kappa=6.25 \cdot 10^{-5}$ and $\kappa=1.25 \cdot 10^{-5}$ respectively.

It can be concluded from the said figures that as η gets larger, the amount of water transmitted to and stored in the blocks becomes more, so that the rate of the flow from the stream to the aquifer increases.

$\eta=1$ means storage coefficients of the fractures and the blocks are equal. For this case, the aquifer functions as a single porosity aquifer and transition does not occur.

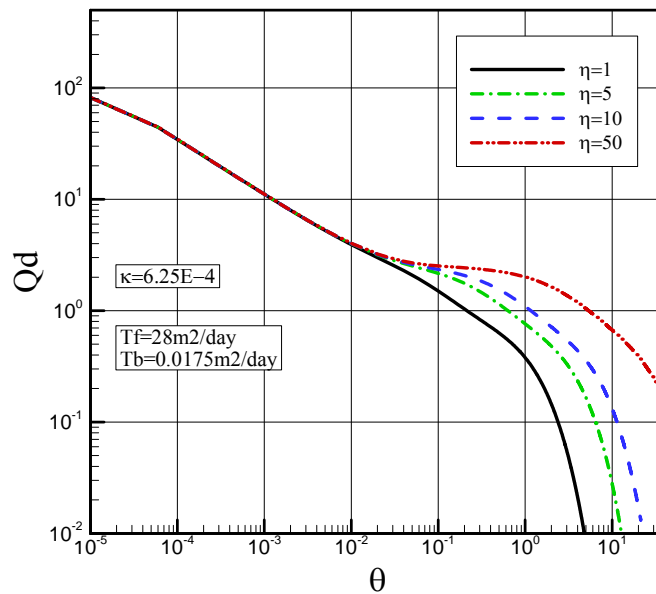


Figure 4.37: Q_d versus θ curves for different storativity contrasts, η , when $\kappa=6.25 \cdot 10^{-4}$.

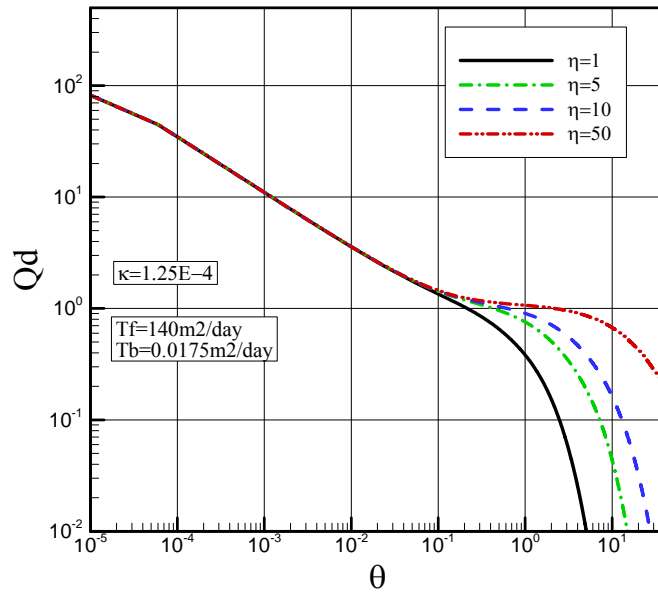


Figure 4.38: Q_d versus θ curves for different storativity contrasts, η , when $\kappa=1.25 \cdot 10^{-4}$.

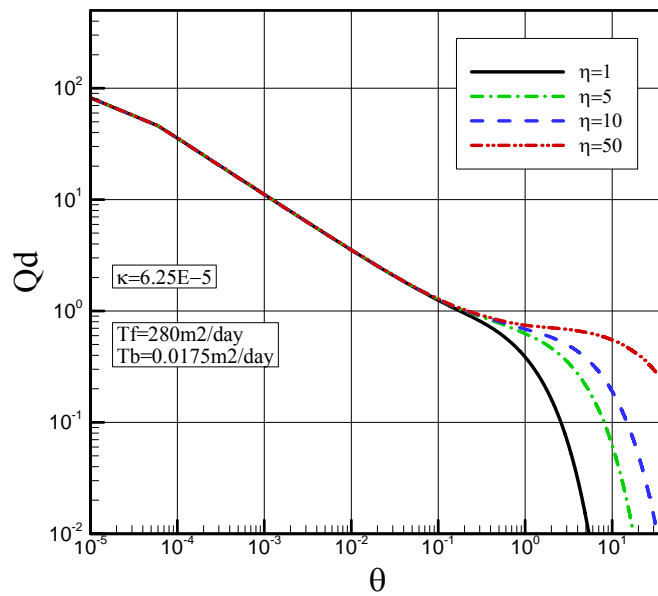


Figure 4.39: Q_d versus θ curves for different storativity contrasts, η , when $\kappa=6.25 \cdot 10^{-5}$.

For the other cases, i.e. $\eta=5$, $\eta=10$ and $\eta=50$, the effect of the transition is significant and starting points of deviation from the single porosity aquifer is dictated by the conductivity contrast, κ .

As κ decreases, deviation takes place later so that total flow from the stream to the aquifer decreases.

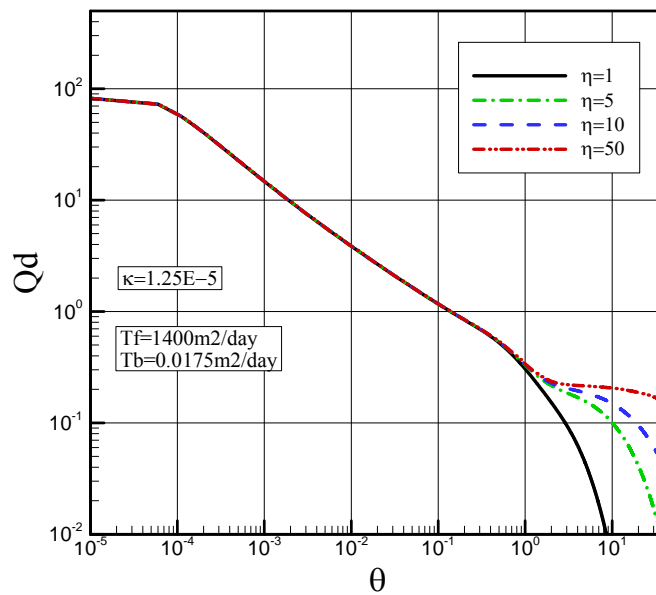


Figure 4.40: Q_d versus θ curves for different storativity contrasts, η , when $\kappa=1.25 \cdot 10^{-5}$.

4.11 Effect of the Conductivity Contrast, κ , on the Flow Rate

The effect of fracture and block transmissivities on the flow rate was investigated by keeping the storativity contrast and the other parameters constant and changing the conductivity contrast in numerical calculations. *Figures 4.41, 4.42 and 4.43* demonstrate dimensionless flow rate versus dimensionless time curves of the fractures for different conductivity contrasts, κ for $\eta=1$, $\eta=10$ and $\eta=50$ respectively.

When $\eta=1$, as in *Figure 4.41*, the aquifer acts almost as a single porosity aquifer, therefore conductivity contrast does not affect the flow rate significantly. Flow in the aquifer is mainly dictated by the storativity contrast and the influence of transition on the flow rate is not considerable.

For the case $\eta=10$ as in *Figure 4.42*, the effect of transition on the flow rate is significant. As the storage coefficient of the blocks becomes large, more water is transferred from the fractures to the blocks. In this regard, more water is transmitted to and stored in the aquifer so that the rate of the flow from the stream to the aquifer is more.

Figure 4.43 shows the case $\eta=50$ where the storage coefficient of the blocks is much larger than that of the fractures. In this case, the effect of conductivity contrast on the flow rate is more significant.

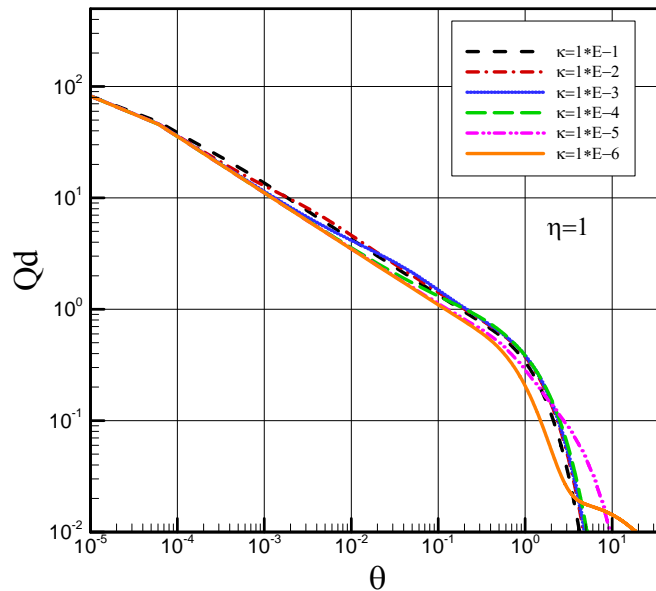


Figure 4.41: Q_d versus θ curves for different conductivity contrasts, κ , when $\eta=1$.

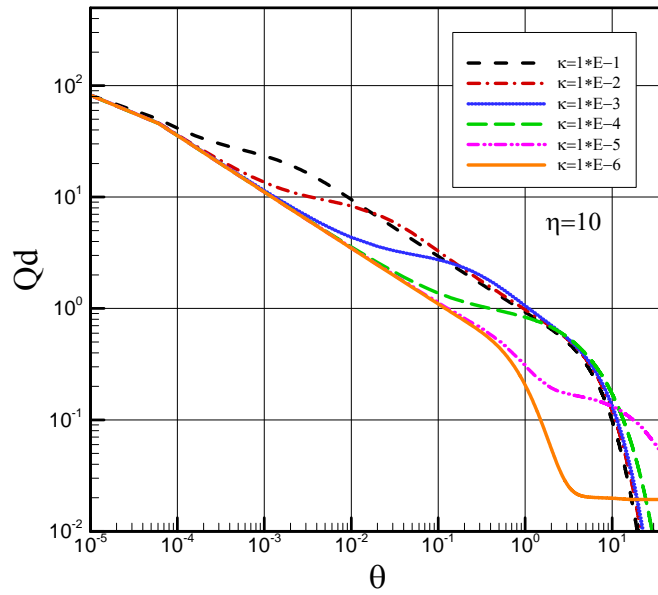


Figure 4.42: Q_d versus θ curves for different conductivity contrasts, κ , when $\eta=10$.

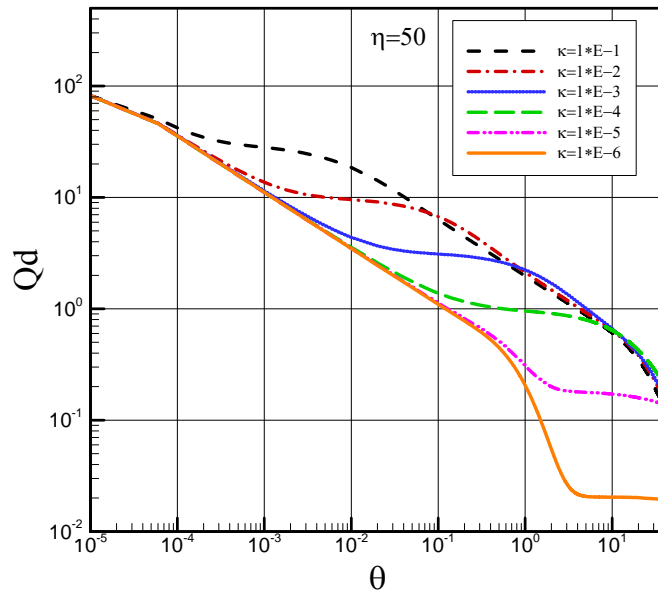


Figure 4.43: Q_d versus θ curves for different conductivity contrasts, κ , when $\eta=50$.

On the other hand, starting and finishing times of the transition are controlled by the conductivity contrast, κ . As κ decreases, transition takes place later. However, the duration of the transition for all cases is almost equal.

For a very small value of κ , i.e. $\kappa=1.25*10^{-6}$, the transition takes place quite lately and the flow rate is less. Given that the total flow is the area under each curve, earlier transition results in more flow.

4.12 Linear Rise in the Stream Level

Numerical calculations have been carried out in order to evaluate the drawdown response of the aquifer to a linear rise in the stream level.

The boundary condition at the stream side is arranged according to the stage hydrograph which is shown in *Figure 4.44*. The dimensionless drawdown in the stream linearly increases to 1 by $\theta=1$, and then stays constant.

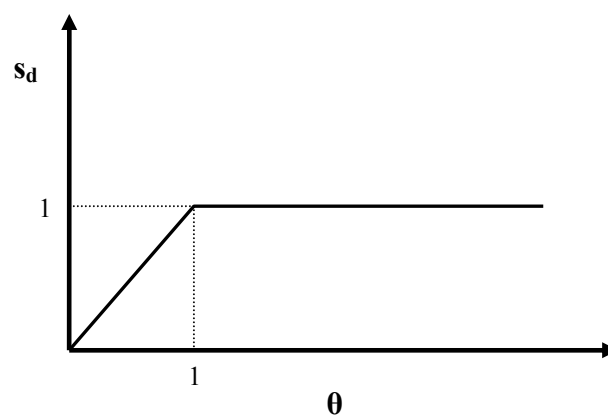


Figure 4.44: Stage hydrograph for linear rise in the stream level.

Figure 4.45 presents the dimensionless drawdown versus dimensionless space curves for the fractures and the blocks for the case $\eta=10$, $\delta=10$ and $\kappa=6.25*10^5$. It is apparent from the figure that the drawdown in the fractures increases faster than the drawdown in the blocks and there exists a lagging between them. However, the difference between the drawdown in the fractures and the drawdown in the blocks is not as large as in the case of step rise in the stream level. For the linear rise case, the drawdown in the blocks gets closer to the drawdown in the fractures at early times and they approach to 1 as the time goes to the infinity.

Figure 4.46 gives the dimensionless drawdown versus dimensionless time curves for the fractures and the blocks at dimensionless locations $\lambda=0.1, 0.2, 0.4$ and 0.8 for the same combination of the dimensionless parameters. It is obvious in the figure that the drawdown behavior of the fractures and the blocks are quite similar and the linear rise in the stream level does not lead transition.

The reason for this is that rapid flow does not take place in the fractures as the drawdown in the stream level increases linearly. Fracture to block flow develops at early stages so that the difference between the drawdown in the fractures and the drawdown in the blocks starts to decrease earlier. In this regard, the blocks store and transmit water homogenously in time.

It could also be seen from the drawdown curves of the fractures at $\lambda=0.1$ and 0.2 in the same figure that there exists a turning point at $\theta=1$ which implies the increase in the drawdown in the fractures slows down after the water level in the stream becomes constant.

In addition, it might be said that the far end of the aquifer is not affected much from the linear rise in the stream level.

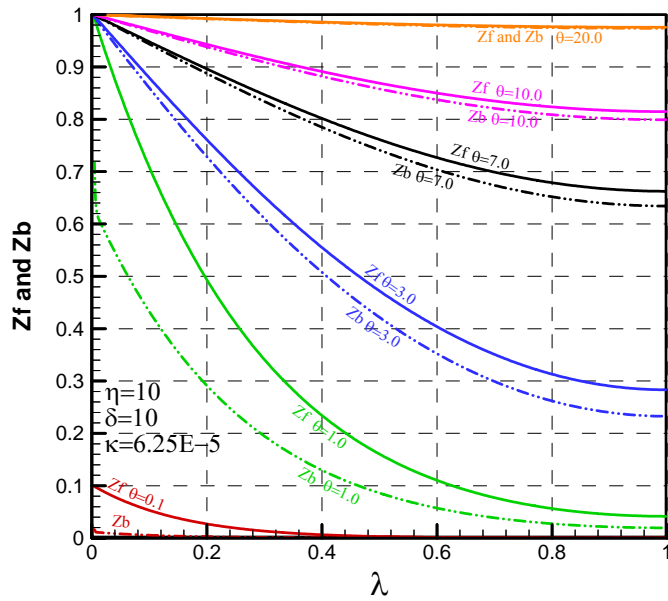


Figure 4.45: Z_f versus λ and Z_b versus λ curves for $\eta=10$, $\delta=10$ and $\kappa=6.25 \cdot 10^{-5}$ at different times θ for the linear rise in the stream level.

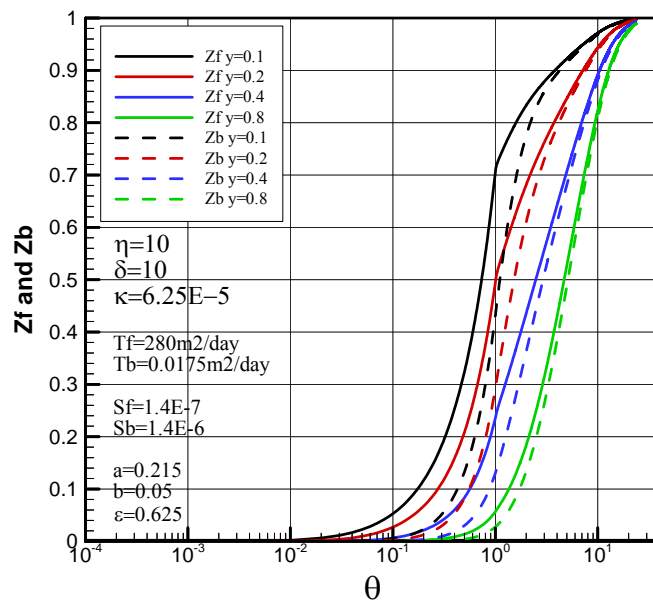


Figure 4.46: Z_f versus θ and Z_b versus θ curves for $\eta=10$, $\delta=10$ and $\kappa=6.25 \cdot 10^{-5}$ at $\lambda=0.1, 0.2, 0.4$ and 0.8 for the linear rise in the stream level.

4.13 Response of the Aquifer to an Arbitrary Stage Hydrograph

Drawdown response of the aquifer to an arbitrary change in the stream stage is studied. *Figure 4.47* shows a hypothetical dimensionless arbitrary stage hydrograph on which calculations are based. It is apparent from the figure that the dimensionless stream stage s_d increases slowly to 0.2 by $\theta=2.2$, gradually to 0.8 between $\theta=2.2$ and $\theta=8.8$, then sharply to 1 by $\theta=11$ and after that time decreases in the same manner.

The boundary condition at the stream side was arranged according to the hydrograph in the computer program. Numerical calculations have been carried out for two cases which are $T_f=280m^2/day^2$ and $T_f=1400 m^2/day^2$. All the other aquifer parameters are fixed in calculations.

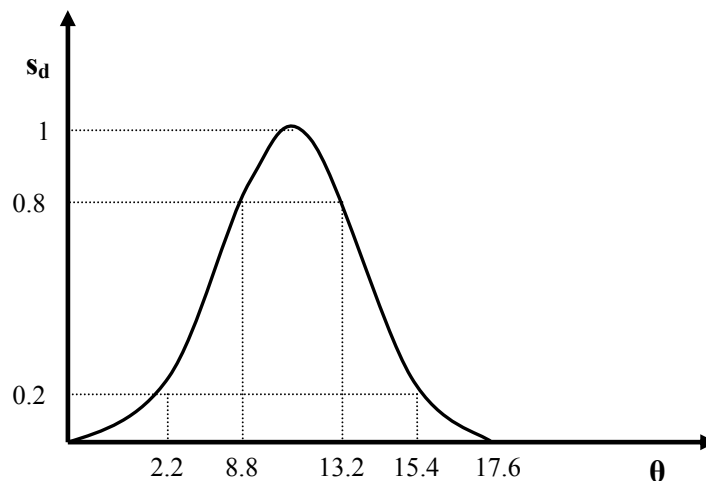


Figure 4.47: Arbitrary stage hydrograph.

Figure 4.48 gives the dimensionless drawdown versus dimensionless time curves for the fractures and the blocks at dimensionless locations $\lambda=0.1, 0.2, 0.4$ and

0.8 for the case $T_f=280 \text{ m}^2/\text{day}^2$. It could be seen in the figure that the drawdown in the aquifer follows the pattern of the stage hydrograph, but delayed in time. Firstly, water flow takes place from the stream to the aquifer and then the water stored in the aquifer flows back to the stream. The drawdown in the aquifer does not reach to 1 except for in the vicinity of the stream. For example, the dimensionless drawdown in the fractures is around 0.94 and 0.77 at dimensionless locations $\lambda=0.1$ and 0.8 respectively.

The drawdown behaviours of the fractures and the blocks in this case are quite similar. In addition, the drawdown in the blocks is very close to the drawdown in the fractures. Transition period does not occur although the stream stage increases sharply at certain stage. It might be said that the exchange of water between the fractures and the blocks is spreaded over the whole flow period.

Figure 4.49 presents the dimensionless drawdown versus dimensionless time curves for the fractures and the blocks at dimensionless locations $\lambda=0.1, 0.2, 0.4$ and 0.8 for the case $T_f=1400 \text{ m}^2/\text{day}^2$.

In this case, the drawdown behaviours of the fractures and the blocks are different. The drawdown response of the blocks is retarded in time. Furthermore, the drawdown in the blocks is not as high as the drawdown in the fractures. These would be explained by the higher fracture transmissivity which results in rapid flow in the fractures that increases the drawdown in the fractures faster than the drawdown in the blocks. The exchange of water between the fractures and the blocks is spreaded over the whole flow period.

The drawdown in the fractures and in the blocks does not reach to 1 except for in the vicinity of the stream. For example, at dimensionless locations $\lambda=0.1$, the drawdown in the fractures is around 0.94 and the drawdown in the blocks is around 0.86.

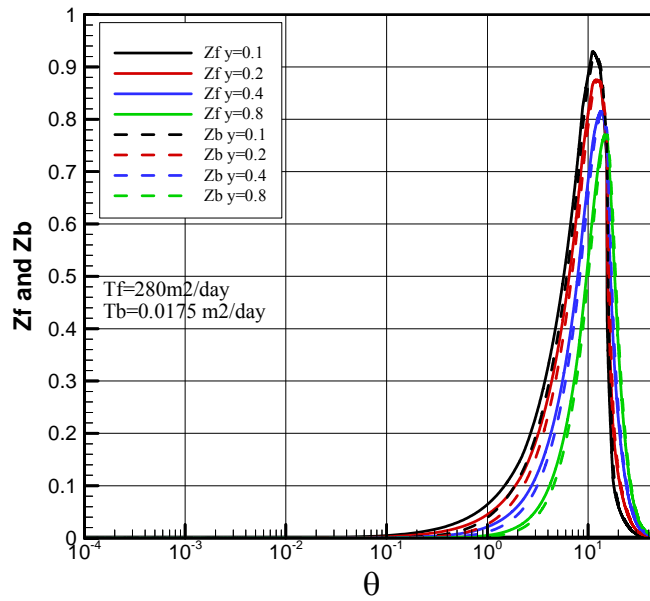


Figure 4.48: Z_f versus θ and Z_b versus θ curves for $T_f=280$ at $\lambda=0.1, 0.2, 0.4$ and 0.8 for the arbitrary stage hydrograph.

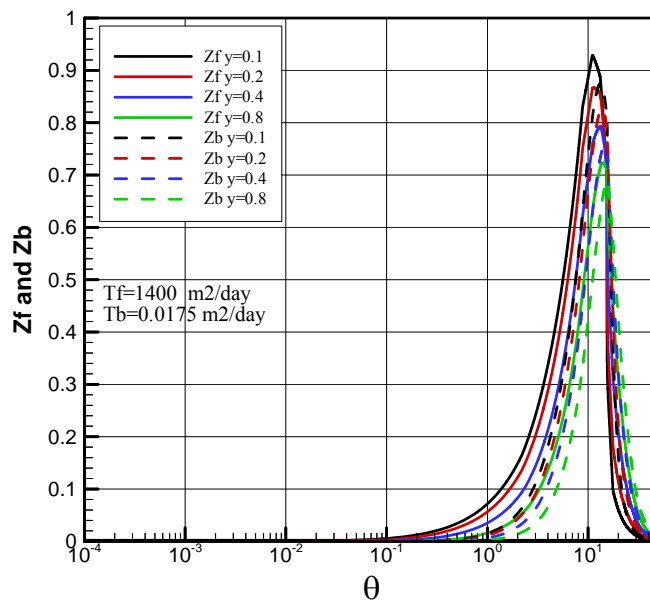


Figure 4.49: Z_f versus θ and Z_b versus θ curves for $T_f=1400$ at $\lambda=0.1, 0.2, 0.4$ and 0.8 for the arbitrary stage hydrograph.

CHAPTER 5

CONCLUSIONS

This study presents a numerical solution for non-Darcian groundwater flow in a finite fractured confined aquifer system. A stream bounds the aquifer at one side and an impervious stratum on the other. The response of the aquifer to three different conditions in the stream level, i.e. sudden rise, linear (gradual) rise and arbitrary change in the stream stage, has been investigated.

The governing equations based on the double porosity conceptual model with quasi-steady transfer of water between the fractures and the blocks have been derived from the continuity equation. The fluid velocity in fractures is often too high for the linear Darcian flow to be valid, so that the governing equation for fracture flow is modified using Forcheimer's equation which incorporates a nonlinear term. On the other hand, the flow in the blocks is Darcian.

The governing equations are solved numerically by Crank-Nicolson implicit scheme. The accuracy of the numerical solution has been verified by comparing it to available analytical solution for the special case of Darcian flow in the fractures. The numerical solution has given good approximation to the analytical solution.

Solution of the governing equations yields drawdown in the fractures and in the blocks with respect to time and space as well as the rate of the flow from the stream to the aquifer.

The behaviour of the drawdown is divided into three periods. Initially, the rate of increase in the drawdown is representative of fracture transmissivity and storage. The drawdown in the fractures increases faster than the drawdown in the

blocks, so that there exists a lagging between them. As fracture to block flow develops, the drawdown response enters into a transitional period and the increase in the drawdown of the fractures is slowed down. The final period of the drawdown response is that of homogenous single porosity medium but delayed in time and the drawdown in the fractures and the blocks increase gradually to reach the steady state condition.

The flow through a finite fractured confined aquifer is controlled by dimensionless parameters representative of aquifer characteristics, namely storativity contrast, η , conductivity contrast, κ , and diffusivity contrast, δ . When the flow in the fractures is non-Darcian, the non-linear term of the Forcheimer's equation, b , has significant effect on the flow.

The storativity contrast dictates the duration of the transition period, on the other hand, the conductivity contrast determines the starting time of the transition.

When the transmissivity of the blocks is equal to 0 , which are the case conductivity and diffusivity contrasts are equal to 0 , the fractured aquifer functions as a single porosity aquifer. Hence, the flow occurs only in the fractures and the drawdown in the blocks is equal to 0 .

The numerical and the analytical solutions give closer results when the aquifer exhibits normal fractured aquifer characteristics which are the fracture transmissivity is much larger than the block transmissivity and the storage coefficient of the blocks are equal or fairly higher than the storage coefficient of the fractures.

The non-Darcian effect primarily depends on the specific discharge which is a function of fracture transmissivity and hydraulic gradient. The specific discharge in the fractures rises as the transmissivity of fractures and the hydraulic gradient increase, so that the non-linear term of the Forcheimer's equation takes effect. The higher the flow rate, the higher the non-linearity.

The non-linear effect on the flow starts to take place when Reynold's number is greater than 0.1 . If Reynold's number is less than this value, the non-Darcian effect is negligible, even non-existent. The non-Darcian effect becomes more and more significant parallel to increase in Reynold's number.

The existing analytical solution is based on the condition that the flow in the blocks and the fractures are Darcian. Consequently, the numerical and the analytical solutions have been compared for the case Reynold's number is less than 0.1 , which is the limit value for Darcian flow, and good approximations have been obtained.

The transition period as well as the effect of the storativity contrast and the conductivity contrast on it could be seen more clearly if the dimensionless flow rate versus dimensionless time curves are examined.

As the storativity contrast increases, more water can be stored in the blocks so that more water is transferred from the fractures to the blocks primarily during the transition period. This also increases the rate of the flow from the stream to the aquifer since more water can be taken by the fractures.

The increase in the conductivity contrast also increases the flow rate. However, the effect of the conductivity contrast on the flow rate depends on the storativity contrast which dictates the duration of the transition period.

The rate of the flow from the stream to the aquifer increases as the non-linear term, b , increases provided that Reynold's number is greater than 0.1 . The increase in the transmissivity of fractures and the hydraulic gradient also makes the non-Darcian effect on the flow rate more significant.

The proposed model is a unique application of non-linear flow models to the fractured aquifers. It can be used in predicting water levels in fractured aquifers and

evaluating time dependent flow rates in the analysis of recession hydrographs and flow towards an excavation site or tunnel located in a fractured aquifer.

In the mathematical formulation of the proposed model the piezometric head, which is the sum of pressure and elevation heads, is selected as main dependent variable. However, in most previous studies, pressure head is taken as dependent variable.

In this study, only one-dimensional flow in the aquifer considered. The study can be extended to two-dimensional flow.

Another valuable method to assess the validity of any flow model and its numerical solution is to compare its results with field observations. Therefore, such a work is recommended.

REFERENCES

Andersen, J. D., “Computational Fluid Dynamics: The Basics with Applications”, McGraw Hill, 1995

Bai, M., Elsworth, D. and Roegiers, J., “Multi-porosity/Multi-permeability Approach to the Simulation of Naturally Fracture Reservoirs”, *Water Resources Research*, Vol. 29(6), 1993, pp. 1621-1633

Barenblatt, G. I., Zheltov, I. P. and Kochina, I. N, “Basic Concepts in the Theory of Seepage of Homogeneous Liquids in Fractured Rocks (Strata) ”, *Journal of Applied Mathematics and Mechanics*, Vol. 24(5), 1960, pp.1286-1303.

Basak, P., “Steady non-Darcian Seepage through Embankments”, *Journal of Irrigation and Drainage*, ASCE, December 1976, pp. 435-443

Basak, P., “Non-Darcy Flow and its Implications to Seepage Problems”, *Journal of Irrigation and Drainage*, ASCE, December 1977, pp. 459-473

Bear, J., “Hydraulics of Groundwater”, McGraw-Hill, 1979

Bordier, C. and Zimmer, D., “Drainage Equations and Non-Darcian Modeling in Coarse Porous Media or Geosynthetic Materials”, *Journal of Hydrology*, Vol. 228, 2000, pp. 174-187

Choi, E. S., Cheema, T. and Islam, M. R., “A New Dual-porosity/Dual-permeability Model with non-Darcian Flow through Fractures”, *Journal of Petroleum Science and Engineering*, Vol. 17, 1997, pp. 331-344

Clossman, P. J., "An Aquifer Model for Fissured Reservoirs", Society of Petroleum Engineers Journal, Vol. 15, 1975, pp. 385-398

Cornell, D. and Katz, D. L., "Flow of Gases through Consolidated Porous Media", Ind. Eng. Chem., Vol. 43, 1953, pp.2145,

Duguid, J. O. and Lee, P. C. Y., "Flow in Fractured Porous Media", Water Resources Research, Vol. 13, No: 3, June 1977, pp. 558-566

Fletcher, C. A. J., "Computational Techniques for Fluid Dynamics", Springer-Verlag, Vol.1, Second Edition, 1991

Gerke, H. H. and van Genuchten, M. T., "A Dual-porosity Model for Simulating the Preferential Movement of Water and Solutes in Structured Porous Media", Water Resources Research, Vol. 29, No: 2, February 1993, pp. 305-319

Gilman, J. R. and Kazemi, H., "Improvements in Simulation of Naturally Fractured Reservoirs", Society of Petroleum Engineers Journal, 1983, pp. 695-707

Henry, J. L. and Palmer, J. R., "Natural and Artificial recharge of Groundwater in the Callide Valley", Proceedings of the Groundwater Recharge Conference, Australian Government Publishing Service, Canberra, Australia, 1980, pp. 72-87

Hirsch, C., "Numerical Computation of Internal and External Flows", John Wiley and Sons Interscience Publications, Vol.1, 1989

Hoffmann, K. A. and Chiang, S. T., "Computational Fluid Dynamics for Engineers", A Publication of Engineering Education System, Wichita, Kansas, Vol. 1, 1993

Huyakorn, P. S. and Pinder, G. F., "Computational Methods in Subsurface Flow", Academic Press NY, 1983

“Introduction to Computational Fluid Dynamics”, Annual Lecture Series Note, von Karman Institute for Fluid Dynamics, Brussels, January 1998

Islam, R. and Nandakumar, K., “Mixed Convection Heat Transfer in Porous Media in the non-Darcy Regime”, The Canadian Journal of Chemical Engineering, Vol. 66, February 1988, pp. 68-74

Kazemi, H., Seth, M. S. and Thomas, G. W., “The Interpretation of Interference Tests in Naturally Fractured Reservoirs with Uniform Fracture Distribution”, Journal of the Society of Petroleum Engineering, Vol. 9, 1969, pp. 463-472

Katz, D. L. and Lee, R. L., “Natural Gas Engineering, Production and Storage” McGraw Hill, 1990

Kohl, T. *et al.*, “Observation and Simulation of Non-Darcian Flow Transients in Fractured Rock”, Water Resources Research, Vol. 33(3), 1997, pp. 407-418

Lane, W. B. and Zinn, P., “Recharge from Weir Storage”, Proceedings of the Groundwater Recharge Conference, Australian Government Publishing Service, Canberra, Australia, 1980, pp. 47-59

Mathews, J. H., “Numerical Methods for Computer Science, Engineering and Mathematics”, Prentice-Hall International Editions, 1988

Neta, B., “Numerical Solution of Partial Differential Equations”, Lecture Notes, Naval Postgraduate School, California, 2003

Önder, H., “Unsteady Groundwater Flow in a Stream-Fractured Aquifer”, Flow and Transport in Porous Media (Edited by Verruijt, A. and Barends, F. B. J.), EUROMEC 143, 1981, pp. 63-68, Balkema, Rotterdam, the Netherlands.

Önder, H., “Non-Steady Flow Type Curves for Strip Aquifers with Constant Drawdown, *Journal of Irrigation and Drainage*, ASCE, Vol. 10, No: 4, July/August 1994, pp. 732-741

Önder, H., “Determination of Aquifer Parameters of Finite Confined Aquifers from Constant Drawdown Non-Steady Type Curves”, *Hydrological Sciences*, 39(3), June 1994, pp. 269-280

Önder, H., “Analysis of One-Dimensional Groundwater Flow in a non-Uniform Aquifer”, *Journal of Hydraulic Engineering*, August 1997, pp. 732-736

Önder, H., “One-Dimensional Transient Flow in a Finite Fractured Aquifer System”, *Hydrological Sciences*, 43(2), April 1998, pp. 243-265

Önder, H., “Predicting Groundwater Flow Behaviour in non-Uniform Aquifers in Contact with a Stream: An Extension to Ditch Drainage”, Kluwer Academic Publishers (Edited by K. W. F. Howard and R. G. Israfiov), 2002, pp. 407-423

Pinder, G. F., Breedhoeft, J. D. and Cooper, H. H., “Determination of Aquifer Diffusivity from Aquifer Response to Fluctuations in River Stage”, *Water Resources Research*, Vol. 5(4), 1969, pp. 850-855

Rorabaugh, M. I., “Use of Water Levels in Estimating Aquifer Constants in a Finite Aquifer”, *Commission of Subterranean Waters*, IAHS Publications, No: 52, 1960, pp. 314-323

Rorabaugh, M. I., “Estimating Changes in Bank Storage and Groundwater Contribution to Stream Flow”, *Commission of Subterranean Waters*, IAHS Publications, No: 63, 1964, pp. 432-441

Smith, G. D., “Numerical Solution of Partial Differential Equations: Finite Difference Methods”, Oxford University Press, Second Edition, 1978

Streltsova, T. D., "Hydrodynamics of Groundwater Flow in a Fractured Formation", *Water Resources Research*, Vol. 12(3), 1976, pp. 405-414

Streltsova, T. D., "Unsteady Unconfined Flow into a Surface Reservoir", *Journal of Hydrology*, Vol. 27, 1975, pp. 95-110

Streltsova, T. D., "Well Testing in Heterogeneous Formations", John Wiley, 1988

Venetis, C., "Finite Aquifers: Characteristic Responses and Applications", *Journal of Hydrology*, Vol. 22, 1970, pp. 53-62

Venkatamaran, P. and Rao, P. R. M., "Darcian, Transitional and Turbulent Flow through Porous Media", *Journal of Hydraulic Engineering*, August 1998, pp. 840-846

Warren, J. E. and Root, P. J., "The Behaviour of Naturally Fractured Reservoirs", *Society of Petroleum Engineering Journal*, Vol. 3, 1963, pp. 245-255

Wu, Y. S., "An Approximate Analytical Solution for non-Darcy Flow towards a Well in Fractured Media", *Water Resources Research*, Vol. 38, No: 3, 2002a

Wu, Y. S., "Numerical Simulation of Single-Phase and Multiphase Non-Darcy Flow in Porous and Fractured Reservoirs", *Transport in Porous Media*, Vol. 49, pp. 209-240, 2002b

APPENDIX A

Computer Program

DOUBLE PRECISION ZB(10000),ZF(10000),FQ(10000),TETA(10000)
DOUBLE PRECISION A(10000),B(10000),C(10000),D(10000)
DOUBLE PRECISION HF(10000),HB(10000),Y(10000)
DOUBLE PRECISION TH(10000),FLOW(10000)
DOUBLE PRECISION SB,SF,TB,TF,EPS,DT,DL,Q

C *CONSTANTS*

C *THICKNESS OF THE AQUIFER, M*
BA=60.

C *LENGTH OF THE AQUIFER, M*
XL=800.

C *INITIAL PIEZOMETRIC HEAD, M*
H0=65.

C *CONSTANT DRAWDOWN IN THE STREAM, M*
S0=2.

C *TRANSMISSIVITY OF THE BLOCKS, M**2/DAY*
TB=0.0175

C *TRANSMISSIVITY OF THE FRACTURES, M**2/DAY*
TF=280.0

C *STORAGE COEFFICIENT OF THE BLOCKS*
SB=0.0000014

C *STORAGE COEFFICIENT OF THE FRACTURES*
SF=0.00000014

C *SHAPE FACTOR, M**-2*
EPS=0.0625

C *CONSTANTS OF THE FORCHEIMER EQUATION, DAY/M, DAY**2/M**2*
AF=0.215
BF=0.05

C *COEFFICIENT OF THE COMBINED METHOD*

C *CRANK-NICOLSON*
GAMA=0.5

C *TIME STEP*
DT=0.00001

C *MESH SIZE*
DX=1.75
DL=DX/XL
N=1/DL

ETA=SB/SF
DELTA=4*XL**2*EPS*TB*SF/(TF*SB)

C INITIAL CONDITIONS

DO I=1,N
ZB(I)=0
ZF(I)=0
HF(I)=H0
HB(I)=H0
END DO

DO I=2,N-1
FQ(I)=AF
END DO

C COMPUTATIONS

C TIME

T=0.

100 T=T+DT

C BOUNDARY CONDITIONS

ZB(1)=1
ZF(1)=1

HF(1)=H0+S0
HB(1)=H0+S0

C FRACTURES

DO I=2,N-1
A(I)=(BA*DT*GAMA/(FQ(I)*TF*DL**2))
B(I)=1+(BA*DT**2*GAMA/(FQ(I)*TF*DL**2))
C(I)=(BA*DT*GAMA/(FQ(I)*TF*DL**2))
D(I)=ZF(I)+(BA*DT*(1-GAMA)/(FQ(I)*TF*DL**2))*(ZF(I+1)-2*ZF(I)
+ZF(I-1)+(XL**2*EPS*TB*DT/TF)*(ZB(I)-ZF(I)))
END DO

B1=ZF(1)

C BN=ZF(N)

BC1=1.
BC2=0.

CALL THOMAS(N,DL,A,B,C,D,B1,BN,BC1,BCN,TH)

DO I=2,N
ZF(I)=TH(I)
HF(I)=S0*ZF(I)+H0

```

      END DO
C  OUTPUT

C  BLOCKS
DO I=2,N-1
A(I)=SF*TB*DT*GAMA/(SB*TF*DL**2)
B(I)=1+SF*TB*DT*2*GAMA/(SB*TF*DL**2)
C(I)=SF*TB*DT*GAMA/(SB*TF*DL**2)
D(I)=ZB(I)+(SF*TB*DT*(1-GAMA)/(SB*TF*DL**2))*(ZB(I+1)-
2*ZB(I)
+ZB(I-1))-(XL**2*EPS*TB*SF*DT/(SB*TF))*(ZB(I)-ZF(I))
END DO

      B1=ZB(1)
C  BN=ZB(N)
      BC1=1.
      BC2=0.

      CALL THOMAS(N,DL,A,B,C,D,B1,BN,BC1,BCN,TH)
DO I=2,N
ZB(I)=TH(I)
HB(I)=S0*ZB(I)+H0
END DO
C  OUTPUT

C  FORCHEIMER EQUATION
DO I=2,N-1
FQ(I)=AF-(BF/(2*AF*2*DX))*(HF(I+1)-HF(I-1))
END DO

C  FLOW RATE
Q=TF*((HF(1)-HF(2))/DX)
C  OUTPUT

C  LOOP
IF(ZF(N-1).LT.0.999) THEN
GO TO 100
ELSE
STOP
ENDIF

      END

C  THOMAS ALGORITHM
SUBROUTINE THOMAS(N,DL,A,B,C,D,B1,BN,BC1,BCN,TH)
DOUBLE PRECISION E(10000),F(10000)

```

```

DOUBLE PRECISION A(10000),B(10000),C(100000),D(10000)
DOUBLE PRECISION TH(10000),DL
IF(BC1.EQ.1.) THEN
E(1)=0
F(1)=B1
ELSE
E(1)=1
F(1)=-B1*DL
ENDIF

DO I=2,N-1
E(I)=A(I)/(B(I)-C(I)*E(I-1))
F(I)=(D(I)+C(I)*F(I-1))/(B(I)-C(I)*E(I-1))
END DO

IF(BC2.EQ.1.) THEN
TH(N)=BN
ELSE
TH(N)=(F(N-1)+BN*DL)/(1-E(N-1))
ENDIF

DO I=N,2,-1
TH(I-1)=E(I-1)*TH(I)+F(I-1)
END DO

END

```

APPENDIX B

Application of Discrete Perturbation Stability Analysis

Stability of the finite difference equations of the fractures and the blocks are investigated by discrete perturbation stability analysis. Basic theory of this method is presented in *Section 3.9*.

The finite difference equation for the fractures is:

$$\begin{aligned}
 & -\left(\frac{1}{2} \frac{B}{F(q)_i^n} \frac{1}{T_f} \frac{\Delta\theta}{\Delta\lambda^2}\right) z f_{i+1}^{n+1} + \left(1 + \frac{B}{F(q)_i^n} \frac{1}{T_f} \frac{\Delta\theta}{\Delta\lambda^2}\right) z f_i^{n+1} \\
 & - \left(\frac{1}{2} \frac{B}{F(q)_i^n} \frac{1}{T_f} \frac{\Delta\theta}{\Delta\lambda^2}\right) z f_{i-1}^{n+1} \\
 & = z f_i^n + \frac{1}{2} \frac{B}{F(q)_i^n} \frac{1}{T_f} \frac{\Delta\theta}{\Delta\lambda^2} (z f_{i+1}^n - 2z f_i^n + z f_{i-1}^n) \\
 & - \frac{L^2 \varepsilon T_b}{T_f} \Delta\theta (z f_i^n - z b_i^n)
 \end{aligned} \tag{3.54}$$

In order to reduce mathematical labor in the application of the method, the following variables have been used.

$$\alpha = \frac{\Delta\theta}{\Delta\lambda^2} \tag{4.6}$$

$$\Gamma = \frac{B}{F(q)_i^n} \frac{1}{T_f} \tag{B.1}$$

$$\Lambda = \frac{L^2 \varepsilon T_b}{T_f} \Delta\theta \tag{B.2}$$

Then, *equation 3.54* takes the form:

$$\begin{aligned}
& -\frac{\Gamma\alpha}{2}zf_{i+1}^{n+1} + (1+\Gamma\alpha)zf_i^{n+1} - \frac{\Gamma\alpha}{2}zf_{i-1}^{n+1} \\
& = zf_i^n - \frac{\Gamma\alpha}{2}(zf_{i+1}^n - 2zf_i^n + zf_{i-1}^n) - \Lambda(zf_i^n - zb_i^n)
\end{aligned} \tag{B.3}$$

In order to determine the disturbance e_i^{n+1} at time level $n+1$ at the node i , a disturbance e_i^n is introduced at node i at time level n .

$$\begin{aligned}
& -\frac{\Gamma\alpha}{2}zf_{i+1}^{n+1} + (1+\Gamma\alpha)(zf_i^{n+1} + e_i^{n+1}) - \frac{\Gamma\alpha}{2}zf_{i-1}^{n+1} \\
& = (zf_i^n + e_i^n) - \frac{\Gamma\alpha}{2}(zf_{i+1}^n - 2(zf_i^n + e_i^n) + zf_{i-1}^n) - \Lambda(zf_i^n + e_i^n)
\end{aligned} \tag{B.4}$$

Subtracting *equation B.3* from *equation B.4* produces the disturbance equation:

$$(1+\Gamma\alpha)e_i^{n+1} = e_i^n - \frac{\Gamma\alpha}{2}(-2e_i^n) - \Lambda e_i^n \tag{B.5}$$

If the mathematical operations are furthered:

$$(1+\Gamma\alpha)e_i^{n+1} = e_i^n - \frac{\Gamma\alpha}{2}(-2e_i^n) - \Lambda e_i^n \tag{B.6}$$

$$(1+\Gamma\alpha)e_i^{n+1} = e_i^n + \Gamma\alpha e_i^n - \Lambda e_i^n \tag{B.7}$$

$$(1+\Gamma\alpha)e_i^{n+1} = (1+\Gamma\alpha - \Lambda)e_i^n \tag{B.8}$$

$$e_i^{n+1} = \frac{(1+\Gamma\alpha - \Lambda)}{(1+\Gamma\alpha)}e_i^n \tag{B.9}$$

$$e_i^{n+1} = \left(1 - \frac{\Lambda}{1 + \Gamma\alpha}\right) e_i^n \quad \text{B.10}$$

For the node $i+1$ at time level $n+1$:

$$\begin{aligned} & -\frac{\Gamma\alpha}{2} z f_{i+2}^{n+1} + (1 + \Gamma\alpha) z f_{i+1}^{n+1} - \frac{\Gamma\alpha}{2} z f_i^{n+1} \\ & = z f_{i+1}^n - \frac{\Gamma\alpha}{2} (z f_{i+2}^n - 2z f_{i+1}^n + z f_i^n) - \Lambda z f_{i+1}^n \end{aligned} \quad \text{B.11}$$

$$\begin{aligned} & -\frac{\Gamma\alpha}{2} z f_{i+2}^{n+1} + (1 + \Gamma\alpha)(z f_{i+1}^{n+1} + e_{i+1}^{n+1}) - \frac{\Gamma\alpha}{2} (z f_i^{n+1} + e_i^{n+1}) \\ & = z f_{i+1}^n - \frac{\Gamma\alpha}{2} (z f_{i+2}^n - 2z f_{i+1}^n + (z f_i^n + e_i^n)) - \Lambda z f_{i+1}^n \end{aligned} \quad \text{B.12}$$

Subtracting *equation B.11* from *equation B.12* produces:

$$(1 + \Gamma\alpha) e_{i+1}^{n+1} - \frac{\Gamma\alpha}{2} e_i^{n+1} = -\frac{\Gamma\alpha}{2} e_i^n \quad \text{B.13}$$

If the mathematical operations are furthered:

$$(1 + \Gamma\alpha) e_{i+1}^{n+1} - \frac{\Gamma\alpha}{2} \left(1 - \frac{\Lambda}{1 + \Gamma\alpha}\right) e_i^n = -\frac{\Gamma\alpha}{2} e_i^n \quad \text{B.14}$$

$$(1 + \Gamma\alpha) e_{i+1}^{n+1} = -\frac{\Gamma\alpha}{2} e_i^n + \frac{\Gamma\alpha}{2} \left(1 - \frac{\Lambda}{1 + \Gamma\alpha}\right) e_i^n \quad \text{B.15}$$

$$(\Gamma\alpha + \Lambda) e_{i+1}^{n+1} = -\frac{\Lambda}{1 + \Gamma\alpha} e_i^n \quad \text{B.16}$$

$$e_{i+1}^{n+1} = -\frac{\Lambda}{(\Gamma\alpha + \Lambda)(1 + \Gamma\alpha)} e_i^n \quad \text{B.18}$$

For the node $i-1$ at time level $n+1$:

$$\begin{aligned} & -\frac{\Gamma\alpha}{2}zf_{i-2}^{n+1} + (1+\Gamma\alpha)zf_{i-1}^{n+1} - \frac{\Gamma\alpha}{2}zf_i^{n+1} \\ & = zf_{i-1}^n - \frac{\Gamma\alpha}{2}(zf_{i-2}^n - 2zf_{i-1}^n + zf_i^n) - \Lambda zf_{i-1}^n \end{aligned} \quad \text{B.19}$$

$$\begin{aligned} & -\frac{\Gamma\alpha}{2}zf_{i-2}^{n+1} + (1+\Gamma\alpha)(zf_{i-1}^{n+1} + e_{i-1}^{n+1}) - \frac{\Gamma\alpha}{2}(zf_i^{n+1} + e_i^{n+1}) \\ & = zf_{i-1}^n - \frac{\Gamma\alpha}{2}(zf_{i-2}^n - 2zf_{i-1}^n + (zf_i^n + e_i^n)) - \Lambda zf_{i-1}^n \end{aligned} \quad \text{B.20}$$

Subtracting *equation B.19* from *equation B.20* produces:

$$(1+\Gamma\alpha)e_{i-1}^{n+1} - \frac{\Gamma\alpha}{2}e_i^{n+1} = -\frac{\Gamma\alpha}{2}e_i^n \quad \text{B.21}$$

If the mathematical operations are furthered:

$$(1+\Gamma\alpha)e_{i-1}^{n+1} - \frac{\Gamma\alpha}{2}\left(1 - \frac{\Lambda}{1+\Gamma\alpha}\right)e_i^n = -\frac{\Gamma\alpha}{2}e_i^n \quad \text{B.22}$$

$$(1+\Gamma\alpha)e_{i-1}^{n+1} = -\frac{\Gamma\alpha}{2}e_i^n + \frac{\Gamma\alpha}{2}\left(1 - \frac{\Lambda}{1+\Gamma\alpha}\right)e_i^n \quad \text{B.23}$$

$$(\Gamma\alpha + \Lambda)e_{i-1}^{n+1} = -\frac{\Lambda}{1+\Gamma\alpha}e_i^n \quad \text{B.24}$$

$$e_{i-1}^{n+1} = -\frac{\Lambda}{(\Gamma\alpha + \Lambda)(1+\Gamma\alpha)}e_i^n \quad \text{B.25}$$

Notice that *equation B.25* is identical with *equation B.18* and, thus, the error propagation is symmetrical in the solution domain.

For the node $i+2$ at time level $n+2$:

$$\begin{aligned} & -\frac{\Gamma\alpha}{2}zf_{i+1}^{n+2} + (1+\Gamma\alpha)zf_i^{n+2} - \frac{\Gamma\alpha}{2}zf_{i-1}^{n+2} \\ & = zf_i^{n+1} - \frac{\Gamma\alpha}{2}(zf_{i+1}^{n+1} - 2zf_i^{n+1} + zf_{i-1}^{n+1}) - \Lambda zf_i^{n+1} \end{aligned} \quad \text{B.26}$$

$$\begin{aligned} & -\frac{\Gamma\alpha}{2}zf_{i+1}^{n+2} + (1+\Gamma\alpha)(zf_i^{n+2} + e_i^{n+2}) - \frac{\Gamma\alpha}{2}zf_{i-1}^{n+2} = (zf_i^{n+1} + e_i^{n+1}) \\ & -\frac{\Gamma\alpha}{2}((zf_{i+1}^{n+1} + e_{i+1}^{n+1}) - 2(zf_i^{n+1} + e_i^{n+1}) + (zf_{i-1}^{n+1} + e_{i-1}^{n+1})) - \Lambda(zf_i^{n+1} + e_i^{n+1}) \end{aligned} \quad \text{B.27}$$

Subtracting *equation B.26* from *equation B.27* produces:

$$(1+\Gamma\alpha)e_i^{n+2} = e_i^{n+1} - \frac{\Gamma\alpha}{2}(e_{i+1}^{n+1} - 2e_i^{n+1} + e_{i-1}^{n+1}) - \Lambda e_i^{n+1} \quad \text{B.28}$$

If the mathematical operations are furthered:

$$\begin{aligned} (1+\Gamma\alpha)e_i^{n+2} & = \left(1 - \frac{\Lambda}{1+\Gamma\alpha}\right)e_i^n \\ & -\frac{\Gamma\alpha}{2}\left(-\frac{\Lambda}{(\Gamma\alpha+\Lambda)(1+\Gamma\alpha)}e_i^n - 2\left(1 - \frac{\Lambda}{1+\Gamma\alpha}\right)e_i^n - \frac{\Lambda}{(\Gamma\alpha+\Lambda)(1+\Gamma\alpha)}e_i^n\right) \\ & -\Lambda\left(1 - \frac{\Lambda}{1+\Gamma\alpha}\right)e_i^n \end{aligned} \quad \text{B.29}$$

$$\begin{aligned} (1+\Gamma\alpha)e_i^{n+2} & = \left(1 - \frac{\Lambda}{1+\Gamma\alpha}\right)e_i^n \\ & -\frac{\Gamma\alpha}{2}\left(-\frac{2\Lambda}{(\Gamma\alpha+\Lambda)(1+\Gamma\alpha)}e_i^n - \left(2 - \frac{2\Lambda}{1+\Gamma\alpha}\right)e_i^n\right) - \Lambda\left(1 - \frac{\Lambda}{1+\Gamma\alpha}\right)e_i^n \end{aligned} \quad \text{B.30}$$

$$(1+\Gamma\alpha)e_i^{n+2} = (1-\Lambda)\left(1-\frac{\Lambda}{1+\Gamma\alpha}\right)e_i^n + \left(\frac{\Gamma\alpha\Lambda}{(\Gamma\alpha+\Lambda)(1+\Gamma\alpha)}e_i^n + \left(\Gamma\alpha - \frac{\Gamma\alpha\Lambda}{1+\Gamma\alpha}\right)e_i^n\right) \quad \text{B.31}$$

$$(1+\Gamma\alpha)e_i^{n+2} = (1-\Lambda)\left(1-\frac{\Lambda}{1+\Gamma\alpha}\right)e_i^n + \frac{\Gamma\alpha\Lambda}{(\Gamma\alpha+\Lambda)(1+\Gamma\alpha)}e_i^n + \Gamma\alpha e_i^n - \frac{\Gamma\alpha\Lambda}{1+\Gamma\alpha}e_i^n \quad \text{B.32}$$

$$e_i^{n+2} = \frac{(1-\Lambda)}{(1+\Gamma\alpha)}\left(1-\frac{\Lambda}{1+\Gamma\alpha}\right)e_i^n + \frac{\Gamma\alpha\Lambda}{(\Gamma\alpha+\Lambda)(1+\Gamma\alpha)^2}e_i^n + \frac{\Gamma\alpha}{(1+\Gamma\alpha)}e_i^n - \frac{\Gamma\alpha\Lambda}{(1+\Gamma\alpha)^2}e_i^n \quad \text{B.33}$$

$$e_i^{n+2} = \left[\frac{(1-\Lambda)}{(1+\Gamma\alpha)}\left(1-\frac{\Lambda}{1+\Gamma\alpha}\right) + \frac{\Gamma\alpha\Lambda}{(\Gamma\alpha+\Lambda)(1+\Gamma\alpha)^2} + \frac{\Gamma\alpha}{(1+\Gamma\alpha)} - \frac{\Gamma\alpha\Lambda}{(1+\Gamma\alpha)^2} \right] e_i^n \quad \text{B.34}$$

$$e_i^{n+2} = \left[\frac{(1-\Lambda)}{(1+\Gamma\alpha)}\left(1-\frac{\Lambda}{1+\Gamma\alpha}\right) + \left(\frac{1}{(\Gamma\alpha+\Lambda)} - 1\right)\frac{\Gamma\alpha\Lambda}{(1+\Gamma\alpha)^2} + \frac{\Gamma\alpha}{(1+\Gamma\alpha)} \right] e_i^n \quad \text{B.35}$$

Applications can be extended further in order to see how the disturbance proceeds. However, it is reasonable to stop here to show the application of the discrete perturbation stability analysis to the finite difference equation for the fractures as the mathematical labour increases substantially during the calculation of disturbance at each neighbouring point. Therefore, a computer program is needed to calculate the disturbance in every node at later time steps.

Discrete perturbation stability analysis has been also applied to the finite difference equation for the blocks. The finite difference equation for the blocks is:

$$\begin{aligned}
& - \left(\frac{1}{2} \frac{S_f}{S_b} \frac{T_b}{T_f} \frac{\Delta\theta}{\Delta\lambda^2} \right) z b_{i+1}^{n+1} + \left(1 + \frac{S_f}{S_b} \frac{T_b}{T_f} \frac{\Delta\theta}{\Delta\lambda^2} \right) z b_i^{n+1} \\
& - \left(\frac{1}{2} \frac{S_f}{S_b} \frac{T_b}{T_f} \frac{\Delta\theta}{\Delta\lambda^2} \right) z b_{i-1}^{n+1} \\
& = z b_i^n + \frac{1}{2} \frac{S_f}{S_b} \frac{T_b}{T_f} \frac{\Delta\theta}{\Delta\lambda^2} (z b_{i+1}^n - 2z b_i^n + z b_{i-1}^n) \\
& + \Delta\theta \frac{S_f}{S_b} \frac{T_b}{T_f} L^2 \varepsilon (z f_i^n - z b_i^n)
\end{aligned} \tag{3.44}$$

Equation 3.44 can be written as in the form of equation B.3, however for this case:

$$\Gamma = \frac{S_f}{S_b} \frac{T_b}{T_f} \tag{B.36}$$

$$\Lambda = \frac{S_f}{S_b} \frac{T_b}{T_f} L^2 \varepsilon \Delta\theta \tag{B.37}$$

Then, equation 3.44 becomes:

$$\begin{aligned}
& - \frac{\Gamma \alpha}{2} z b_{i+1}^{n+1} + (1 + \Gamma \alpha) z b_i^{n+1} - \frac{\Gamma \alpha}{2} z b_{i-1}^{n+1} \\
& = z b_i^n - \frac{\Gamma \alpha}{2} (z b_{i+1}^n - 2z b_i^n + z b_{i-1}^n) + \Lambda (z f_i^n - z b_i^n)
\end{aligned} \tag{B.38}$$

Application of discrete perturbation stability analysis to the finite difference equation for the blocks yields the same disturbance equations with the finite difference equation for the fractures, however Γ and Λ are different. For this reason, there is no need to present the disturbance equations for the blocks here.

APPENDIX C

Comparison of Numerical and Analytical Solutions

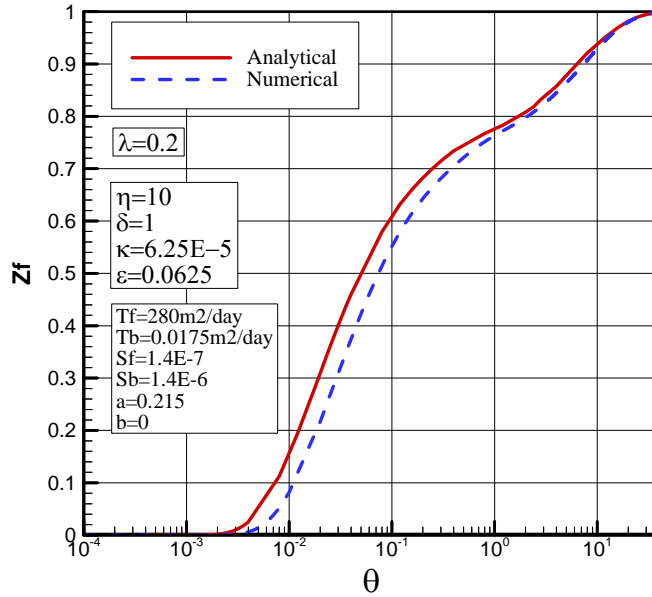


Figure C.1: Comparison of numerical and analytical solutions at $\lambda=0.2$ when $\alpha=2.09$ and $\eta=10$, $\delta=1$ and $\kappa=6.25 \cdot 10^{-5}$.

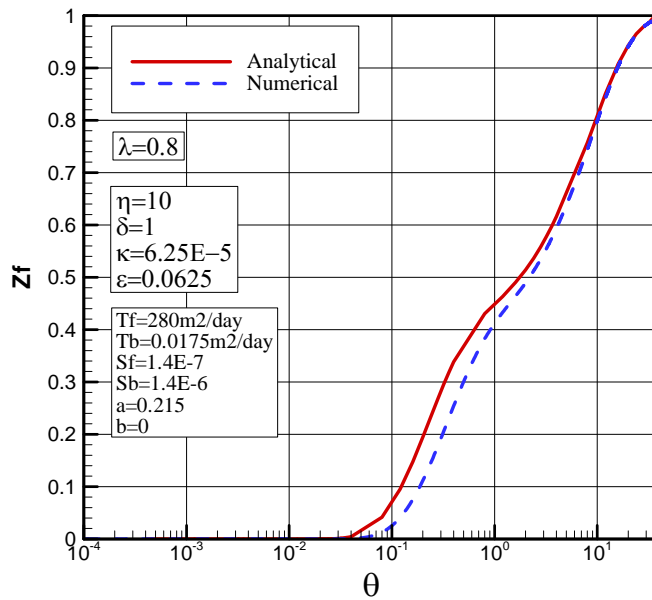


Figure C.2: Comparison of numerical and analytical solutions at $\lambda=0.8$ when $\alpha=2.09$ and $\eta=10$, $\delta=1$ and $\kappa=6.25 \cdot 10^{-5}$.

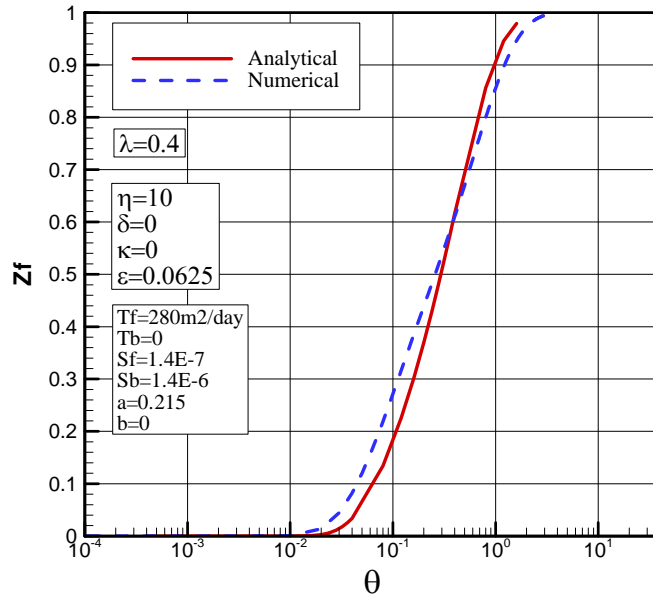


Figure C.3: Comparison of numerical and analytical solutions at $\lambda=0.4$ when $\alpha=2.09$ and $\eta=10$, $\delta=0$ and $\kappa=0$.

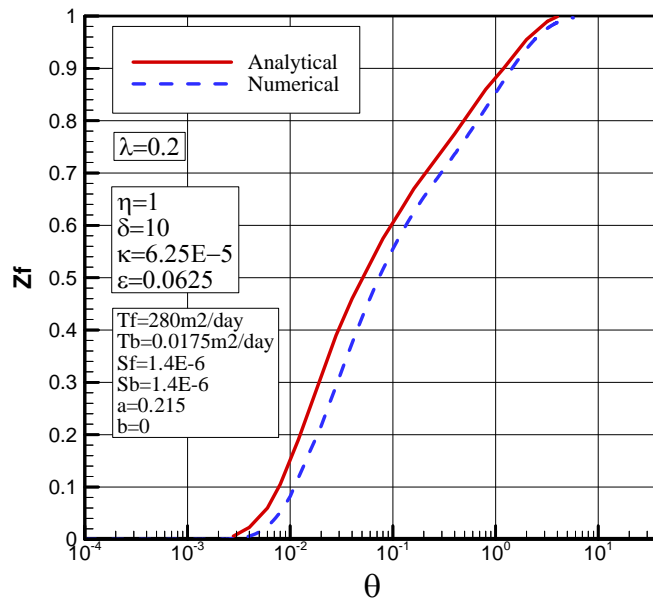


Figure C.4: Comparison of numerical and analytical solutions at $\lambda=0.2$ when $\alpha=2.09$ and $\eta=1$, $\delta=10$ and $\kappa=6.25 \cdot 10^{-5}$.

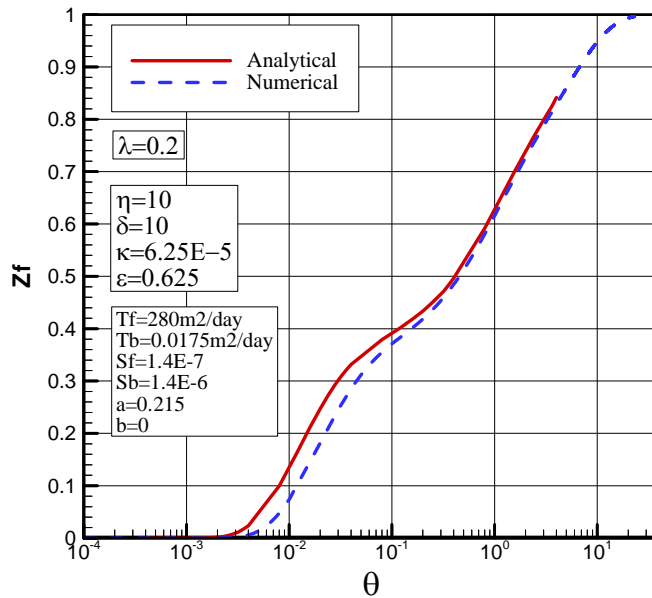


Figure C.5: Comparison of numerical and analytical solutions at $\lambda=0.2$ when $\alpha=2.09$ and $\eta=10$, $\delta=10$ and $\kappa=6.25 \cdot 10^{-5}$.

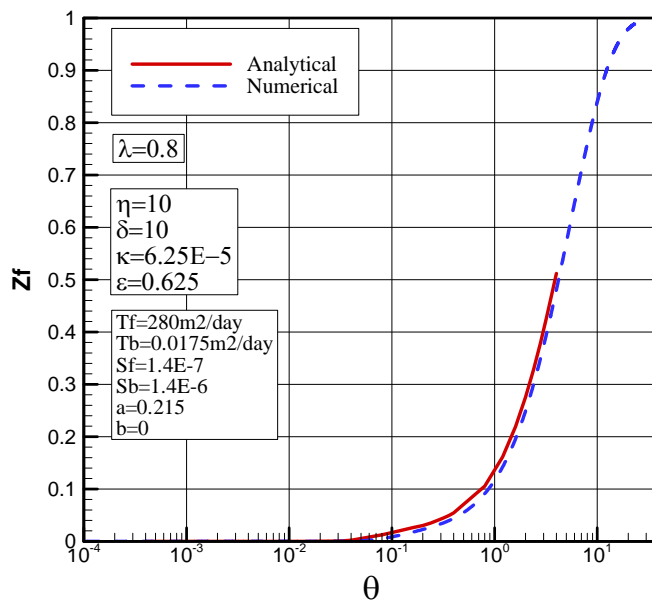


Figure C.6: Comparison of numerical and analytical solutions at $\lambda=0.8$ when $\alpha=2.09$ and $\eta=10$, $\delta=10$ and $\kappa=6.25 \cdot 10^{-5}$.

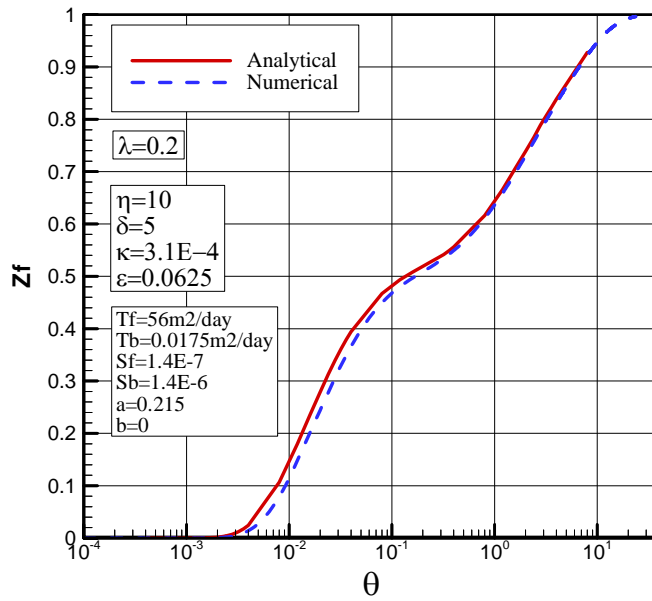


Figure C.7: Comparison of numerical and analytical solutions at $\lambda=0.2$ when $\alpha=2.09$ and $\eta=10$, $\delta=5$ and $\kappa=3.125 \cdot 10^{-4}$.

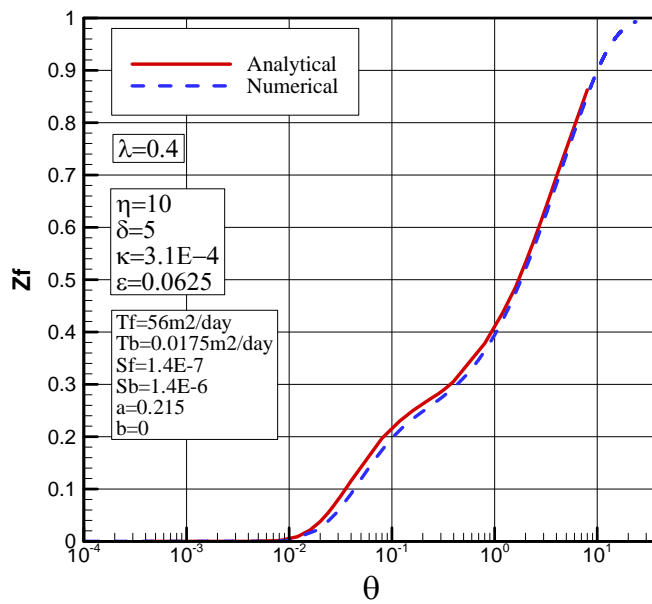


Figure C.8: Comparison of numerical and analytical solutions at $\lambda=0.4$ when $\alpha=2.09$ and $\eta=10$, $\delta=5$ and $\kappa=3.125 \cdot 10^{-4}$.

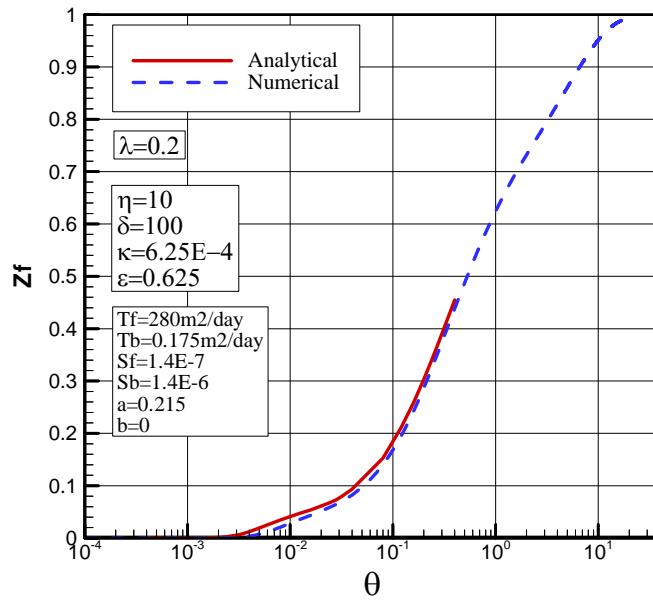


Figure C.9: Comparison of numerical and analytical solutions at $\lambda=0.2$ when $\alpha=2.09$ and $\eta=10$, $\delta=100$ and $\kappa=6.25 \cdot 10^{-4}$.

APPENDIX D

Published Data on Porous Media

Table D.1: Published data on porous media (Venkataraman *et al.*, 1998)

Medium	Particle Size (cm)	Porosity (%)	k (m ²)	b (day ² /m ²)
Glass Spheres	2.50	39.20	6.67	3.7*10 ⁻⁶
Glass Spheres	2.00	38.30	5.02	6.0*10 ⁻⁶
Glass Spheres	2.89	41.31	16.9	3.6*10 ⁻⁶
Crushed Rock	1.31	47.00	2.29	9.0*10 ⁻⁶
Crushed Rock	2.89	48.73	9.28	4.2*10 ⁻⁶
Glass Spheres	1.84	38.27	8.14	7.5*10 ⁻⁶
Gravel	2.83	46.50	8.83	7.5*10 ⁻⁶
Crushed Rock	2.01	45.88	6.59	7.6*10 ⁻⁶
Crushed Rock	2.99	46.60	26.9	3.9*10 ⁻⁶
Glass Spheres	2.89	39.82	33.1	5.2*10 ⁻⁶
Glass Spheres	1.56	39.50	8.49	8.9*10 ⁻⁶
Gravel	8.40	-	204	2.0*10 ⁻⁶
Glass Spheres	1.56	35.53	7.2	1.31*10 ⁻⁵
Gravel	1.30	47.90	3.76	1.74*10 ⁻⁵
Gravel	1.20	37.30	1.69	2.77*10 ⁻⁵
Gravel	1.20	35.70	1.81	2.51*10 ⁻⁵
Crushed Rock	1.44	41.50	4.53	1.54*10 ⁻⁵
Marble	1.58	-	17.5	1.03*10 ⁻⁵
Marble	2.46	-	22.4	8.8*10 ⁻⁶
Marble	1.56	-	24.7	8.4*10 ⁻⁶
Marble	1.56	-	12	1.38*10 ⁻⁵
Gravel	0.64	47.00	0.85	5.23*10 ⁻⁵
Crushed Rock	1.40	44.40	9	1.63*10 ⁻⁵

Table D.1 (continued)

Crushed Rock	1.90	44.08	14.2	1.45×10^{-5}
Sand	0.0625	40.70	0.03	3.35×10^{-4}
Marble	1.60	-	11.9	1.57×10^{-5}
Sand	0.49	-	1.4	4.93×10^{-5}
Glass Spheres	1.56	35.58	13.5	1.94×10^{-5}
Glass Beads	0.027	37.00	0.01	9.41×10^{-4}
Glass Beads	0.038	37.00	0.01	6.70×10^{-4}
Glass Beads	0.32	-	0.67	8.35×10^{-5}
Glass Spheres	0.30	-	0.64	8.58×10^{-5}
Gravel	0.17	43.60	0.23	1.47×10^{-4}
Gravel	0.29	42.30	0.35	1.18×10^{-4}
Gravel	0.40	38.40	0.98	7.10×10^{-5}
Crushed Rock	1.68	44.50	15.9	1.72×10^{-4}
Crushed Rock	0.29	42.00	0.29	1.26×10^{-4}
Gravel	1.10	-	10.3	2.14×10^{-5}
Sand	0.16	39.90	0.12	2.35×10^{-4}
Crushed Rock	1.07	44.11	8.5	2.81×10^{-5}
Crushed Rock	0.69	47.20	4.24	4.07×10^{-5}
Crushed Rock	0.93	43.00	5.36	34.6×10^{-5}
Sand	0.14	-	0.10	32.1×10^{-4}
Sand	0.26	-	0.22	2.21×10^{-4}
Marble	0.47	-	1.7	7.68×10^{-5}
Gravel	2.50	-	40	1.62×10^{-5}

APPENDIX E

Raw Data

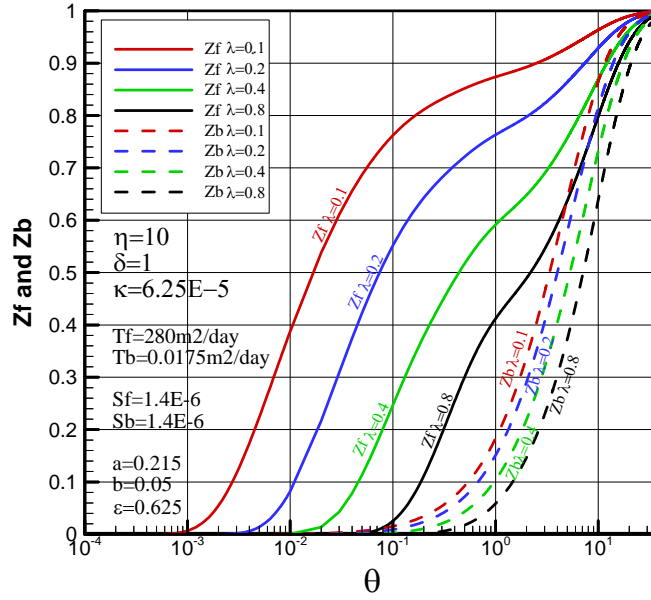


Figure E.1: Z_f versus θ and Z_b versus θ curves for $\eta=10$, $\delta=1$ and $\kappa=6.25 \cdot 10^{-5}$ at $\lambda=0.1, 0.2, 0.4$ and 0.8 .

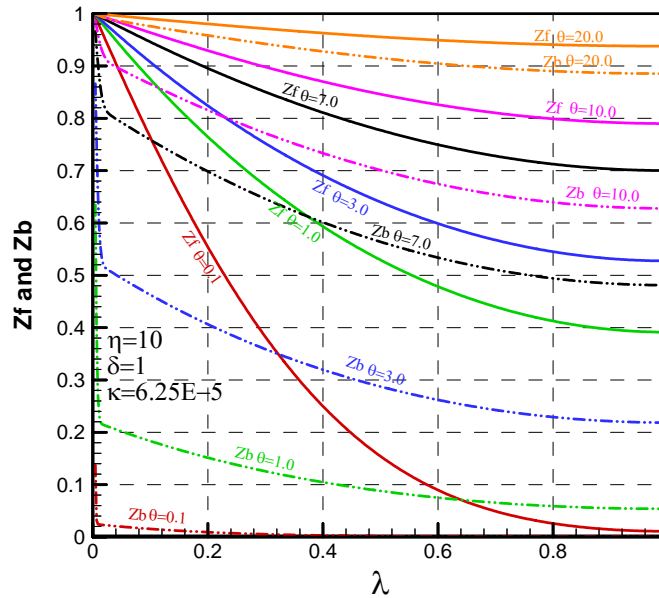


Figure E.2: Z_f versus λ and Z_b versus λ curves for $\eta=10$, $\delta=1$ and $\kappa=6.25E-5$ at different times θ .

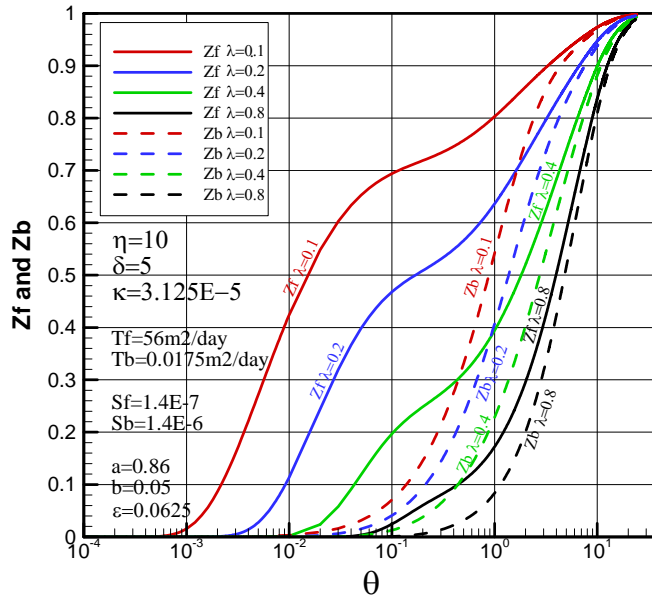


Figure E.3: Z_f versus θ and Z_b versus θ curves for $\eta=10$, $\delta=5$ and $\kappa=3.125 \cdot 10^{-5}$ at $\lambda=0.1, 0.2, 0.4$ and 0.8 .

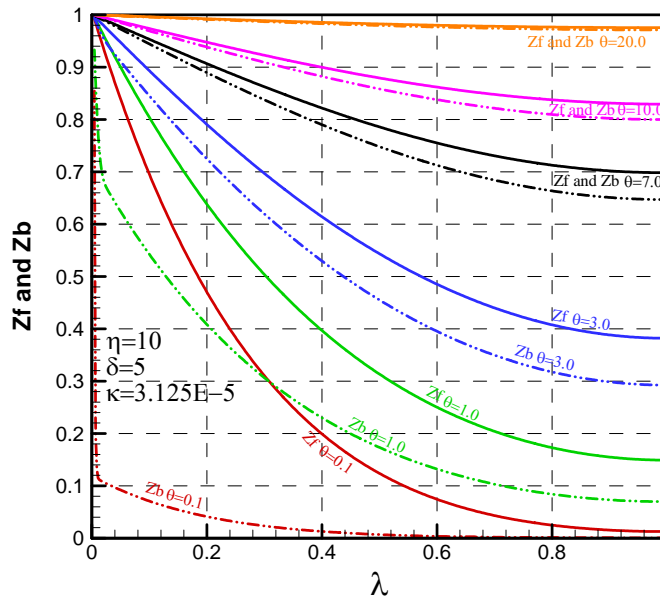


Figure E.4: Z_f versus λ and Z_b versus λ curves for $\eta=10$, $\delta=5$ and $\kappa=3.125 \cdot 10^{-5}$ at different times θ .

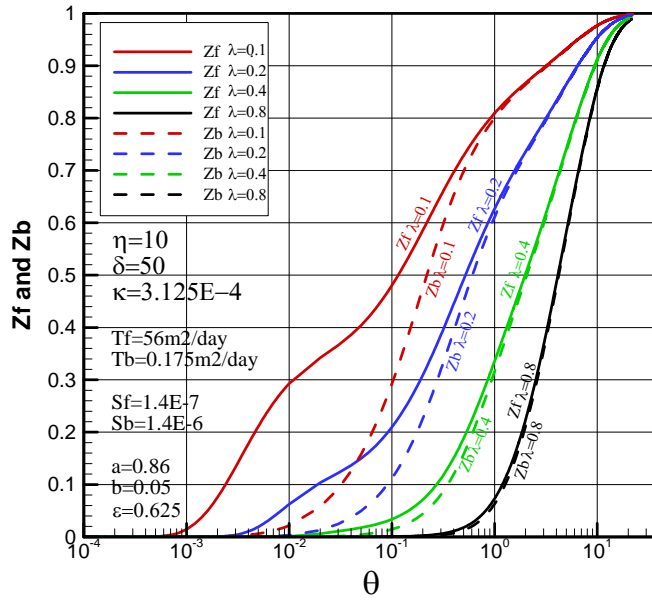


Figure E.5: Z_f versus θ and Z_b versus θ curves for $\eta=10$, $\delta=50$ and $\kappa=3.125 \cdot 10^{-4}$ at $\lambda=0.1, 0.2, 0.4$ and 0.8 .

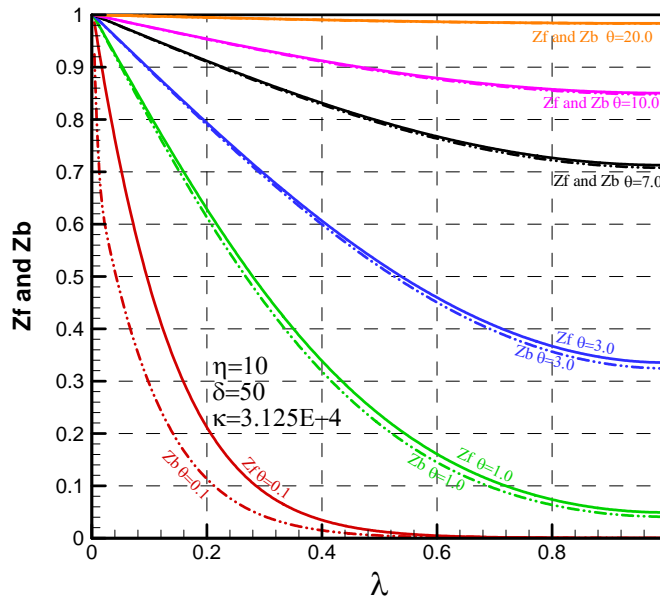


Figure E.6: Z_f versus λ and Z_b versus λ curves for $\eta=10$, $\delta=50$ and $\kappa=3.125 \cdot 10^{-4}$ at different times θ .

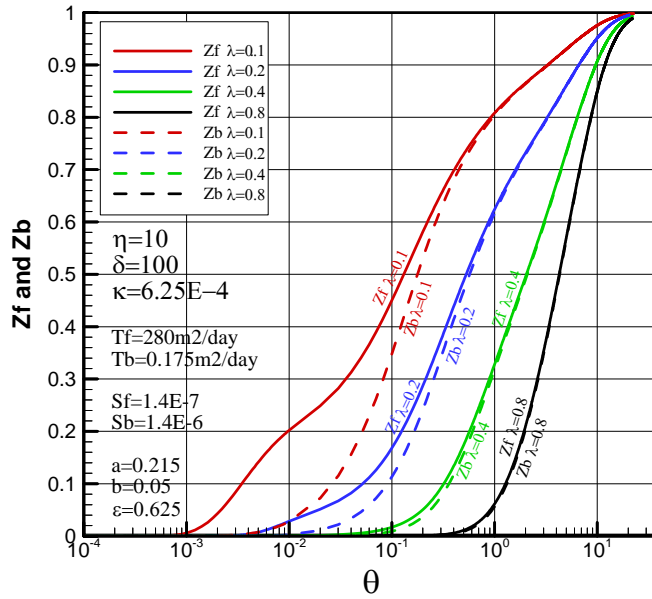


Figure E.7: Z_f versus θ and Z_b versus θ curves for $\eta=10$, $\delta=100$ and $\kappa=6.25 \cdot 10^{-4}$ at $\lambda=0.1, 0.2, 0.4$ and 0.8 .

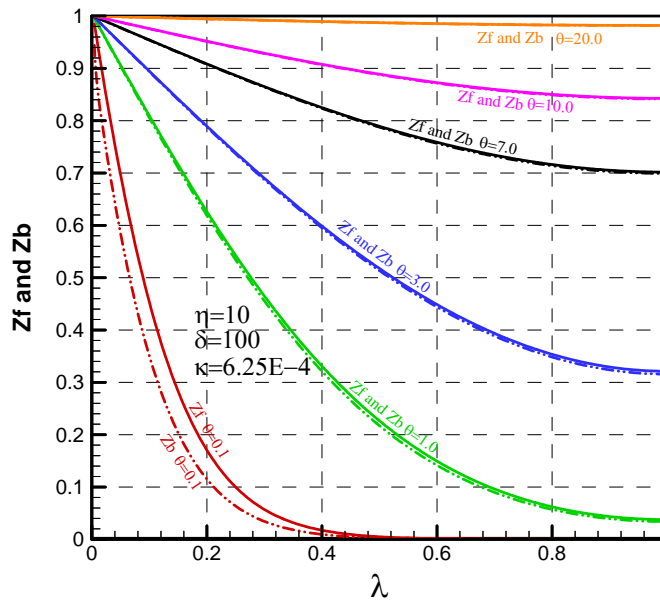


Figure E.8: Z_f versus λ and Z_b versus λ curves for $\eta=10$, $\delta=100$ and $\kappa=6.25 \cdot 10^{-4}$ at different times θ .

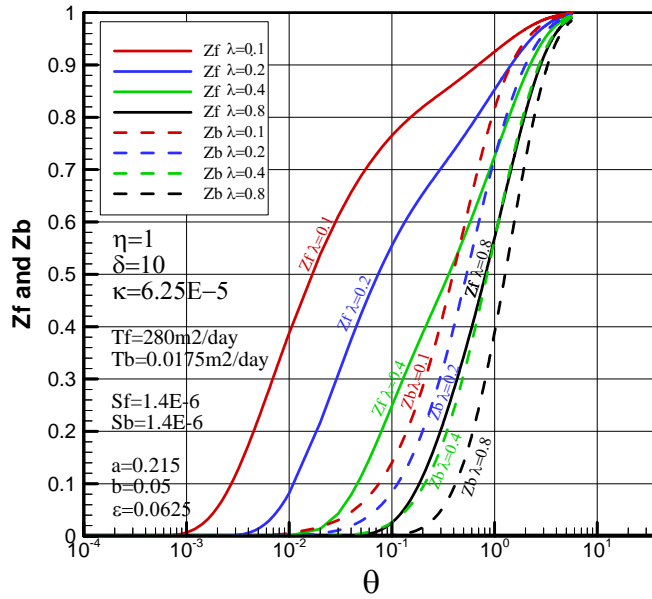


Figure E.9: Z_f versus θ and Z_b versus θ curves for $\eta=1$, $\delta=10$ and $\kappa=6.25 \cdot 10^{-5}$ at $\lambda=0.1, 0.2, 0.4$ and 0.8 .

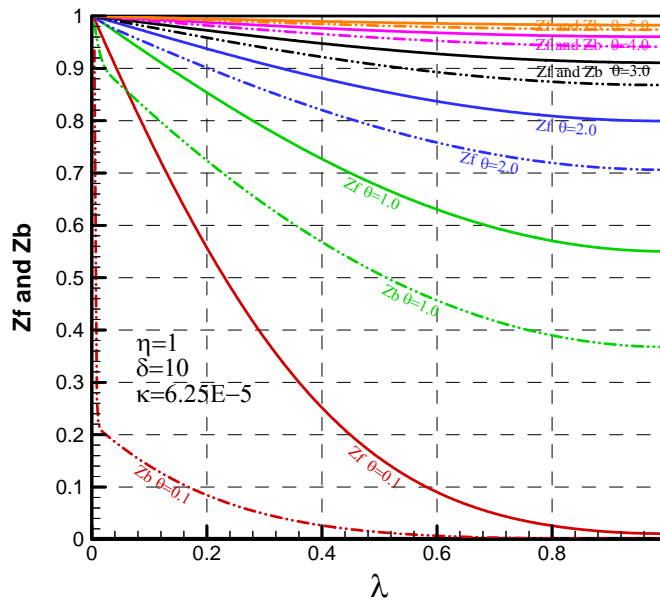


Figure E.10: Z_f versus λ and Z_b versus λ curves for $\eta=1$, $\delta=10$ and $\kappa=6.25 \cdot 10^{-5}$ at different times θ .

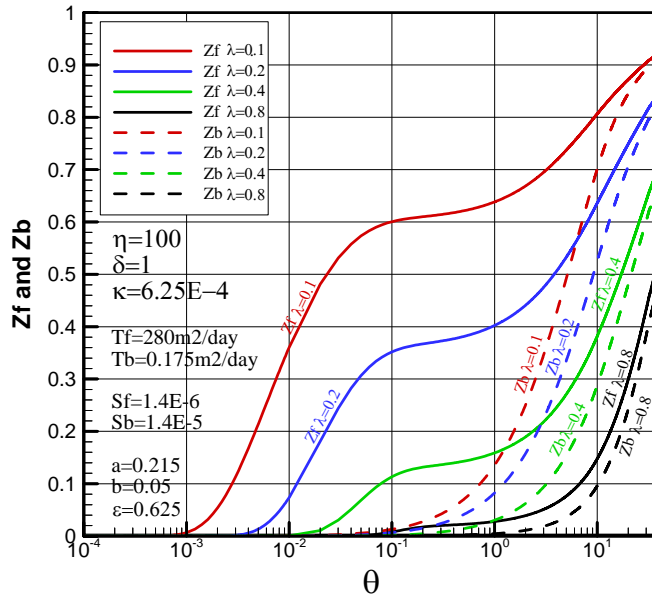


Figure E.11: Z_f versus θ and Z_b versus θ curves for $\eta=100$, $\delta=1$ and $\kappa=6.25 \cdot 10^{-4}$ at $\lambda=0.1, 0.2, 0.4$ and 0.8 .

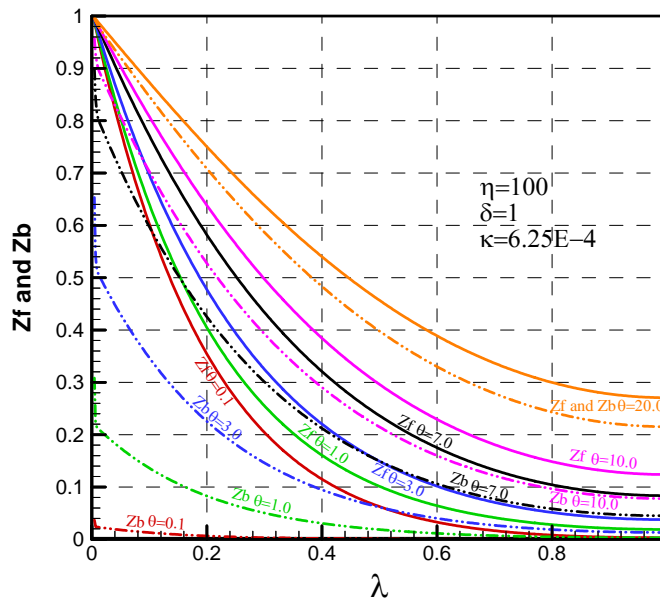


Figure E.12: Z_f versus λ and Z_b versus λ curves for $\eta=100$, $\delta=1$ and $\kappa=6.25 \cdot 10^{-4}$ at different times θ .

APPENDIX F:
Some Examples to the Results of the Discrete Perturbation
Stability Analysis

Fractures, $\alpha=1$

<i>n=2</i>		<i>n=20</i>	
<u><i>i</i></u>	<u><i>e</i></u>	<u><i>i</i></u>	<u><i>e</i></u>
1	0.999987330983642	1	1.00014531858685
2	1.214456593200893E-005	2	1.777678436649515E-005
3	2.665947541869868E-006	3	2.809499480667030E-006
4	5.691843983674877E-007	4	3.983568626902148E-007
5	1.176595204951565E-007	5	4.522843568367277E-008
6	2.335725688740841E-008	6	2.102011617557553E-009
7	4.386226494641318E-009	7	-9.080741835615392E-010
8	7.556432872267478E-010	8	-4.185284881320092E-010
9	1.106008834601498E-010	9	-1.215503505513980E-010
10	1.004114355561356E-011	10	2.914915436903099E-011
11	-1.360395117703012E-012	11	-6.080627655557356E-012
12	-1.169343858051408E-012	12	-1.089217874111837E-012
13	-4.645839187422533E-013	13	-1.509278946542314E-013
14	-1.505227927949204E-013	14	-7.523447271485539E-015
15	-4.411431248209550E-014	15	4.995266250001851E-015
16	-1.214530798077058E-014	16	2.690547025812294E-015
17	-3.196997436422308E-015	17	9.476056158153797E-016
18	-8.119958777633418E-016	18	2.824815454374401E-016
19	-1.999427168407695E-016	19	7.622157493475481E-017
20	-4.782466202477497E-017	20	1.909209349061834E-017
21	-1.110929348986663E-017	21	4.478191742461287E-018
22	-2.499810141503706E-018	22	9.818212612082294E-019
23	-5.418446738369576E-019	23	1.981872488140921E-019
24	-1.119205208147700E-019	24	3.586244780027734E-020

n=40

<i>i</i>	<i>e</i>
1	1.00020691569197
2	2.063251242749762E-005
3	2.199179723618916E-006
4	1.687948501916633E-007
5	-1.495265194121089E-010
6	-3.393417556139809E-009
7	-8.151943958838417E-010
8	-1.149463346067754E-010
9	-4.787914048719059E-012
10	3.150905691085266E-012
11	1.322139711959445E-012
12	3.406691617290022E-013
13	6.600585746674639E-014
14	8.871439779862425E-015
15	1.682522632475994E-016
16	-4.008468020762001E-016
17	-1.776255223206486E-016
18	-5.379773285173396E-017
19	-1.338450022525268E-017
20	-2.807213926440180E-018
21	-4.990332915931270E-019
22	-3.623664312032857E-020
23	-1.309673206609401E-020
24	1.921554484513330E-020
25	-8.051662946666679E-021

n=80

<i>i</i>	<i>e</i>
1	1.00028788862618
2	2.226910774632987E-005
3	1.596473530552725E-006
4	6.154626522551607E-008
5	-4.922500084129996E-009
6	-1.238488458332900E-009
7	-9.188292398146603E-011
8	1.060828813648876E-011
9	4.395414005447673E-012
10	6.598039574199019E-013
11	1.765968841147041E-014
12	-1.869970369584940E-014
13	-5.953930242505560E-015
14	-9.956933343447358E-016
15	-8.058111050625546E-017
16	3.952770192238805E-017
17	-1.986436392329295E-018
18	1.307547382772330E-017
19	-6.991234290453813E-018
20	4.904082453009036E-018
21	-2.908694466218092E-018
22	1.536904344359163E-018
23	-7.329636665031148E-019
24	3.038094323020712E-019
25	-1.093975631774749E-019

Blocks, $\alpha=0.028$

<i>n=2</i>		<i>n=20</i>	
<i>i</i>	<i>e</i>	<i>i</i>	<i>e</i>
1	0.999997500000897	1	1.00005065702351
2	-0.880929406001033	2	-0.880971251064848
3	-1.488377666900599E-007	3	-1.488519067483620E-007
4	-2.514694212995627E-014	4	-2.515052572888492E-014
5	-4.248711281755626E-021	5	-4.249518581966272E-021
6	-7.178426491153233E-028	6	-7.180131481823250E-028
7	-1.212833809399204E-034	7	-1.213179494116068E-034
8	-2.049148028519368E-041	8	-2.049829431288974E-041
9	-3.462145934787928E-048	9	-3.463461682932932E-048
10	-5.849481983216952E-055	10	-5.851982917117074E-055
11	-9.883014788074100E-062	11	-9.887709799227779E-062
12	-1.669788565577820E-068	12	-1.670661147553091E-068
13	-2.821197694755010E-075	13	-2.822806012014251E-075
14	-4.766565418500617E-082	14	-4.769509235118791E-082
15	-8.053368940108594E-089	15	-8.058725332195135E-089
16	-1.360660047458392E-095	16	-1.361629691887871E-095
17	-2.298908417729225E-102	17	-2.300655921630779E-102
18	-3.884129561221574E-109	18	-3.887266629825770E-109
19	-6.562446042655817E-116	19	-6.568058131318091E-116
20	-1.108760595751720E-122	20	-1.109761476977400E-122
21	-1.873310730024976E-129	21	-1.875090795024948E-129
22	-3.165059350659440E-136	22	-3.168217277638470E-136
23	-5.347538202091645E-143	23	-5.353127823492740E-143
24	-9.034953741664127E-150	24	-9.044827090277840E-150
25	-1.526504085227134E-156	25	-1.528244788719437E-156

<i>n=40</i>		<i>n=80</i>	
<i>i</i>	<i>e</i>	<i>i</i>	<i>e</i>
1	1.00010661480228	1	1.00021853964696
2	-0.881015300647803	2	-0.881103406421415
3	-1.488667921087004E-007	3	-1.488965661787224E-007
4	-2.515429830608529E-014	4	-2.516184459230804E-014
5	-4.250368475233430E-021	5	-4.252068580491992E-021
6	-7.181926471333388E-028	6	-7.185517258136418E-028
7	-1.213543434854866E-034	7	-1.214271507410521E-034
8	-2.050546837235713E-041	8	-2.051982079594113E-041
9	-3.464846984829786E-048	9	-3.467618523750154E-048
10	-5.854616120839586E-055	10	-5.859884503291687E-055
11	-9.892653241415202E-062	11	-9.902544204351747E-062
12	-1.671579923575863E-068	12	-1.673418302566143E-068
13	-2.824499514044826E-075	13	-2.827888169365575E-075
14	-4.772609046979004E-082	14	-4.778811925694599E-082
15	-8.064365701316070E-089	15	-8.075652785359053E-089
16	-1.362650768330827E-095	16	-1.364694146584942E-095
17	-2.302496161719044E-102	17	-2.306178988351873E-102
18	-3.890570256260859E-109	18	-3.897181969319341E-109
19	-6.573968329211203E-116	19	-6.585797147595472E-116
20	-1.110815549821454E-122	20	-1.112925276727627E-122
21	-1.876965506879040E-129	21	-1.880717883466293E-129
22	-3.171543194051796E-136	22	-3.178200515035705E-136
23	-5.359014934460721E-143	23	-5.370799312410637E-143
24	-9.055226169401047E-150	24	-9.076043047397701E-150
25	-1.530078224883763E-156	25	-1.533748535169277E-156

CURRICULUM VITAE

Personal Information

Surname, Name: Altınörs, Adnan Altay
Nationality: Turkish
Date and Place of Birth: 21 April 1972, Ayvalık, Turkey
Marital Status: Married
Phone: +32 2 289 62 55, +32 2 476 55 70 15
Fax: +32 2 511 04 50
E-mail: aaltinors@mfa.gov.tr

Education

<u>Degree</u>	<u>Institution</u>	<u>Graduation</u>
Ph. D.	METU, Ankara, Turkey	2005
Postgraduate Diploma	von Karman Institute for Fluid Dynamics, Brussels, Belgium	1998
MS	METU, Ankara, Turkey	1997
Visiting Scholar	Monash University, Melbourne, Australia	1996
BS	METU, Ankara, Turkey	1995

Work Experience

<u>Year</u>	<u>Place</u>	<u>Position</u>
2003-Present	Permanent Delegation of Turkey to the European Union, Brussels, Belgium	Advisor
1999-2003	Ministry of Foreign Affairs, Ankara, Turkey	Advisor
1998	Tempo Engineers and Consultants, Ankara, Turkey	Design Engineer
1995	Yüksel Construction, Ankara, Turkey	Site Engineer

Foreign Languages

English, French